



Prepared for:

European Union MAST-III SAFE



RWS-RIKZ

Laboratory experiments on sediment dynamics and density gradation

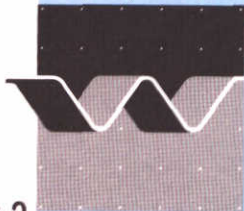
Part II: Time-dependent measurements

Data Report

June 2000



Groningen State University-KVI (partner)



wl | delft hydraulics

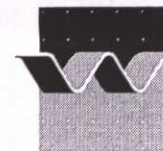
Laboratory experiments on sediment dynamics and density gradation

Part II: Time-dependent measurements

Judith Bosboom and Ronald Koomans

Data Report

June 2000



CLIENT: European Union MAST-III SAFE
&
Rijkswaterstaat/Rijksinstituut voor Kust en Zee (RIKZ)

TITLE: Laboratory experiments on sediment dynamics and density gradation
Part II: time-dependent measurements

ABSTRACT:

The data presented in this report were obtained and analysed within the framework of the EU-sponsored MAST-III SAFE project. The measurements of hydrodynamics, suspended sediment concentrations, sediment transport and radiometry were carried out on a natural 2DV beach under erosive conditions in WL|DELFT HYDRAULICS' Scheldt flume. Besides dune sand (series A), also various mixtures of dune sand and heavy minerals were used to investigate selective transport phenomena of minerals with a different density (series B through D). Time-mean sediment concentrations, radiometry (bed composition), bed profile evolution (data report part I: Time-averaged measurements (Koomans and Bosboom, 2000) and time-dependent measurements (surface elevations and time-dependent velocities and sediment concentrations at one elevation above the bed; data report part II: Time-dependent measurements (Bosboom and Koomans, 2000) were measured for all mixtures.

REFERENCES:

VER.	ORIGINATOR	DATE	REMARKS	REVIEW	APPROVED BY
1.0	J. Bosbom	15-6-00		M.J.F. Stive	T. Schilperoort

PROJECT IDENTIFICATION:

KEYWORDS:

CONTENTS:	TEXT PAGES	59	TABLES	44	FIGURES	42	APPENDICES	
STATUS:	<input type="checkbox"/> PRELIMINARY	<input type="checkbox"/> DRAFT	<input checked="" type="checkbox"/> FINAL					

Contents

List of Figures

List of Tables

1 Introduction.....	1
1.1 Background and aim of study	1
1.2 Outline of report	1
1.3 Acknowledgements.....	2
2 Experimental set-up.....	3
2.1 Scheldt flume	3
2.2 Measurement programme and test procedures	3
2.3 Steering and wave conditions	5
2.4 Sediment	6
2.5 Instrumentation	6
2.5.1 General.....	6
2.5.2 Measurements during runs.....	7
2.5.3 Measurements between runs.....	10
2.5.4 Sample analysis.....	10
3 Instrumentation and calibration	12
3.1 General.....	12
3.2 Wave height meters (WHM).....	12
3.3 Optical concentration meter (OPC)	12
3.3.1 Instrument description	12
3.3.2 OpCon calibration.....	15
3.3.3 Discussion of non-linearity in calibration	19
3.4 Acoustic Doppler Velocity meter (ADV)	25
3.4.1 Instrument description	25
3.4.2 Set-up and calibration	26

4 Data analysis and validation	29
4.1 General.....	29
4.2 Data storage	29
4.3 File conversion and correction.....	32
4.3.1 Conversion to physical values	32
4.3.2 Division between instruments and filtering.....	32
4.4 Derived time-averaged parameters	33
4.4.1 Surface elevation	33
4.4.2 Velocity	36
4.4.3 Sediment concentration	37
4.4.4 Sediment fluxes.....	37
4.4.5 Data retrieval; description of programme collec_sf	37
4.5 Surface elevation.....	38
4.5.1 Results.....	38
4.5.2 Statistical analysis.....	39
4.5.3 Long waves	45
4.6 Concentration.....	46
4.6.1 Visual inspection of time-series.....	46
4.6.2 Results.....	47
4.6.3 Comparison with suction system	48
4.7 Velocity	49
4.7.1 ADV files.....	49
4.7.2 Spike detection filter.....	52
4.7.3 Results.....	53
4.8 Sediment fluxes.....	55
5 Conclusions and recommendations	57

List of Figures

Figure 1 Schematic set-up of the experiment with x-axis, locations of wave height meters (WHM) and positions of measuring verticals (vertical dashed lines) in which the measurement carriages were deployed. The grey box on the left-hand side of the figure shows the location of the wave generator with $x=0$ corresponding to the mean position of the wave board.	4
Figure 2 Grain-size distribution for Quartz and Zircon	6
Figure 3 Measurement carriage 1 during the A-series, looking into the direction of the wave board. From left to right equipped with: suction tube d-side (not visible), ADV, depth-reference rod, OPCON, suction tube w-side and WHM.	10
Figure 4 Schematic diagram of OPCON probe with the two stems and the transmitted light beam	13
Figure 5 Calibration curves for OpCon1 and OpCon 2 with different zero level shiftings for quartz sand of $d_{50}=129\text{ }\mu\text{m}$	16
Figure 6 Calibration constant K1 OpCon, D^* influence	18
Figure 7 Calibration constant K1 OpCon, D_{50} influence	18
Figure 8 Calibration factor γ for sand S3. Upper panel: from transmission signal V. Lower panel: from linearised transmission signal W. From Bosman (1984)	21
Figure 9 Calibration factor γ obtained from linearised transmission signal W. Upper panel: sand S2. Lower panel: sand S4. From Bosman (1984)	22
Figure 10 Calibration factor γ for Scheldt flume calibration measurements from linearised transmission signal W for both OpCons (without zero level shift).	23
Figure 11 Schematic diagram of the ADV probe with the transmitter at the bottom part of the probe surrounded by the three receive transducers	26
Figure 12 The difference in the still water level before and after each test	40
Figure 13 Set-up with zerolevel before test (upper plot) and with average of zerolevel before and after test (middle plot) and initial bed level (%A100) and bed after ~30 hours (%A904) (lower plot). Error bars indicate twice the standard deviation from mean.	41
Figure 14 The difference in the still water level before and after each test	42
Figure 15 Kurtosis (first plot), standard deviation (second), skewness (third plot) and initial bed level (%A100) and bed after ~30 hours (%A904) (fourth plot) for surface elevation signal of series A. Error bars indicate twice the standard deviation of data.	44
Figure 16 Development of cross-correlation coefficient between long wave surface elevation and wave envelope (squares) and low wave energy (triangles) in time for WHM04	46

Figure 17 Comparison between mean concentration measured with the OPCON (corrected for grain-size) and determined from the suction system with $\alpha = 0.77$ for all measurements in series A	48
Figure 18 Comparison between mean concentration measured with the OPCON (uncorrected for grain-size) and determined from the suction system with $\alpha = 0.77$ for all measurements in series A	49
Figure 19 Percentage of samples with correlation > 70% and SNR > 15 Db as a function of the distance from the bed as measured by the ADV.	51
Figure 20 Time-mean vertical velocity versus settling velocity	55
Figure A-21 Schematic drawings of suspension vessel	2
Figure A-22 Surface elevation spectra Series A	2
Figure A-23 Surface elevation spectra Series C	2
Figure A-24 Integral surface elevation data Series A	2
Figure A-25 Integral surface elevation data Series C	2
Figure A-26 Time-variation in m0 surface elevation spectra series A	2
Figure A-27 Mean concentration measured by OPCON without grain-size correction Series-A.....	2
Figure A-28 Standard deviation of OPCON signal without grain-size correction Series-A ..	2
Figure A-29 Standard deviation of low-passed filtered OPCON signal without grain-size correction Series-A	2
Figure A-30 Standard deviation of high-passed filtered OPCON signal without grain-size correction Series-A	2
Figure A-31 Concentration data at $z=0.01$ m without grain-size correction Series-A	2
Figure A-32 Concentration data at $z=0.03$ m without grain-size correction Series-C.....	2
Figure A-33 Horizontal velocity, correlation and SNR, and sediment concentration for A305 carriage 1 ($x=23$ m, $z=9$ cm).....	2
Figure A-34 Horizontal velocity, correlation and SNR, and sediment concentration for A305 carriage 2 ($x=30.5$ m, $z=0.5$ cm).....	2
Figure A-35 Quality of ADV signals in A-series: percentage good (%) and time-averaged correlation (%).....	2
Figure A-36 Mean horizontal velocity, Series-A	2
Figure A-37 Standard deviation of horizontal velocity signal, Series-A.....	2
Figure A-38 Mean vertical velocity, Series-A	2
Figure A-39 Standard deviation of vertical velocity signal, Series-A	2
Figure A-40 Velocity data, Series-A	2
Figure A-41 Horizontal velocity moments, Series-A	2
Figure A-42 Velocity data, Series-C	2

Figure A-43 Horizontal velocity moments, Series-C.....	2
Figure A-44 Sediment flux, Series-A	2
Figure A-45 Sediment flux, Series-C.....	2
Figure A-46 Total sediment flux, Series-A.....	2
Figure A-47 High frequency sediment flux, Series-A	2
Figure A-48 Low frequency sediment flux, Series-A.....	3
Figure A-49 Current related sediment flux, Series-A.....	3
Figure A-50 Time-mean load (upper plot), sediment transport (second plot) derived from profile deformation (line) and from flux profiles (diamond) and initial bed and bed after 30 hours (lower plot), Series-A	3
Figure E-51: The relation between concentration and Voltage. Dark squares represent the raw measurements, the open circles are the raw data when the background correction is done in V, the grey squares are the concentrations, after background correction in g/l. These data-points are used to fit the calibration curves.....	1
Figure E-52: Calibration curves for OpCon1 and OpCon2 with different zero level shiftings. The calibration curve with a zero level shifting of -7.97V (and a shift of - 2V at the OpCon), is based on the data points from the measurements with a -2V zero shifting. These data points are translated with -5.97V. The calibration curve with a zero level shifting of -7.97V (and a shift of -0V at the OpCon), is based on the data points from the measurements with a -0V zero shifting. These data points are translated with -7.97V.....	2

List of Tables

Table 1 Initial geometry, sediment composition and total duration of the various experiments	3
Table 2 The grain size properties (in μm) and activity concentrations (with external uncertainties) of ^{40}K , ^{238}U and ^{232}Th for Quartz and Zircon.	6
Table 3 Overview of the use of the different ADV's, OPC's, number of tubes of the transverse suction system that are used during the experiment, PROVO, MEDUSA, Wave height meters, settling tube and KVI in-house BGO detector	7
Table 4 Co-ordinates of the fixed and mobile wave height meters (WHM).....	7
Table 5 Locations of instruments on the carriages during series A and C.	9
Table 6 Grain size characteristics of some of the samples in Bosman (1984) and of the Scheldt flume	20
Table 7 A/D Conversion	30
Table 8 Overview of instrument names and channel numbers for data acquisition	31
Table 9 File names containing physical quantities	32
Table 10 Surface elevation (η) signal names in W*** files	32
Table 11 Velocity (u,v,w) signal names in A*** files	33
Table 12 Concentration (c) signal names in O*** files.....	33
Table 13 Parameters computed with programme WAVES using downwards as zero crossing type for total signals WHM0*	34
Table 14 Parameters computed with programme SPECTPER for total signals WHM0*	34
Table 15 Parameters computed with programme STATIST for total signals WHM0* with N number of samples	35
Table 16 Parameters computed with programme MOMENTS for signals ADV01, ADV03, ADV*01 and ADV*03	36
Table 17 Parameters computed with programme MOMCOMB for u-velocity signals stored in sections ADV30*.....	36
Table 18 Parameters in S***.PAR files computed with programme FLUX.....	37
Table 19 Outliers in set-up values in A-series	42
Table 20 Outliers in A-series: standard deviation, skewness and kurtosis of surface elevation.....	45
Table 21 Outliers in C-series: standard deviation, skewness and kurtosis of surface elevation.....	45
Table 22 Outliers in concentration measurements.....	47

Table 23 Outliers in comparison between suction and Opcon measurements.....	49
Table 24 Quality of ADV signals in C-series: Percentage good (%), averaged correlation (%) and SNR (dB).....	52
Table C-25 Positions of the measuring verticals	1
Table C-26 Positions of carriage 2 in the correlation measurements and distance of carriage 2 landwards of carriage 1.....	2
Table C-27 Positions of the carriages during each half-hour run of series A (in chronological order).....	3
Table C-28 Measured vertical positions, name of the series and carriage number for vertical 1	4
Table C-29: Measured vertical positions, name of the series and carriage number for vertical 2	5
Table C-30 Measured vertical positions, name of the series and carriage number for vertical 3	5
Table C-31 Measured vertical positions, name of the series and carriage number for vertical 4	5
Table C-32 Measured vertical positions, name of the series and carriage number for location near vertical 4	5
Table C-33 Measured vertical positions, name of the series and carriage number for vertical 5	6
Table C-34 Measured vertical positions, name of the series and carriage number for location near vertical 5	6
Table C-35 Measured vertical positions, name of the series and carriage number for vertical 6	6
Table C-36 Measured vertical positions, name of the series and carriage number for location near vertical 6	6
Table C-37 Measured vertical positions, name of the series and carriage number for vertical 7	7
Table C-38 Measured vertical positions, name of the series and carriage number for vertical 8	7
Table D-39 Overview of uncorrected and corrected set-up values; mean and standard deviation over several tests (series A)	1
Table D-40 zero level values WHM before test (series A).....	2
Table D-41 zero level values WHM after test (series A).....	3
Table D-42 Overview of uncorrected and corrected set-up values; mean and standard deviation over several tests (series C)	4
Table D-43 zero level values WHM before test (series C).....	4
Table D-44 zero level values WHM after test (series C).....	5

Table E-45: Overview of 0-shift combinations during the various experiments	2
Table E-46: Coefficients of the polynomials fitted through the calibration measurements with different zero shifting according to the function $(c)=A_0+A_1V+A_2V^2+A_3V^3+A_4V^4$ (where (c) is the sediment concentration (g/l) and V the measured voltage) the internal uncertainties of the fitted parameters are within brackets. The χ^2_{red} shows the quality of the fit.	3
Table E-47: Sediment concentrations calculated with the polynomial fits when the output voltage does not deviate from base level and their uncertainties.	3
Table E-48: Overview of the differences in the concentration due to the fitting with the wrong calibration curve. The uncertainty in the difference of OpCon1=1.1 g/l, the uncertainty in the difference of OpCon2 =0.8g/l.....	4

I Introduction

I.1 Background and aim of study

Within the framework of the EU-sponsored MAST-III SAFE project a programme of detailed measurements of hydrodynamics, sediment transport and radiometry has been carried out in WL|DELFT HYDRAULICS' Scheldt flume.

The objective of the study was twofold: 1) the generation of high quality and high resolution data on hydrodynamics and sediment transport dynamics on a natural 2DV beach under erosive conditions with special attention to near-bottom resolution; and 2) the generation of data of selective transport phenomena of minerals which differ in density.

During the project, WL|DELFT HYDRAULICS made available the Scheldt Flume and took care of expert assistance in running the facility and carrying out the experiments. The team from WL|DELFT HYDRAULICS was led by J. Bosboom (project manager) and consisted of P. Pasterkamp and A. ter Veen. R. de Vries provided assistance for the operation of the experiments. P. Pasterkamp took care of the AUKE-PC postprocessing.

The team from the University of Groningen (KVI) consisted of R.L. Koomans assisted by several other researchers during different parts of the experiments: P.W. Groen, R. ten Have, P.G.H.M. Hendricks, J. Limburg and L.B. Venema. Two students of Delft University of Technology, L. Barends and W. Kuiper, assisted in experiments. H. Demaie (Sogreah, France) assisted in the preparation of the final experiments.

The total duration of the project was four weeks (in August and September 1998), inclusive of the preparation of the Scheldt flume, the positioning and testing of the instruments. The actual experiments were carried out in 15 days.

I.2 Outline of report

This data report consists of two parts: part I: Time-averaged measurements (Koomans and Bosboom, 2000) and part II: Time-dependent measurements (this report). The first two chapters of both reports are identical and aim to give an overview of the experimental set-up and the type of data that were collected. In chapter 3, a more elaborate discussion on the measuring techniques and calibration procedures is given. In part I, time-averaged measuring techniques and their calibration are presented, while in part II the time-dependent techniques are discussed. Chapter 4 of part I and II focuses on data validation and provides a discussion on the uncertainties in the time-averaged and time-dependent measurements respectively. Where necessary, results are shown, but detailed descriptions and interpretations of experimental data will not be given in this data report.

1.3 Acknowledgements

This work is undertaken in the SAFE project, in the framework of the EU-sponsored Marine Science and Technology Programme (MAST-III), under contractno. MAS3-CT95-0004. It is cosponsored by the Dutch Ministry of Transport and Public Works (Rijkswaterstaat). This work is also part of the Nuclear Geophysics programme of the Kernfysisch Versneller Instituut, Rijksuniversiteit Groningen and the Netherlands Centre of Coastal Research.

2 Experimental set-up

2.1 Scheldt flume

The experiments were carried out in WL|DELFT HYDRAULICS' Scheldt flume, location the Voorst, see Appendix B. This facility has a length of 55 m, a width of 1.0 m and a total depth of 1.2 m. The facility consists of a concrete/iron bottom and glass walls. For the location of the instruments in the facility, we adopted the following co-ordinate system (see also Figure 1) :

- the x-direction was parallel to the channel axis, the positive x-direction was from the wave-board towards the "beach face", and $x=0$ was located at the mean position of the wave board.
- the y-direction was in the horizontal plane parallel to the channel bed and orthogonal to the x-direction, the positive y-direction was then to the right when looking from the wave board to the "beach face", and $y=0$ was located inside the channel at the glass window to the left. For practical reasons, the two sides of the flume were named as D and W-side. The D-side is located at $y=1\text{m}$, the W-side is located at $y=0\text{m}$.
- the z-direction was directed vertically upward with $z=0$ is located at the top of the concrete bed at the horizontal part of the flume. However, in this report z is used to define the distance of the instruments with respect to the ripple tops at a specific location along the flume.

2.2 Measurement programme and test procedures

Measurement programme

The measurement programme globally consisted of four series (see Table 1):

Table 1 Initial geometry, sediment composition and total duration of the various experiments

Series	Initial geometry	Sediment	Total wave duration (hrs:min)
A	plane, 1:40	Quartz	29:37
B	end profile series A	Quartz + Zircon placers	3:32
C	plane, 1:40	70% Quartz, 30% Zircon	14:33
D	end profile series C	70% Quartz, 30% Zircon	-

In series A special attention was paid to high-resolution measurements of hydrodynamics and sediment transport. In Series A the focus was on the collection of instantaneous velocity and concentration data at several locations along the beach profile and for varying distances from the sandy bed. The set-up of the measurement programme was so as to enable the identification of the spatial correlation (in both horizontal and vertical direction) of

concentration, the time-dependent near-bottom response of the concentration to water velocity and the contribution of the various velocity components to the sediment fluxes.

These experiments were carried out on an initially plane, 1 in 40, beach consisting of dune sand (see Figure 1). During the operation quantities were measured by a number of instruments attached to two movable carriages (see Section 2.5). Moreover, four wave-gauges at a fixed position throughout the experimental programme measured the water elevation. The instruments on the carriage measured at a fixed horizontal and vertical position for about half an hour and were then moved to other locations. The sediment profile was measured at several time periods between runs.

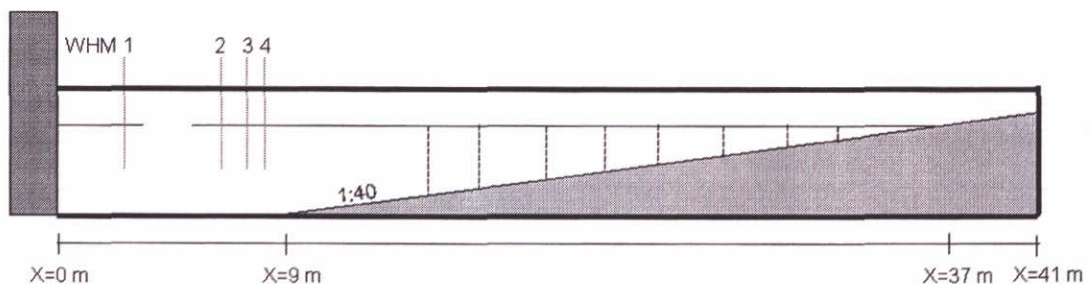


Figure 1 Schematic set-up of the experiment with x-axis, locations of wave height meters (WHM) and positions of measuring verticals (vertical dashed lines) in which the measurement carriages were deployed. The grey box on the left-hand side of the figure shows the location of the wave generator with $x=0$ corresponding to the mean position of the wave board.

Series B focused on the selective transport of placers of Zircon. Thin layers of Zircon were placed at several x -positions on the single-barred final profile of series A. In these experiments only the sediment profile and composition was measured.

The C-series aimed at measurements of selective transport processes. The series started again from a 1 in 40 beach, in which the upper 10 cm of the bed consisted of a mixture of 60% sand and 40% Zircon by mass. During runs hydrodynamic parameters and sediment concentrations were recorded; in between the runs, profile and sediment composition were measured.

The objective of the D-series was to test a new device to record “friction” sound. These experiments were carried out with still water on the end profile of Series C.

The test conditions (see Section 2.3) and beach geometry were chosen according to test 1 of Roelvink and Stive (1989).

In Appendix C, an overview is given of the measurements carried out, the measuring positions per wave half-hour and the corresponding code names. The instrumentation used in the respective series is described Section 2.5.

Test procedures

Series A were subdivided in a number of "wave half-hours". During each wave half-hour, a time series of exactly 35 minutes (the steering signal + 4.5 minutes) was generated, starting at the same position in the steering signal. To be able to compare the time dependent measurements, the post-processing of these data will be done on the final part of the time-series with the length of the steering signal. The time-averaged suction system was operated during the last part of the time series corresponding to the length of the steering signal. In series C, besides half-hour runs also hour runs were carried out in which during 65 minutes waves were generated. For these measurements, the analysed time-series will be twice the length of the steering signal. Also suction system was operated during a period twice the steering signal. All instruments with time-dependent measurements were sampled simultaneously at 50 Hz. To avoid aliasing, a low-pass 25Hz analogue filter filtered each signal before storage.

At specific time intervals (mostly the end of the day) profile measurements were conducted by an automatic sounding system. As a standard procedure, measurements were made along two parallel trajectories, each running 33 cm from one of the side-walls of the flume. The profile data were stored at 0.04 m intervals and were stored on a separate PC. In addition, in some of the cases also the profile in the middle of the flume was measured. For selected profiles in the A-series and for all profiles in the C-series, the MEDUSA detector was attached to the carriage carrying the profiler. The MEDUSA logging PC was connected to the profile logging PC with an RS232 coupling for position information.

2.3 Steering and wave conditions

Random waves were generated by a wave board equipped with an active wave absorption system (Klopman, 1995), such that at the same time waves were generated and reflected waves were absorbed. The latter prevented the re-reflection of free, long waves travelling offshore towards the wave board. The reflection compensation was operated such that waves with periods up to 60 seconds are completely absorbed by the wave board. Note that according to Dean and Dalrymple (1984) in the present set-up, a period of natural oscillation of $1.642L/\sqrt{gh} = 50s$ is expected, with $L = 41m$ being the length from wave board to the maximum water line and $h = 0.7m$ being the maximum water depth.

The wave generation was according to a second-order Stokes wave theory. This second-order wave board control includes corrections for the suppression of spurious free subharmonic and superharmonic components. The random wave fields generated were of the Jonswap type with a peak enhancement factor of approximately 3.3 representing a young sea state as expected under normal sea conditions. An improved method for wave generation (Klopman, 1998) was used which is closer to the theoretical second-order spectrum with respect to the energy content for frequencies larger than the peak frequency. The incident wave conditions at deep water (water depth $h = 0.7 m$) and geometry are $H_{m0} = 0.17 m$ and a peak period $T_p = 2 s$. The wave-board control signal repeated itself every 1820.44 seconds.

2.4 Sediment

The sediment properties of the Quartz and Zircon used in series A-C are summarised in Table 2 and Figure 2. The grain size distribution in Figure 2 shows that the Zircon is somewhat smaller than the Quartz (14 μm for the D_{50}) but that the distribution is similar. The activity concentrations for ^{238}U and ^{232}Th in Table 2 clearly show the enhanced activity concentrations for the Zircon. The activity concentration of ^{40}K is smaller than the external uncertainty due to the high concentrations of ^{238}U and ^{232}Th . The results of the sample analysis imply that with the radiometric fingerprinting method as described in Venema *et al* (1999), the Zircon concentration in the sediment can be determined with an absolute accuracy of $\sim 5\%$.

Table 2 The grain size properties (in μm) and activity concentrations (with external uncertainties) of ^{40}K , ^{238}U and ^{232}Th for Quartz and Zircon.

Sediment	D_{10} (μm)	D_{50} (μm)	D_{90} (μm)	^{40}K (Bq/kg)	^{238}U (Bq/kg)	^{232}Th (Bq/kg)
Quartz	93	129	187	6.8 (0.9)	5.6 (0.3)	4.82 (0.15)
Zircon	83	115	153	<580	12400 (400)	2300 (100)

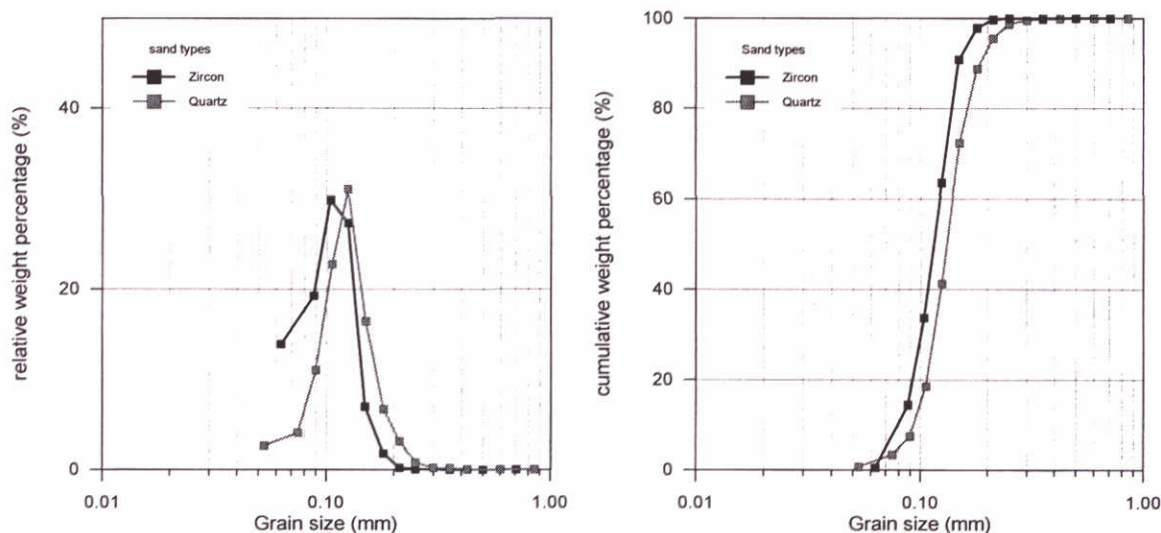


Figure 2 Grain-size distribution for Quartz and Zircon

2.5 Instrumentation

2.5.1 General

Within the experiments, the instrumentation was adjusted to the specific queries of each series. In this section the instrumentation is described. A more detailed description of the time-averaged and time-dependent instruments and their calibration can be found in chapters 3 of data report part I (Koomans and Bosboom, 2000) and part II (this report), respectively.

Table 3 gives a general overview of the instruments that were sampled in each series. The OpCon and ADV on carriage 1 and carriage 2 are named OPC01 and ADV01 and OPC02 and ADV02 respectively.

Series	ADV 01	ADV 02	OPC 01	OPC 02	# tubes	Provo	MEDUSA	WHM	Settling tube	BGO detector
A	*	*	*	*	4	*	*	6	*	
B						*	*			
C		*		*	8	*	*	5		*
D						*	*			

Table 3 Overview of the use of the different ADV's, OPC's, number of tubes of the transverse suction system that are used during the experiment, PROVO, MEDUSA, Wave height meters, settling tube and KVI in-house BGO detector

2.5.2 Measurements during runs

During the runs the following instruments were deployed for time-averaged and time-dependent measurements:

- Transverse suction system;
- Wave height meters (WHM);
- Optical concentration meter (OPC);
- Acoustic Doppler Velocity meter (ADV) and
- video and photo camera.

Photographs and video recordings were made of ripple structures, ripple movement and experimental set up. Some of the photo's are used as illustration.

The free surface elevation, with respect to still water level was recorded continuously with wave height meters (WHM). Four resistance-type twin-wire WHM's were placed in the model at the following locations (Table 4):

Table 4 Co-ordinates of the fixed and mobile wave height meters (WHM).

Code	x (m)	y (m)
WHM01	2.8	0.5
WHM02	6.56	0.5
WHM03	7.97	0.5
WHM04	8.44	0.5
WHM05	Carriage I	0.18
WHM06	Carriage II	0.21

The locations were chosen such that in principle the incoming bound, incoming free, the reflected free and reflected bound components may be separated. Besides the four wave gauges at a fixed position, two wave gauges were located on the measurement carriages.

Measurement carriages

Most of the instruments that were operated during the runs were situated on a measurement carriage. Since the general objectives of the A and C series differed, special assemblies were used for each experiment.

During series A two measurement carriages (number 1 and 2) were used each equipped with:

- Transverse suction system (2 separate suction tubes at equal height but different y-location at each carriage)
- Acoustic Doppler Velocity meter (ADV)
- Optical Concentration Meter (Opcon)
- one resistance type wave gauge

During series C one measurement carriage (number 2) was used equipped with:

- Transverse suction system (8 suction tubes distributed in vertical direction)
- Acoustic Doppler Velocity meter (ADV)
- Optical Concentration Meter (Opcon)
- one resistance type wave gauge

The instruments that were placed on the both measurement carriages (Figure 3) during the A-series were similar except for the ADV's. For the carriages two different ADV's were employed. ADV01 refers to the ADV placed on carriage 1 and has a sampling volume located 0.10 m below the probe tip, whereas for ADV02 (located on carriage 2) the sampling volume is located 0.05 m below the probe tip. The smaller distance between sampling volume and probe tip for ADV02 means that the second carriage can be deployed up to lower water depths than carriage 1, consequently carriage 1 is located offshore of carriage 2 in case of simultaneous deployment (series A only).

In the C-series, only carriage 2 is used.

The carriages were placed on wheels and can be moved along the x-axis of the flume. Moreover, the OpCon, ADV and suction tubes on the carriages are moved jointly in vertical direction to allow measurements at various locations above the bed. The wave height meters (WHM's) on the carriages are not connected to the other instruments and are kept to a fixed position with respect to the water level.

To determine the vertical positions of the instruments with respect to the sediment bed, the carriages were equipped with a 'depth-reference rod', a metal rod with on the lower end a PVC 'foot' which can be rotated in the x-z plane (2nd left instrument in Figure 3). In this way it can be placed on the sloping sand bed over the rippled structures. Before each new run, this 'depth-reference rod' was placed on the sediment and with a marker on the metal rod, the instruments could be placed at 10cm above the sediment. By the use of a measuring rod attached to the carriages the relative position of the instruments with respect to the sediment could be adjusted. The uncertainty in the position of the instruments with respect to the bed (due to cross-flume morphologic variations and uncertainties the deployment the

metal rod) is estimated as 0,5cm. These measurements were repeated after the experiments to determine bed-level variations.

The y-locations of the various instruments on the measurement carriages with respect to the glass wall on the w-side of the flume are given in Table 5 (see also Figure 3 which is a photograph of carriage 1 during series A).

Table 5 Locations of instruments on the carriages during series A and C.

y-locations (cm from w-side) of various instruments	Series A Carriage 1	Series A Carriage 2	Series C Carriage 2
WHM	18.2	21.1	21.1
Suction tube w-side	32.3	31.2	
OPC	49.2	47.8	47.8
'Peilvoetje'	62.5	59.5	59.5
ADV	75.5	73.0	73.0
Suction system			31.2
Suction tube d-side	93.5 ¹	92.8 ²	

¹ 87.5 cm during series A1* and A2*

² 87.2 cm during series A1* and A2*

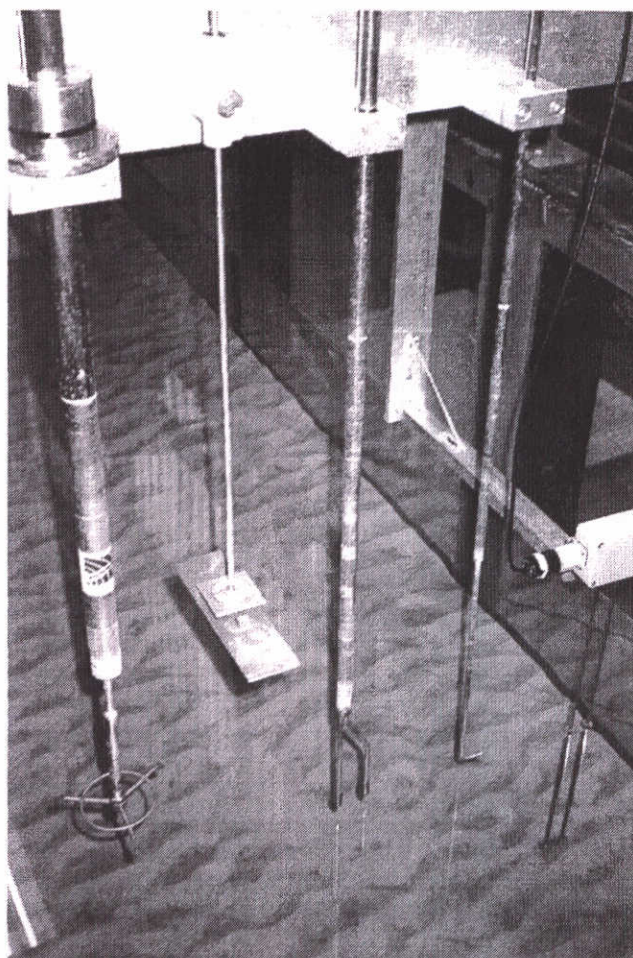


Figure 3 Measurement carriage 1 during the A-series, looking into the direction of the wave board. From left to right equipped with: suction tube d-side (not visible), ADV, depth-reference rod, OPCON, suction tube w-side and WHM.

Appendix C gives an overview of the x- and z-locations of the two carriages.

2.5.3 Measurements between runs

Between the runs, profile measurements (with the PROVO system) and measurements of sediment composition (with the MEDUSA system) were conducted. The PROVO is an automatic sounding system to measure bed height whilst the MEDUSA-system measures γ -ray spectra from the sediment and friction sound generated in the movement of the detector over the sediment. An elaborate description of both instruments can be found in chapter 3 of data report part I (Koomans and Bosboom, 2000) and in Koomans et al. (1999). An overview of the profile measurements can be found in Appendix C.

2.5.4 Sample analysis

Suspended sediment, collected in the suction system during the A series, was analysed on grain size with a settling tube located at “de Voorst”. The collected sediments from the suction system in the C series and samples that were taken from the bed at the end of series

C were analysed radiometrically on the Zircon concentration on a BGO detector located at KVI. The sample locations are listed in Appendix C.

3 Instrumentation and calibration

3.1 General

This chapter describes the measuring techniques and calibration procedures for the time-dependent measurements. Subsequently, the wave height meters, the optical concentration meters and the acoustic Doppler velocity meters are discussed. For the time-averaged measuring techniques (profile follower, medusa, transverse suction system, settling tube and BGO detector) one is referred to part I (Koomans and Bosboom, 2000) of this data report

3.2 Wave height meters (WHM)

The free surface elevation, with respect to still water level was recorded with resistance-type twin-wire wave height meters (WHM's). The output signal range, from -10 to 10 V, corresponds to a water elevation measuring range from -0.25 m to 0.25 m. The wave height meters were at least recalibrated every week.

3.3 Optical concentration meter (OPC)

3.3.1 Instrument description

Principle of operation

An optical concentration meter (OpCon) was used to measure time-dependent suspended-sediment concentrations. The principle of the OPCON is based on the extinction of infrared light by sediment particles, which have diameters much larger than the light wave length. The extinction of the light beam between a transmitter and receiver, that are placed in the flow, is a measure for the concentration of sediment particles.

Figure 4 shows a schematic diagram of the OpCon probe consisting of a stem with on one side the transmitter and on the other side the receiver. The distance between the optical transmitter and the receiver is 30 mm. The thickness of the transmitted light beam (sensing volume) is 2.6 mm. Note that two identical OpCons were used. These OpCons are named OPC01 and OPC02 for measurement carriage 1 and 2 respectively.

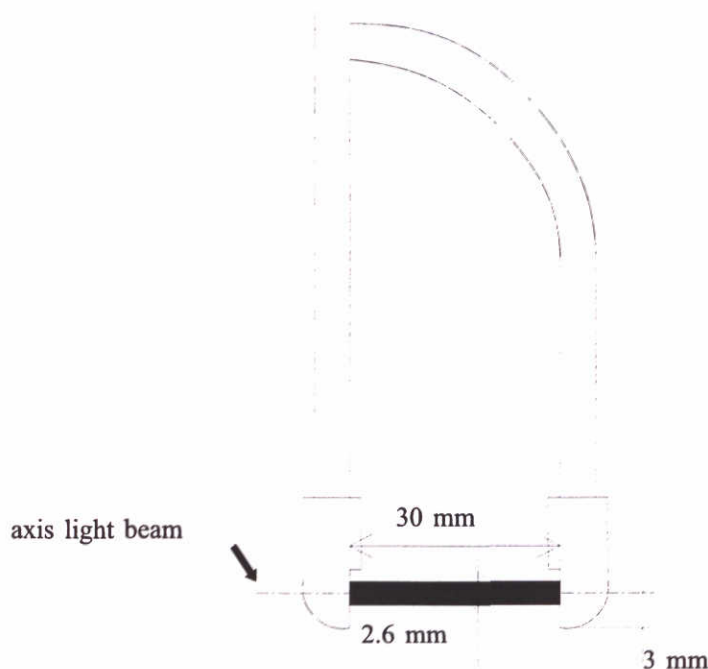


Figure 4 Schematic diagram of OPCON probe with the two stems and the transmitted light beam

Neglecting possible mutual shielding of particles, the light extinction per particle is proportional to the particle cross-section. Thus the extinction of a light beam containing N identical spherical particles with diameter D is proportional to ND^2 . As the concentration C is proportional to volume, i.e. proportional to ND^3 , the light extinction is proportional to C/D . As a consequence any light extinction device must be calibrated for the relation between the output signal and the concentration for each investigated grain size. The calibration procedure may be simplified when a theoretical relationship between the output signal V and C/D is available.

Theoretical approach for small volume concentrations

The OpCon design is based on the statistical theory for the description of light extinction as presented by Bosman (1981, 1984). In order to describe the probability that a certain number of particles is found in a sensing volume, Bosman assumes that the particles are Poisson distributed in space. This assumption means amongst others that the validity of the theory is restricted to suspensions in which the particles are not too close. The latter means in practice that the distance r between the particles must be large compared to the effective particle diameter D^* . Since the volume concentration is of the order $(D^*/r)^3$ this means that the validity of the theory is expected to be limited to volume concentration up to about 1%.

Bosman's derivation accounts for the fact that the relationship between light extinction and concentration is not uniquely defined, but depends on the accidental positioning of the particles in the measuring volume. By taking the stochastic nature into account, he includes the possible occurrence of mutual shielding of the particles. The relation between

the *expected (averaged) value* of the light intensity and *expected concentration* was found to obey the classic (deterministic) Beer's law.

The extinction of light due to the presence of particles in a light beam reads according to Beer's law:

$$I = I_0 e^{-al} \quad (3.1)$$

Here I is the light intensity at a distance l from the light source and I_0 is the intensity at the position of the light source. Further $a = a_0 C$ is the light extinction coefficient of the suspended matter per unit length, with the constant a_0 defined exclusively by the particle characteristics (shape, size and density) and C the concentration by mass.

The OpCon design is based on Beer's law for the expected quantities. The transmitted light is converted proportionally to a transmission signal V . The expected value of the transmission signal then reads:

$$E\{V\} = E\{V_0\} e^{-(\beta + \beta_1)} \quad (3.2)$$

where β is the dimensionless light extinction coefficient defined by $\beta = \gamma C_v$ where C_v is the concentration by volume of the suspended material. The parameter γ is the (dimensionless) calibration constant depending only on the transmission length l of the specific OPCON and the particle size distribution through the effective particle diameter D^* :

$$\gamma = \frac{3}{2} \frac{l}{D^*} \quad (3.3)$$

Further, the instrumental constant V_0 is the transmission signal without particles blocking the light and β_1 is the light extinction coefficient due to turbidity, which is regarded as background. The next section deals with the effect of turbidity in more detail. Note that γ is constant within the validity range of the Bosman's theoretical approach.

From (3.2) it can be seen that a logarithmic relationship exists between the concentration and the averaged transmission signal. The OPCON design is based on this finding by application of a logarithmic amplifier which linearises the relation between concentration and transmission signal. The amplifier performs a logarithmic operation on the transmission signal V to obtain the output voltage signal $W = \ln(V)$.

Within the validity range of the theory, the volume concentration of suspended sediment is thus linearly dependent on the linearised output voltage signal W through:

$$C_v = \frac{1}{\gamma} \frac{E\{W\}}{E\{a_c\}} - \frac{1}{\gamma} \beta_1 \quad (3.4)$$

where a_c is an electronic conversion value of the log/divider amplifier.

Effect of turbidity

The contribution from fines contained in the sand (turbidity) to the extinction of light is relatively large and variable, such that we need to correct for the turbidity for each separate measurement. The turbidity coefficient β_1 during the experiment is unknown and needs to be estimated. In the present experiments and in the calibration measurements, it was decided to estimate β_1 from the turbidity in the water, measured after the experiments (see Section 3.3.2).

3.3.2 OpCon calibration

Suspension vessel

The calibration curves were constructed according to the OpCon technical manual based on the findings of Bosman. A known amount of sediment was stirred in a cylindrical beaker (see Figure A-21) containing a known volume of water (1.8 dm^3). The glass beaker with a magnet stirrer at the bottom was designed to create homogeneous suspensions. The region near the bottom is not accessible for measurements, as the stirrer might damage the probe. In the near-bottom region and the near-surface region, where a relatively large variation in the concentration occurs, the concentration is not well known. Bosman concluded that this results in errors in the concentration of 10% at most. The measurements were carried out with each OpCon connected to the electronics that were used in the experiments. For each concentration of sediment, 18 measurements were conducted at 3 locations in the horizontal plane and 6 locations in the vertical plane covering the total height of the vessel except for the near-bottom and near-surface region. The standard deviation in these measurements ranged from 2% to 5% for voltages up to 10 V. The used concentrations were 2.6 g/l and 10 g/l to 130 g/l with intervals of 10 g/l.

Calibration curves

In previous experiments and in the design of the OpCons, it was assumed that the output signal of the OpCon is linearly dependent on sediment volume concentrations in the range 0.005-2.0 % (= 0.1-50 g/l). The linear calibration for the OpCon Eq (3.4) can be written as:

$$c_{opc}(\text{g/l}) = K_1 W_v(V) \quad (3.5)$$

where c_{opc} is the sediment concentration in g/l, W_v the output signal of the OpCon in V (from which the turbidity effect is subtracted) and K_1 the calibration factor :

$$K_1 = \frac{\rho_s}{a_c a_g \gamma} \quad (3.6)$$

where ρ_s is the sediment density, a_c an electronic conversion factor for the log-amplifier which is fixed electronically by a log/divider amplifier, the amplification factor $a_g = 1$ and γ is a grain-size dependent calibration factor for the OpCon probe (see above).

However, in the present experiments, the maximum concentrations were significantly higher than 1%. Therefore, calibration curves for the quartz sediment used in the flume ($d_{50}=129\text{ }\mu\text{m}$) were constructed for both OpCons (Figure 5) in the measured voltage range. Appendix E gives more information on the construction of the calibration curves.

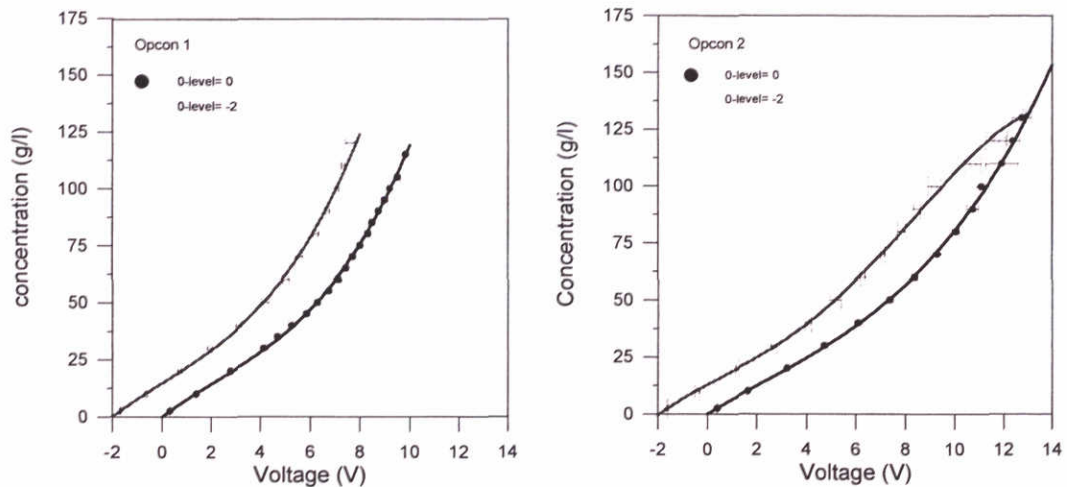


Figure 5 Calibration curves for OpCon1 and OpCon 2 with different zero level shiftings for quartz sand of $d_{50}=129\text{ }\mu\text{m}$

In the beginning of the experiments, the zero shift of the OpCon was set to zero. During the experiments, it became apparent that the measured voltages exceeded 10V (which was designed as the maximum voltage for the detector). Since the amplifier was already at its minimum, the zero shift was set to -2V to gain extra space for measuring. In principle this should not change the calibration curve, although the sensitivity to temperature variations and therefore the relative random error in the electronic conversion factor a_c slightly increases. In order to check the effect of this zero shifting on the calibration curve, two calibration curves per instrument were constructed, one curve without a zero shift and one curve with a zero shift of -2V (see Appendix E).

Figure 5 shows that the calibration curves is linear up to 30 g/l ($C_v \approx 1\%$), but that for larger concentrations the assumption of linearity no longer holds. Therefore three second-order polynomials and one third-order polynomial were fitted through the data points in order to describe the relation between output signal and suspended sediment concentrations. The chi-square of the different fits was used to decide which order of polynomial was appropriate. Appendix E shows the calibration coefficients for OpCon 1 and OpCon 2 with different 0-level shiftings and describes which coefficients should be used for which series. In the analysis of OpCon signals A701-C404, the translated calibration curve of -2V is used instead of the translated calibration curve of 0V . Appendix E estimates the inaccuracy introduced by this. Further, in A301-A303 for the A3 parameter is wrongly used 0.103 instead of 0.0103. At the moment of writing of this report this has not been corrected yet.

Note that since the output signal of the OpCon is inversely proportional to the signal of transmitted light, for higher output voltages the input signal is weaker. At an output signal of approximately 10 V, the input signal is reduced to ~ 1 mV which can be regarded as noise. The maximum voltage range in which accurate concentration measurements can be made is therefore 10 V. Although due to the zero-level shift the voltage range could be larger than 10 V, the measurements with peaks exceeding this range should be considered with care.

Effects of grain size on calibration

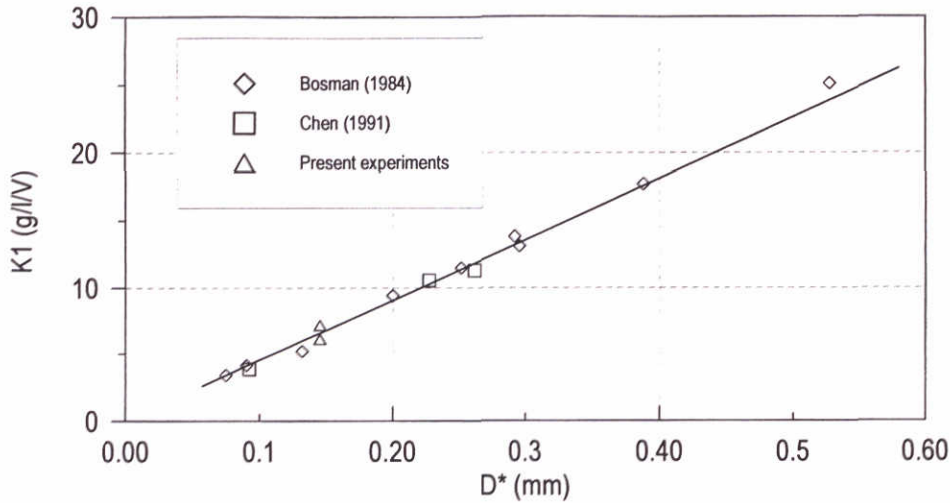
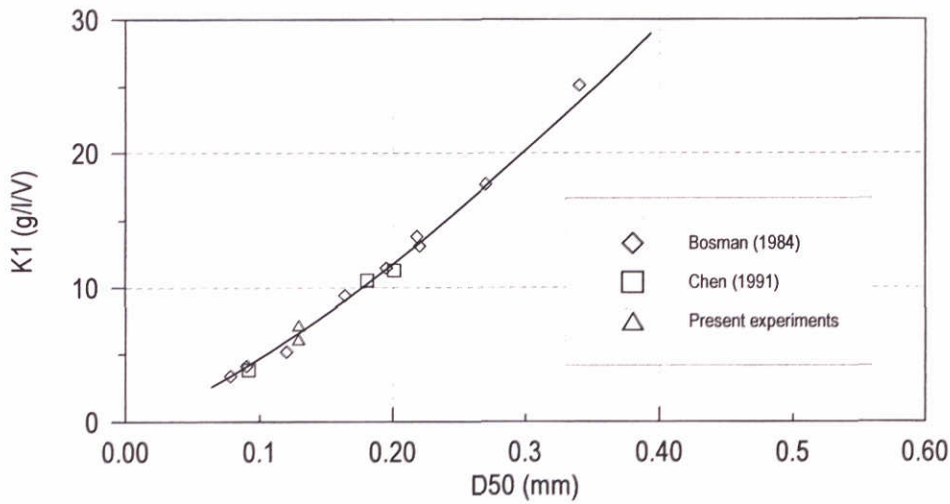
The calibration of the OpCon depends strongly on grain-size. The calibration curves determined for the D_{50} of the bed material need to be adjusted taking into account the measured grain size variations over the vertical from the sediments collected with the suction system. These measurements show that grain size ranges from $66 \mu\text{m}$ to $120 \mu\text{m}$ in the present experiments (see part I, Koomans and Bosboom, 2000).

Bosman (1984) has shown theoretically that the γ - value is inversely proportional to an effective diameter D^* (see Equation (3.3)). In addition, Bosman (1984) analysed sediment samples with median diameters ranging from 0.078 mm up to 0.34 mm and determined for each sample a representative constant γ - value disregarding the non-linear behaviour for larger volume concentrations (see Section 3.3.3). Based on these measurements the effective grain diameter in the theoretical expression for γ (Equation (3.3)) was found to be:

$$D^* = \left(\frac{D_{50}}{9 \cdot 10^{-5}} \right)^{0.33} D_{50} \quad (3.7)$$

with D_{50} in meters.

Chen (1991, see Katopodi et al., 1994) calibrated the same OPCON probe as used for Bosman's experiments for two sand types in the linear low voltage range. Figure 7 shows the corresponding K_I values (in $\text{g l}^{-1} \text{ Volt}^{-1}$) with $a_g = 1$ (Equation (3.6)) for Bosman's and Chen's experiments as a function of the median diameter together with the theoretical relationship (3.3) for small volume concentrations using the fit (3.7). Although different OPCONS were used in the Scheldt flume experiments, the K_I values for the low-voltage part of the present calibration curves are also given. Figure 6 confirms the proportionality of K_I with D^* or equivalently of γ with $1/D^*$ (see Equation (3.3)), at least at low-voltages. For the suspended sediment grain size range from $66 \mu\text{m}$ to $120 \mu\text{m}$ in the present experiments $D^* \approx D_{50}$. For simplicity we therefore use that the calibration coefficient K_I is (approximately) linearly dependent on D_{50} (see also Figure 7).

Figure 6 Calibration constant K1 OpCon, D^* influenceFigure 7 Calibration constant K1 OpCon, D_{50} influence

It is unclear at the moment whether this dependency still holds in the high concentration range where the concentration is no longer linearly dependent on the output voltage. For now we assume that also for higher output voltages, the output voltage is determined by $C_v/D^* \approx C_v/D_{50}$, the ratio of concentration over grain diameter.

The non-linear calibration coefficients $A_{1..4}$ of the polynomial fit through the calibration curves (Figure 5 and Appendix E) are based on the median grain size of the well-mixed sediment in the calibration vessel. Since due to sorting effects the grain size of the suspended sediment in the experiments was smaller, these parameters need to be adjusted for grain-size. Based on the linear relationship between K_1 and D_{50} for the grain-sizes considered, we suggest that the fit parameters $A_{1..4}$ be corrected linearly according to:

$$A_{1..4, \text{cor_diam}} = \frac{D_{50, \text{suc}}}{D_{50, \text{cal}}} A_{1..4} \quad (3.8)$$

Here $D_{50,cal}$ is the grain size of the well-mixed sediment in the calibration vessel (Table 2), and $D_{50,suc}$ is the grain size of the suspended sediment samples from the suction system. The AUKE-PC data files contain the calibration factors $A_{1..4}$ without a grain-size correction. The grain-sizes per test, computed from the measured fall velocities of the suction samples, are given in part I (Koomans and Bosboom, 2000).

Therefore, the actual calibration coefficients for each OpCon measurement depend on the zero shift and on the grain size measurements from the suction system. In part I, the grain-sizes for all tests are listed, from which the correction factor is easily computed. The actual fit parameters for all tests without correction for grain-size are given in Table E-46.

Turbidity during experiments

Upon visual inspection it appeared that the turbidity increases rapidly after the start of the experiments, because the fines contained in the sandy material are stirred up immediately after initiation of motion. Therefore, the turbidity measured shortly after the experiments, when only the sand has settled, is estimated to be representative for the turbidity during the experiments. It was decided to use the OpCon value measured 6 minutes after the test (in still water and after the sand has settled) as a zero-level correction value.

Effect of density

Equation (3.6) shows that the calibration coefficient K_i also depends on sediment density. For the C-series experiments, a mixture of Quartz and Zircon is used and effects of sediment density should be accounted for. Measurements of sediment composition of the samples from the suction system showed that at 3 cm above the bed, where all measurements in series C were made, Zircon can be present up to 20% by mass. Since the major component of the suspended sediments is Quartz, we use the calibration curves for quartz and account for changes in bulk density of the suspended sediment through:

$$A_{1..4_cor_diam_dens} = \frac{D_{50,suc}}{D_{50,cal}} \frac{\rho_{suc}}{\rho_{cal}} A_{1..4} \quad (3.9)$$

where ρ_{suc} is the density of the suspended material and ρ_{cal} is the specific density of the material from the calibration. $A_{1..4}$ are the calibration coefficients from the polynomial fit. This correction has not been included in the AUKE-PC data files in which the coefficients $A_{1..4}$ are used.

3.3.3 Discussion of non-linearity in calibration

The non-linear relationship between sediment concentration and voltage may be surprising since the OpCons were designed to have a linear relationship. However, some of the calibration tests performed by Bosman show similar non-linearity for higher concentrations. Bosman (1984) analysed 9 sediment samples (S1 through S9), with median diameters ranging from 0.078 mm up to 0.34 mm (Table 6). Sample S3, although better-sorted, is best comparable to the sand in the present calibration measurements. In the suspended sediments in the flume experiments the median diameter is 0.1 mm on the average with minimum values of

0.053 mm and maximum values up to 0.12 mm. For that reason also the samples S1 and S2 of Bosman are considered here. The remaining 6 samples from Bosman's investigation have larger grain-sizes.

Table 6 Grain size characteristics of some of the samples in Bosman (1984) and of the Scheldt flume

Sample	Specification	D_{10} (mm)	D_{50} (mm)	D_{90} (mm)	D_{90}/D_{10}
S1	sorted	0.064	0.078	0.083	1.30
S2	sorted	0.076	0.090	0.110	1.45
S3	sorted	0.102	0.120	0.134	1.31
S4	sorted	0.150	0.164	0.180	1.20
Scheldt flume	unsorted	0.093	0.129	0.187	2.01

Bosman found that for the larger concentrations the measured γ -value drops fast with increasing concentration for the samples S1, S2 and S3. For S1 and S2 the drops starts near $C_v \approx 0.5\%$ and for S3 near $C_v \approx 1\%$ (see Figure 8 for S3 and the upper panel of Figure 9 for S2). In Figure 8 the results obtained from the linearised transmission signal W as well as from the transmission signal V are shown.

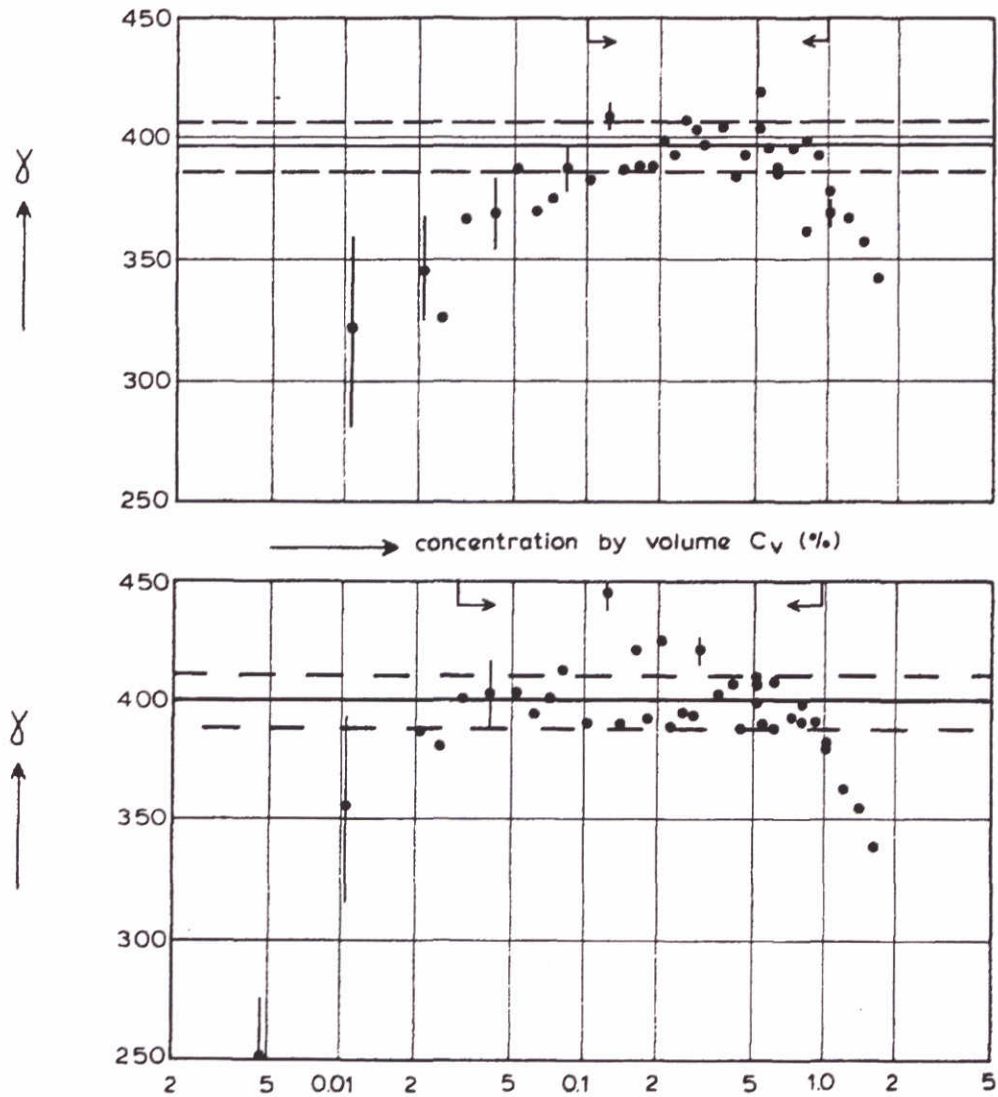


Figure 8 Calibration factor γ for sand S3. Upper panel: from transmission signal V. Lower panel: from linearised transmission signal W. From Bosman (1984)

For the coarser samples such a fast drop is not observed, which does not exclude its occurrence above the largest measured concentration (see the lower panel of Figure 9 for sand S4). A possible fast drop for γ for the coarser material should be above $C_v \approx 3\%$ (largest measured concentration for the coarser samples). Also for small concentrations ($C_v \leq 0.1\%$) γ is not a constant for samples S1 through S3. The latter is the result of errors in the estimation of the turbidity. Since the relative turbidity contribution decreases with sediment concentration it is only relevant for the smaller concentrations. For this reason the lowest concentration used in the calibration curves for the Scheldt flume experiments is performed for $C_v \approx 0.1\%$.

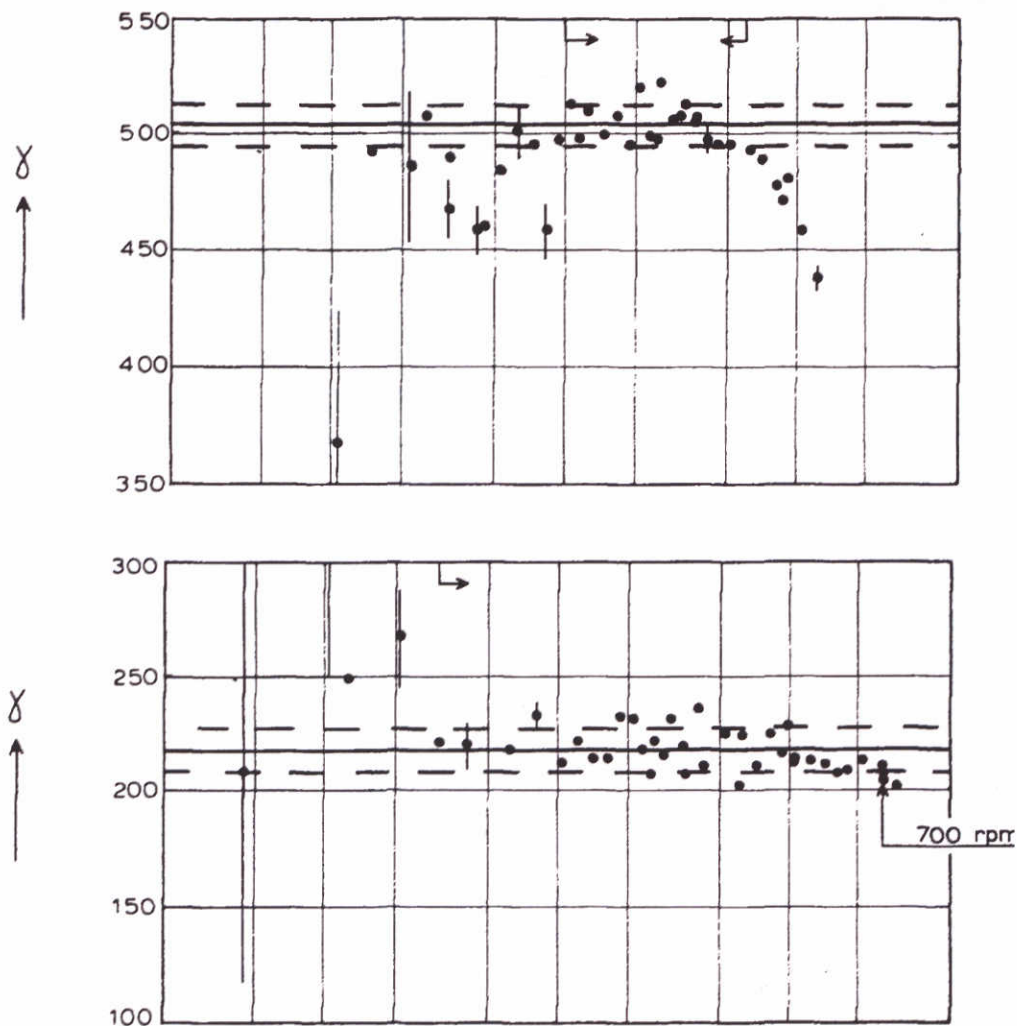


Figure 9 Calibration factor γ obtained from linearised transmission signal W. Upper panel: sand S2. Lower panel: sand S4. From Bosman (1984)

Figure 10 shows the calibration measurements for both OpCons used in the Scheldt flume presented similar to Figure 8 and Figure 9. Note that the figure corresponds to Figure 5 for the situation without zero-level shift. For simplicity, the electronic conversion factor a_c is assumed to be 1.303 for both OpCons in order to compute γ .

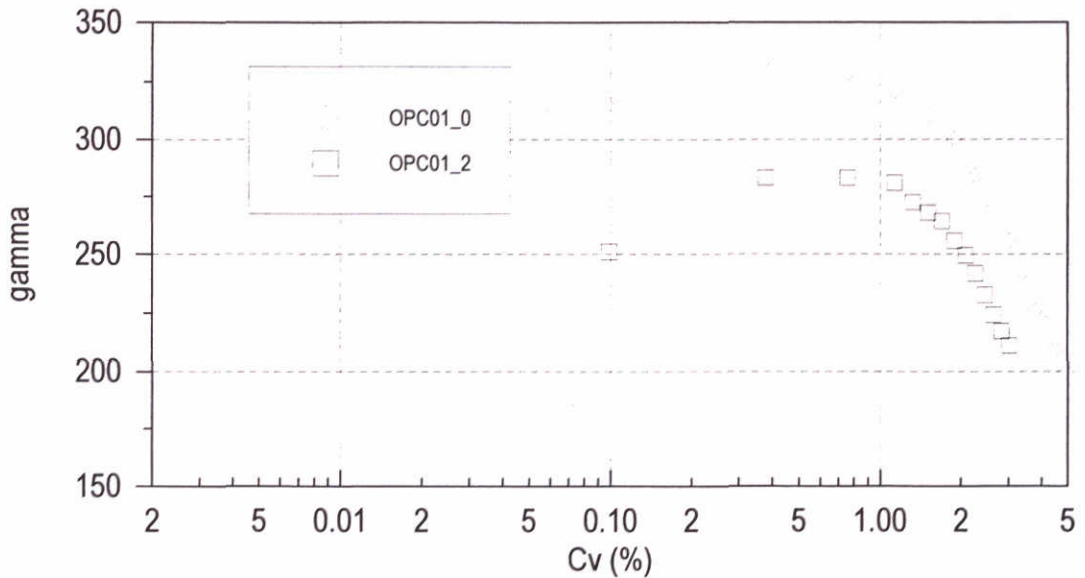


Figure 10 Calibration factor γ for Scheldt flume calibration measurements from linearised transmission signal W for both OpCons (without zero level shift).

The observed difference between the calibration factors for OPC01 and OPC02 shows the dependency of γ on the specific OPCON (transmission length) and the instrumental constant a_c (an electronic conversion value of the log/divider amplifier). The trend however is identical and analogous to the results of Bosman. From the present calibration, it is seen that the γ -value systematically decreases for increasing volume concentration, also for concentrations higher than $C_v = 1.5\%$, the highest concentration in the Bosman experiments. In the present experiment, the drop of the γ -value for low concentrations is observed as well.

It is important to identify the source of the non-linearity in order to ascertain the validity of the non-linear calibration curve. Possible explanations of the deviation from the theoretical linear relationship between concentration and output voltage (see also Bosman (1984)) are:

- For volume concentrations above 1% the assumptions underlying the derivation by Bosman and therefore the derived linear relationship may no longer be valid. This concerns the assumption of the Poisson distribution
- For large light extinction coefficients, say $\beta + \beta_1 > 1$ ($C_v \sim 0.3\%$), electronics non-linearity may become significant
- For the linearised transmission signal W, the log-nonconformity of the log/divider-amplifier may be significant for $\beta + \beta_1 > 5$ ($C_v \sim 1.5\%$)
- For large volume concentrations the concentration in the unmeasured regions of the calibration vessel may be significantly higher than in the measured region as a result of insufficient mixing for higher concentrations; related to the latter is the effect of the stirrer velocity of the magnetic stirrer on the concentration distribution.

Electronics non-linearity may occur when the assumption that light transmittance is converted proportionally to an output voltage is violated. As light transmittance decays exponentially with concentration, the transmission may vary over a few decades and the assumed

proportionally may be violated over such a range. Bosman argues from investigation of the qualitative effects of electronics non-linearity that due to electronics non-linearity (only) the observed non-linear behaviour cannot be explained.

The linearised transmission signal W is the output signal of a log/divider-amplifier. Non-linearity may be introduced if the log-amplifier does not perform an ideal logarithmic operation. Tests on the log-conformity of the log/divider-amplifier showed no significant deviations from a perfect logarithmic operation in the range up to 10V. Besides, Figure 9 indicates that the γ -values for sand S3 obtained from the linearised transmission signal W and directly from the transmission signal V give similar results. The log-conformity of the log/divider-amplifier is therefore out of the question as a source of non-linearity.

The velocity of the magnetic stirrer during the Scheldt flume calibration measurements was 550 rpm. Bosman carried out tests for the coarser samples with larger stirring velocity (700 rpm instead of 550 rpm) and concluded that the concentration distribution is not affected by the stirrer velocity (see Figure 9 for sand S4). For the Scheldt flume calibration measurements, the maximum voltage deviation for a single measurement point in the vessel from the overall averaged voltage based on the total of 18 measuring points is order of 5% for the majority of the calibration concentrations, in line with Bosman's finding of deviations of 10% at most. An incidental maximum of 16% occurred. Although for concentrations of 2.6 and 10 g/l and concentrations larger than 100 g/l slightly higher values were found than for the intermediate concentration range, it can be concluded that requirement of a homogeneous mixture in the measured region of the vessel was met in all situations. In view of this homogeneity, it is unlikely, though not impossible, that for large volume concentrations the concentration in the unmeasured regions of the calibration vessel is significantly higher than in the measured region as a result of insufficient mixing. If this effect would occur, it should be expected that the non-linearity is more significant for coarser material, which is more difficult to stir up. Bosman's experiments on the contrary, show that for the larger concentrations the sudden decrease of the measured γ -value occurs near $C_v \approx 0.5\%$ for S1 and S2 and near $C_v \approx 1\%$ for S3. Further, such a decrease is not observed for the coarser sediment. Thus it appears that the volume concentration, above which a drop in the γ -value is observed, increases for increasing particle size. The volume concentration for which the non-linearity becomes significant therefore increases with increasing grain-size. Therefore it can be concluded that concentration variations in the measured region of the vessel and between the measured and unmeasured region of the vessel cannot explain the non-linearity.

We follow Bosman's tentative conclusions in speculating that the deviations from the theoretical linear relation between concentration and output voltage for higher concentrations most likely arise from violation of the assumption of a limited number of Poisson distributed suspended particles underlying the derivation of theory. In more detail, a Poisson distribution requires a homogeneous distribution in space of independent and non-multipliable particles.

Based on the above, the calibration procedure is regarded as valid throughout the complete concentration range and the non-linear calibration curve should be used for the Scheldt flume experiments.

3.4 Acoustic Doppler Velocity meter (ADV)

3.4.1 Instrument description

An Acoustic-Doppler Velocity meter, developed by the U.S. Army Engineering Station (WES), as implemented by SonTek, was used for velocity measurements. The ADV is based on the Doppler principle to measure the three components (u , v and w) of the velocity at a single point. The system includes three modules: a measurement probe, a signal conditioning module and a signal processing module. The measurement probe consists of four ultrasonic transducers; a transmit transducer located at the bottom end of the stem and three receive transducers, slanted 30° from the axis of the transmit transducer and pointed at the sampling volume. This sampling volume is located about 0.10 m and 0.05 m below the probe tip for ADV01 and ADV02 respectively, which means that the flow in the sampling volume is not disturbed too much by the probe. A schematic diagram of the measurement probe of the ADV is presented in Figure 11.

The recorded signals can be stored and analysed by specific ADV software (processing module). However, it is also possible to record the signals on a different data acquisition system, via three analogue outputs. In the present experiments, signals were recorded using both methods. The first has the advantage that the raw ADV signals and information on the quality of the data are stored, the latter has the advantage of simultaneous sampling of all instruments (OpCons, WHM's, ADV's).

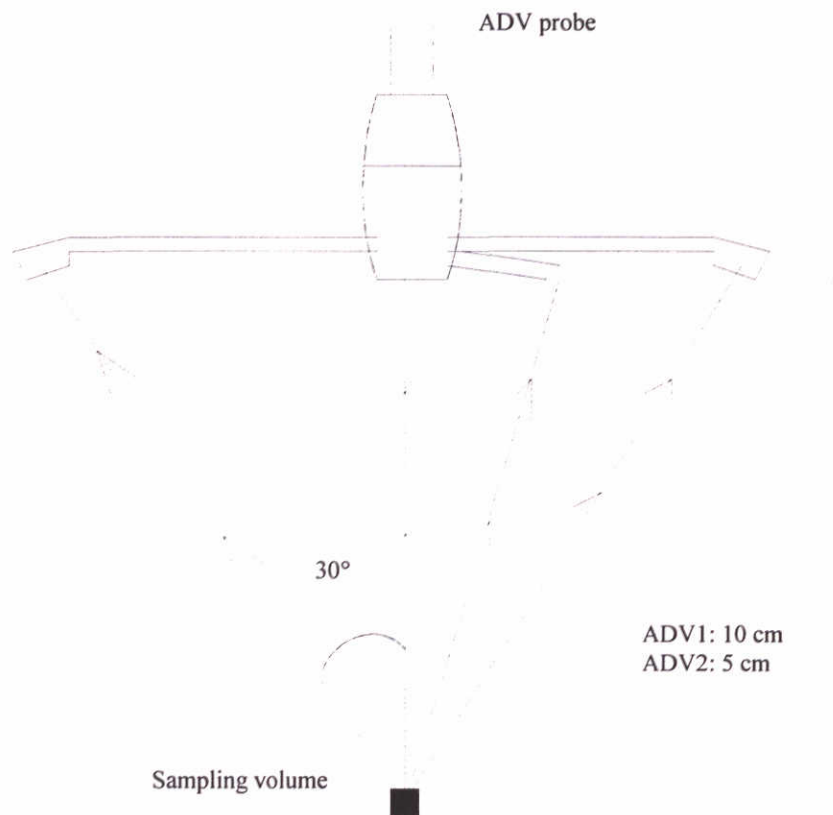


Figure 11 Schematic diagram of the ADV probe with the transmitter at the bottom part of the probe surrounded by the three receive transducers

3.4.2 Set-up and calibration

ADV set-up

The sampling volume of the ADV can be set to 3, 6 or 9 mm. In order to resolve turbulence quantities, the sampling volume should be taken as small as possible. However, statistics decrease with decreasing measuring volume and increasing sampling rate such that the data will be noisier. Especially in our situation with high concentrations of suspended sediment, which are likely to reduce the quality of the ADV data, the 9 mm sampling volume was considered the best choice. Only in the A101 through A104 series the 6 mm sampling volume was chosen.

Another important setting for the ADV operation is the velocity range. The conversion from output voltage to velocity, scales with the pre-defined velocity range. In principle this range should be taken as small as possible since the Doppler noise is approximately proportional to the velocity range. In the A1* series, the velocity range was set to 10 cm/s, which unfortunately resulted in spikes imposed on the signal. We then increased the velocity range to 30 cm/s which strongly reduced the amount of spikes in the velocity signal.

Before every measurement the actual water temperature was set which is required for calculating the speed of sound, which determines the scale factor used to convert Doppler frequency shift to velocity.

Calibration of analogue outputs

The calibration of the analogue output comprises the conversion from measured voltage to velocity (dependent on the velocity range) as well as corrections due to small differences between the voltage as read by the ADV and the AUKE data acquisition system. The proper calibration factors for each measurement are stored in the AUKE-PC files.

Re-calibration of ADV2

Another aspect which has to be taken into account is correction of the signals of the ADV02. Just before the start of the experiments, one of the three receive transducers was accidentally bent. The probe was checked using standard ADVCHECK software indicating a slight displacement in the signal of one of the receive transducers. The displacement was such that it was estimated by NORTEK that the influence on the velocity signal could be expected to be very small. It was therefore decided to continue with the ADV02 and perform a recalibration after the experiments.

The three velocity components measured by the three receiver arms of the ADV have an angle of 15° with the vertical, such that mainly vertical velocities are measured. These three components are then converted into velocity components (u,v,w) in (x,y,z) direction. When one (or more) receiver arms are bent, all three components (u,v,w) could be influenced, depending on the plane in which the arm is bent. In principle, a 3 by 3 correction matrix is needed to convert the three measured velocity components (u,v,w) to three corrected velocity components.

After the experiments NORTEK performed a recalibration of the ADV02. The correction matrix was approximated by NORTEK as a matrix with main diagonal components, only. The reasoning behind this was as follows. NORTEK performed two separate tests with an imposed velocity in purely x and y direction respectively. In the first test, the x-velocity deviated from the measured velocity with -5.5%, whereas the velocities in y and z-direction were zero. The second test showed a deviation of -10.2% in the y-velocity, whereas the velocities in x and z-direction were zero. NORTEK therefore reasons that there are negligible couplings between the velocity deviations and suggest to use a correction matrix with a main diagonal of $[1.055 \ 1.01 \ 0]$. The vertical velocity is thought to be within the specifications of 1%. Due to the small angle of 15° between measured velocity and the vertical, the horizontal components are more sensitive to bent receiver arms than the vertical components. For instance, a 1° error in the angle in the (x,z) plane would cause an error of a 6% in the u velocity but only an error of 0.5% in the vertical velocity.

According to NORTEK the findings are consistent with the way the probe was bent. They argue that the receiver arms were bent up or down, which does not induce coupling between the horizontal components. However, if the receiver arm pointing in x-direction, which is marked with a red tip, was bent in the x-z plane, this would not induce deviations in the y-

velocities. In case another receiver arm was bent, this would automatically mean a coupling between the deviations in x- and y-direction.

We have used the correction matrix with the mean diagonal $[1.055 \ 1.01 \ 0]$ as a good approximation. Note that the w-velocities are relatively insensitive to bent receiver arms. For the u-velocities any cross-terms are thought to be small, since the u-velocities are significantly larger than the v- and w-velocities.

4 Data analysis and validation

4.1 General

All instruments (OpCons, WHM's, ADV's) were sampled simultaneously at 50 Hz using WL|DELFT HYDRAULICS AUKE-PC data acquisition system. In order to avoid aliasing, each signal was low-pass filtered by an analogue filter at 25 Hz before storage. Besides sampling and storage of the ADV signals by AUKE-PC via three analogue outputs, the recorded signals are also stored directly by the ADV data acquisition system. Although the time-synchronisation with the other data is lost in the latter case, in these files information on the quality of the data is stored as well. The files can be viewed and processed using a viewer and postprocessing programme like WinADV which is public domain software. In the analysis of the ADV data we mainly used the data sampled by AUKE-PC. Inspection of some of the ADV files (for instance A305.ADV) showed that the data storage by the ADV acquisition system occasionally lags behind the data sampling. Also spikes can be present in the locally stored data, which are not found in the data sampled by AUKE-PC. When using the ADV files one should therefore carefully compare the data in the ADV files with the data sampled and stored by AUKE to analyse whether for the specific series phase differences are introduced in the ADV files. The file names of the ADV file start with the test name (for instance A101 or C204) and have the extension .ADV

The analysis of the data can roughly be divided in the analysis of the time-dependent data (WHM, ADV, OPC) and the time-averaged data from radiometry and sound, suction system and profile measurements. In this chapter, the time-dependent data are described; for the time-averaged data one is referred to Koomans and Bosboom (2000). Sections 4.2 and 4.3 deal with the data storage in AUKE-PC files and the conversion of the original AUKE-PC files to the files used as a basis of further analysis, respectively. The latter files have been used to derive a number of relevant parameters, which are described in Section 4.4. The data are analysed with the several subprograms of the AUKE-PC package. The results are described in Sections 4.5 through 4.8 for the surface elevation, sediment concentration, velocity and sediment fluxes. These sections also pay attention to the validity of the measurements through a statistical analysis of some of the time-averaged quantities derived from the time-dependent measurements.

4.2 Data storage

The data of each test were stored into two files within WL|DELFT HYDRAULICS AUKE-PC package format, namely a data file with extension .DAT and an administration file with extension .SEQ. The SEQ-files contain all information required to convert the binary data in the DAT-file into physical values. Per instrument, the zero-level, calibration factor and location in the flume are given. The original datafiles names start with # followed by the test name (for instance #A101, #C204). The naming convention for the test series is given in Appendix C.

The signal voltages were sampled and converted into two-byte integers. The integers are stored in binary format into the DAT-file.

The conversion of the voltages to the two-byte integers was done applying the formula:

$$store_value = voltage_value \cdot \left[\frac{highstored - lowstored}{highused - lowused} \right]$$

(4.1)

where voltage_value is the measured voltage, store_value is the value as stored in the DAT-file and highused, lowused, highstored and lowstored are the values as found in the SEQ-file in the following line:

‘A/D-CONVERSION,LOWSTORED=-32768,LOWUSED=-10.,HIGHSTORED=32752,HIGHUSED=10.’,

where the italicised names actually are variables which were kept constant during all tests. Their constant values were:

Table 7 A/D Conversion

LOWUSED	-10V
HIGHUSED	+10V
LOWSTORED	-32768
HIGHSTORED	-32752

This means that the measurable signal-voltage range lay between -10V and +10V, and that -10V was mapped in the integer -32768 and +10V was mapped on the integer +32752. Due to the 12-bit A/D-conversion, the resolution of the 2-byte integers was 4 bits, corresponding with steps of 16 in the integer values.

In every time-step all 15 signals were measured simultaneously and the corresponding 2-byte integer values were stored consecutively in the DAT-file. Thus the first 15 samples are the values measured at time 0.00 s, the second 15 values are the measured values at time 0.02 s and so on. The sequence of the data per instrument was according to the sequence of the instruments in the SEQ-files. An overview of the used instruments in all tests and the corresponding channel numbers is given in Table 8.

Table 8 Overview of instrument names and channel numbers for data acquisition

Name of recorded quantity	Instrument name	Data	Channel number (sequence in SEQ-file)	
			series A	series C
WHM01	WHM01 (fixed)	surface elevation (m)	1 (1) ³	1 (1)
WHM02	WHM02 (fixed)	surface elevation (m)	2 (2)	2 (2)
WHM03	WHM03 (fixed)	surface elevation (m)	3 (3)	3 (3)
WHM04	WHM04 (fixed)	surface elevation (m)	4 (4)	4 (4)
WHM05	WHM05 (Carriage 1)	surface elevation (m)	5 (5)	
WHM06	WHM06 (Carriage 1)	surface elevation (m)	6 (6)	6 (5)
ADV01	ADV01 (Carriage 1)	u-velocity (m/s)	7 (7)	
ADV02	ADV01 (Carriage 1)	w-velocity (m/s)	8 (8)	
ADV05	ADV01 (Carriage 1)	y-velocity (m/s)	14 (13)	
ADV03	ADV02 (Carriage 2)	u-velocity (m/s)	9 (9)	9 (6)
ADV04	ADV02 (Carriage 2)	w-velocity (m/s)	10 (10)	10 (7)
ADV06	ADV02 (Carriage 2)	y-velocity (m/s)	15 (14)	15 (9)
OPC01	OPC01 (Carriage 1)	concentration (g/l)	11 (11) ⁴	
OPC02	OPC02 (Carriage 2)	concentration (g/l)	13 (12)	13 (8)
DPM01	Displacement meter at wave board (DPM01)	displacement of wave board (m)	16 (15) ⁵	16 (10)

For the A-series and for test #C101 the measurement duration is 2100 seconds ($> 1 \cdot$ steering signal cycle), whereas for the rest of the C-series 3900 s were recorded ($> 2 \cdot$ steering signal cycle). The DAT-files therefore were exactly 3,150,000 byte (15 channels \cdot 2100 s \cdot 50Hz \cdot 2 byte/channel) for the half-hour tests #A***, 2,100,000 byte (10 channels \cdot 2100 s \cdot 50Hz \cdot 2 byte/channel) for the half-hour tests #C101 and 3,900,000 byte (10 channels \cdot 3900 s \cdot 50Hz \cdot 2 byte/channel) for the hour tests #C2** and #C3**.

The SEQ-files contain all information required to convert the binary data in the DAT-file into physical values.

The SEQ-files were subdivided into sections, each beginning on a new line with a section heading (LOGGING, STO, GENERAL, SERIES) and ending on a new line with corresponding END statement (e.g. END LOGGING).

The first section LOGGING contains comments about the test without a fixed format. The second SECTION STO (for storage) gives details of how the sampled data was stored. The third GENERAL describes the project and gives information on the A/D conversion. The next sections are all headed SERIES, quantity_name where quantity_name is the name of the quantity recorded at the respective channel according to the first column in Table 8.

Each section contained the measured zero-level, the calibration factors, the dimensions of the measured quantity and the location of the instrument in the channel.

³ During #A706 and #A707 WHM01: 16 (15) instead of DPM01

⁴ During #A705 OPC01 11 (11) also as OPC11 at 16 (15) instead of DPM01, during #A706 and #A707 OPC01: 11 (11) also as OPC21 at 1 (1) without amplifier

⁵ Not recorded for #A705 through #A707

4.3 File conversion and correction

4.3.1 Conversion to physical values

The raw datafiles (starting with #) are converted to .DAT and .SEQ files in which zerolevel and calibration are taken into account via:

$$physical_value = \sum_i C_i \cdot (voltage_value)^i - zerolevel_value$$

where the calibration coefficients C_i and the zero-level values are given in the SEQ-file. Only for the OPC, i is larger than 2 (3 or 4, see 3.3.2). The grain-size influence on the OPCON calibration was not taken into account. Note that for all instruments but the ADV signals, the zero-level correction (in terms of physical values) was accounted for. The zero-levels are the measured offsets just before the tests. For the ADV, the proper offsets are already taken into account in the ADV calibration. For the OPC, variations in the zero-level are due to variation of the fine material content in still water. Note that for the OPC, the zero-level measured a few minutes after the test is taken to be representative for offsets due to fines in the water (see Section 3.3.2) and are stored in the .SEQ files.

The new .DAT files (without #, see Table 9) contain physical values. The first few minutes of the data series is disregarded and only the signal with a length equal to a multiple of the steering signal (1820.44 s) is stored. The new SEQ-files therefore range from 279.56 s up to 2099.98 s for series A and C101 and from 259.12 to 3899.98 s for series C2** and C3**. Note that in either case the time range stored in the new DAT and SEQ-files corresponds to the period during which the suction system was operated.

4.3.2 Division between instruments and filtering

The new .DAT files and .SEQ files are produced for each instrument type. The file names are according to Table 9

Table 9 File names containing physical quantities

quantity	filename
surface elevation	W***
velocity	A***
concentration	O***

In order to facilitate further analyses, the WHM, ADV and OPC time series are analysed into a high-frequency part and a low-frequency part (de-meaned), except for the v-velocity components (in cross-flume direction). For all series, half the peak frequency (0.25 Hz) is used for the lowest short wave frequency. The coding of these series is given in Table 10, Table 11 and Table 12, for the surface elevation, velocity and concentration, respectively.

Table 10 Surface elevation (η) signal names in W*** files

quantity	WHM01	WHM02	WHM03	WHM04	WHM05	WHM06
η -signal	whm01	whm02	whm03	whm04	whm05	whm06
η -low	whm101	whm102	whm103	whm104	whm105	whm106
η -high	whm201	whm202	whm203	whm204	whm205	whm206

Table 11 Velocity (u,v,w) signal names in A*** files

quantity	ADV01	ADV02
u-signal	adv01	adv03
w-signal	adv02	adv04
v-signal	adv05	adv06
u-low	adv101	adv103
w-low	adv102	adv104
u-high	adv201	adv203
w-high	adv202	adv204

Table 12 Concentration (c) signal names in O*** files

quantity	OPC01	OPC02
c-signal	opc01	opc02
c-low	opc101	opc102
c-high	opc201	opc202

4.4 Derived time-averaged parameters

From the W***.DAT and .SEQ, A***.DAT and .SEQ and O***.DAT and .SEQ files, a number of integral parameters was computed and stored into ASCII-files named W***.PAR, A***.PAR and O***.PAR, respectively. In addition sediment fluxes were computed from the A***.DAT and .SEQ and the O***.DAT and SEQ files and stored into S***.PAR files. The PAR-files are subdivided into sections. Each section starts on a new line with a section heading SERIES and ends on a new line with corresponding END statement (END SERIES). All sections are headed SERIES, signal_name where signal_name is the name of the signal in the ***.DAT and .SEQ files according to Table 10, Table 11 and Table 12. Each line in the respective sections contains the parameter name, the parameter unity, the name of the used AUKE-PC programme and last the value of the parameter. The list of computed parameters is given in the following sections for the respective PAR files. The names that are used in the data files are given first, followed by the symbol and a brief description.

4.4.1 Surface elevation

The parameters derived from the W***. DAT and .SEQ files are given in the tables below for the unfiltered signals WHM0*. Table 13 shows the parameters computed with the WAVES programme, which determines the development of series values between two zero-crossings. Here we use downwards baseline crossings for wave detection, where the baseline is the mean of the signal.

Table 13 Parameters computed with programme WAVES using downwards as zero crossing type for total signals WHM0*

parameter	symbol	description
H1/3d	$H_{1/3}$ (m)	mean of the highest 1/3 of the waves
T1/3d	$T_{1/3}$ (s)	mean of the highest 1/3 of the periods
H1/10d	$H_{1/10}$ (m)	mean of the highest 1/10 of the waves
T1/10d	$T_{1/10}$ (s)	mean of the highest 1/10 of the periods
Tmd	T_m (s)	the average wave period
Hmaxd	H_{max} (m)	the maximum of all wave heights
Tmaxd	T_{max} (s)	the maximum of all wave periods
Hmd	H_m (m)	the average wave height
Hrmsd	H_{rms} (m)	the root mean square wave height
gammad	γ (-)	linear correlation coefficient for wave heights (Eqs (4.2) and (4.3))
kappa (t)	κ (-)	correlation parameter kappa (Eqs (4.2) and (4.3))
Nd	N (-)	number of waves in a record
H1%d	$H_{1\%}$ (m)	1% exceeded wave height
H10%d	$H_{10\%}$ (m)	10% exceeded wave height

The linear correlation coefficient for wave heights (H) reads, with N is the number of waves in the record,

$$r(H) = \frac{N}{N-1} \frac{\sum_{i=1}^{N-1} (H_i - \bar{H})(H_{i+1} - \bar{H})}{\sum_{i=1}^N (H_i - \bar{H})^2} \quad (4.2)$$

We then have:

$$\begin{aligned} \gamma &= r(H); \\ \kappa &= \sqrt{r(H^2)} \end{aligned} \quad (4.3)$$

Table 14 Parameters computed with programme SPECTPER for total signals WHM0*

parameter	symbol	description
m-1..m4	m_i (m ² /s ⁴)	spectral moments, $i = -1, 0, 1, 2, 4$
TpD	T_{pd} (s)	dominant peak period for total spectrum
kappa (f)	κ (-)	spectral correlation parameter kappa
Hm0	H_{m0} (m)	significant wave height $4\sqrt{m_0}$

The programme SPECTPER uses a periodogram, being an amplitude spectrum, as input to compute the spectrum. The periodogram is computed with the programme FILTER. Using the periodogram information and a user-defined frequency interval (0.01 Hz in this case), the energy density spectrum is derived.

Table 15 Parameters computed with programme STATIST for total signals WHM0* with N number of samples

parameter	formula	description
mean	$\langle x \rangle = \frac{\sum_{i=1}^N x_i}{N}$	the mean of all samples of series x
st-dev	$\sigma_x = \sqrt{\frac{\sum_{i=1}^N (x_i - \bar{x})^2}{N-1}}$	the standard deviation of the series samples
minimum		the minimum value of all series values
t-minimum		the time corresponding to the minimum value
maximum		the maximum value of all series values
t-maximum		the time corresponding to the maximum value
skewness	$S_k = \frac{1}{N} \sum_{i=1}^N \left(\frac{x_i - \bar{x}}{\sigma_x} \right)^3$	the skewness of the series
kurtosis	$K_u = \frac{1}{N} \sum_{i=1}^N \left(\frac{x_i - \bar{x}}{\sigma_x} \right)^4 - 3$	the kurtosis of the series
GF	$GF = \frac{\sigma\{(x^2)_{low-pass}\}}{\langle (x^2)_{low-pass} \rangle}$	the groupedness factor of the series: the standard deviation of the squared and low-passed filtered signal over the mean of the squared and low-passed filtered signal.
Rms	$x_{rms} = \sqrt{\frac{\sum_{i=1}^N x_i^2}{N}}$	
mean-pos		the mean value of the positive series values
st-dev pos		the standard deviation of the positive series values
mean-neg		the mean value of the negative series values
st-dev-neg		the standard deviation of the negative series values

For the low- and high-pass filtered signals WHM10* and WHM20* respectively parameters are only computed with the programme SPECTPER. Note that for all series, half the peak frequency (0.25 Hz) is used for the lowest short wave frequency. Also, the correlation coefficient between the low-pass filtered surface elevation and the wave envelope as measured for WHM0* is stored in the sections WHM10* and WHM20*. The wave envelope is derived through high-pass filtering, squaring, de-meaning, and low-pass filtering of the elevation signal. Therefore the correlation coefficient (programme CORR) pertaining to e.g. the surface elevation recorded by WHM01 is stored in the section headed WHM101 as well as WHM201. Besides, for all signals, the X (and Z) positions are stored, the latter representing the still-water level of 70 cm for the fixed wave height meters and the distance of the other instruments on the measurement carriage above the ripple tops.

4.4.2 Velocity

For the velocity related A***.DAT and .SEQ files, besides the x-position and z-position (distance above the ripple tops), for all series shown in Table 11, the parameters computed with STATIST are stored in the A***.PAR files. Moreover, for the u-velocity components (total, low-pass and high-pass filtered signals), velocity moments are computed using the programme MOMENTS (Table 16). As for the surface elevation, for the u-velocity components, the correlation coefficient between the low-pass filtered velocity and the slowly varying short wave variance as measured for ADV01 and ADV03 is stored in the sections ADV101 and ADV201 and ADV103 and ADV203, respectively.

Table 16 Parameters computed with programme MOMENTS for signals ADV01, ADV03, ADV*01 and ADV*03

parameter	formula	description
gu2,gu3,gu5	$\langle u(t) ^n \rangle ((\text{m/s})^n)$	total even velocity moments, $n = 2, 3, 5$
gu2ux,gu3ux	$\langle u(t) u(t) ^n \rangle ((\text{m/s})^{n+1})$	total odd moments, $n = 2, 3$

In addition, in the A***.PAR files two extra sections are defined, ADV301 and ADV302, pertaining to the first and second carriage respectively. In those sections for the respective carriages the following velocity parameters, analysed with the programme MOMCOMB, are stored:

Table 17 Parameters computed with programme MOMCOMB for u-velocity signals stored in sections ADV30*

parameter	formula	description
guus	$\langle u_{high}(t) u_{high}(t) ^2 \rangle (\text{m}^3/\text{s}^3)$	third order velocity moment (short waves)
guls	$\langle 3u_{low}(t) u_{high}(t) ^2 + 3u_{high}(t) u_{low}(t) ^2 + u_{low}(t) u_{low}(t) ^2 \rangle (\text{m}^3/\text{s}^3)$	third order velocity moment (long-short wave interaction)
gusc	$\langle 3\bar{u}(t) u_{high}(t) + u_{low}(t) ^2 \rangle (\text{m}^3/\text{s}^3)$	third order velocity moment (mean flow-wave interaction)
guc	$\langle \bar{u} \bar{u} ^2 \rangle (\text{m}^3/\text{s}^3)$	third order velocity moment (mean flow-wave interaction)
guzx	$\langle u_{high}(t)w_{high}(t) \rangle (\text{m}^3/\text{s}^3)$	wave induced Reynolds stress

4.4.3 Sediment concentration

For the concentration related O***.DAT and .SEQ files, besides the x-position and z-position (distance above the ripple tops), the parameters computed with STATIST are stored in the O***.PAR for all series shown in Table 12.

4.4.4 Sediment fluxes

Two new variables are defined and stored in the S***.PAR files, namely SFL01 and SFL02, pertaining to the first and second carriage respectively. The section headings starting with SFL0* contain sediment flux parameters according to Table 18 and computed from the ADV and OPC signals.

Table 18 Parameters in S***.PAR files computed with programme FLUX

parameter	formula	description
uca	$\langle u \rangle \langle c \rangle$ (kg/(m ² s))	mean flow contribution to time-averaged sediment flux
uc	$\langle u(t)c(t) \rangle$ (kg/(m ² s))	total time-averaged sediment flux
uchigh	$\langle u_{high}(t)c_{high}(t) \rangle$ (kg/(m ² s))	short wave contribution to time-averaged sediment flux
uclow	$\langle u_{low}(t)c_{low}(t) \rangle$ (kg/(m ² s))	long wave contribution to time-averaged sediment flux

4.4.5 Data retrieval; description of programme collec_sf

Data from the parameter files *.PAR can be selected quite conveniently by a utility programme COLLEC_SF.EXE. The programme must be run from the directory immediately above sub-directory PARFILES in which the parameter files are stored. To make a selection of the data type <collec_sf>.

The program asks for a test name. Type the code of the test you want. Legal codes are given in the file "tests", which can be edited. The code you type may include one or more '*' as wild characters, thus A101 for test A101, A1** for all tests from the first day etc. Note that the input is case-sensitive; use capitals.

Next the programme asks for an instrument name. Legal names are defined in the file 'instrum'. This file can be adapted by the user. Again the input is case-sensitive (capitals only) and '*' is allowed as a wild character. For instance, type 'OPC0*' for the data of the two opcons, or type WHM10* for parameters compute from the low-pass filtered wave height meter signals.

Finally the programme asks for a variable name; legal variable names are listed in the file 'varnames'. The input is case-sensitive, refer to the file for the names and case. Here no wild characters are allowed. For instance, type 'mean' to get the average value of each selected instrument in each selected test.

The programme then asks for x_{min} , x_{max} , z_{min} and z_{max} . Only those parameters are selected for which the measuring location was in the here defined range. If no selection on position is desired, type for instance '0', '50', '0', '1'.

The programme writes the X,Y,Z values, the parameter values, the instrument and test codes to the file 'collec.out'. The file 'collec.pp' omits the instrument and test codes. These files are overwritten every time the program is run. To save your results copy the files to different filenames.

The file 'malfun' contains series, instruments and variables which are incorrect due to for instance malfunctioning instruments (see Sections 4.5 through 4.7). The parameters mentioned in this file are not selected.

4.5 Surface elevation

4.5.1 Results

Some of the measured and smoothed spectra ($df = 0.01$) for series A and C are given in Figure A-22 and Figure A-23, respectively. The spectra indicate how both the superharmonic and subharmonic components develop as the waves shoal. The slightly different shape of the spectra for series A and C is due to the difference in length of the processed series (1 and 2 times the length of the steering signal respectively). Also differences in bed level, can give rise to differences between the spectra in the respective series. Figure A-24 and Figure A-25 show the integral surface elevation data, comprising significant wave height, set-up, peak period and cross-correlation coefficient between the low-pass filtered surface elevation and the wave envelope. The lower plot of the figures shows the initial bottom profile together with the single-barred bottom profile at the end of series A and C respectively.

The figures clearly show the onset of breaking around $x = 18\text{ m}$ and the intensification of the breaking process around $x = 23\text{ m}$ from where the wave height strongly reduces and a positive gradient is observed in the mean water level in landward direction. From the bar crest towards the beach, the cross-correlation coefficient, which equals -1 in a complete bound long-wave situation, increases from the offshore value of -0.83 to 0.23 at the most landward measuring location. The changes in the correlation are explained by the increasingly important short-wave modulation through the depth variations induced by the presence of the long waves for smaller depths. Also the release of long waves in the surf zone could play a role.

During series A, the surface elevation signal for the first four horizontal positions was recorded 48 times and for the 8 locations on the profile the recording of the surface elevation signal was repeated on average 10 times (ranging from 4 times at the most landward measuring location to 22 times at $x = 20.5\text{ m}$). In series C, the surface elevation signal for the first four horizontal positions was recorded 12 times, whereas for the 8 locations on the profile the recording of the surface elevation signal was performed 1 to 2 times.

The small variations in the wave height at the various locations are satisfactory. The variations in the cross-correlation coefficient between long wave surface elevation and wave envelope can for the greater part be explained from an increase of free long waves reflected from the beach as a result of the changing bottom profile (see Section 4.5.3). The deviating value for the correlation coefficient at $x = 23 \text{ m}$ corresponds to WHM05 in series A305 (see Section 4.5.2). The set-up variations can be largely attributed to the deployment of the suction system; during each measurement in the A and C series 8 respectively 28 buckets of water corresponding to 0.08 and 0.28 m^3 are withdrawn from the flume, whereas a variable amount of water is put back in the flume. A correction to the set-up data using the zero level recordings after the tests, greatly reduces the standard deviation of the measured value, is described in Section 4.5.2.

4.5.2 Statistical analysis

Information about the statistical distribution of the WHM data is obtained by computation of the mean, standard deviation, skewness and kurtosis for each wave height meter. Where the standard deviation yields information on the spreading of the data around its mean value, the skewness characterises the degree of asymmetry around its mean. The kurtosis indicates the relative peakedness or flatness of a distribution compared to the normal distribution. By computing the mean and standard deviation of these parameters for the fixed wave height meters for all tests and for the wave height meters on the carriages for the tests in one vertical, possible outliers can be detected. Chauvenet's criterion is used for deciding whether a data point is bad; a limit is selected on the probability that a bad point had come up in the data set of this size. The probability is calculated using the standard deviation of the whole set. The lower limit of probability is set to 50 %, therefore if a point gets a probability smaller than 50% is gets thrown out. For a data point in a series of n measurements, the probability is equal to n times the probability on a single measurement according to a normal distribution.

Mean water level

In first instance, the mean water level was computed with a correction for the zero level shift recorded before each measurement. The standard deviation of the mean surface elevation, is of the order of 0.5 mm for all WHM's, except for the A3** series with WHM05 at $x=23 \text{ m}$ (Table D-39). These variations in the set-up, can be largely attributed to the deployment of the suction system; during each measurement in series A, 8 buckets of water (0.08 m^3 in total) corresponding to a 2 mm water level fall are withdrawn from the flume, whereas a variable amount of water is put back in the flume at varying moments in time. Therefore, in all measurements a more or less wandering offset occurs, which can be expected to decrease not more than 2 mm in the situation that water is only withdrawn from the flume, as is the case for the first measurement on a day. In the situation that besides the continuous withdrawal of water, the maximum amount of water (the 8 buckets withdrawn during the respective measurement and 8 buckets during the previous measurement, therefore $16 \text{ buckets} \equiv 4 \text{ mm}$) is put back in the flume on regular intervals, we estimate the net water level rises 2 mm .

In Table D-40 and Table D-41 the zero level values are listed, which are recorded before and after each measurement, respectively. In Figure 12, the difference in still water level before and after the tests is shown.

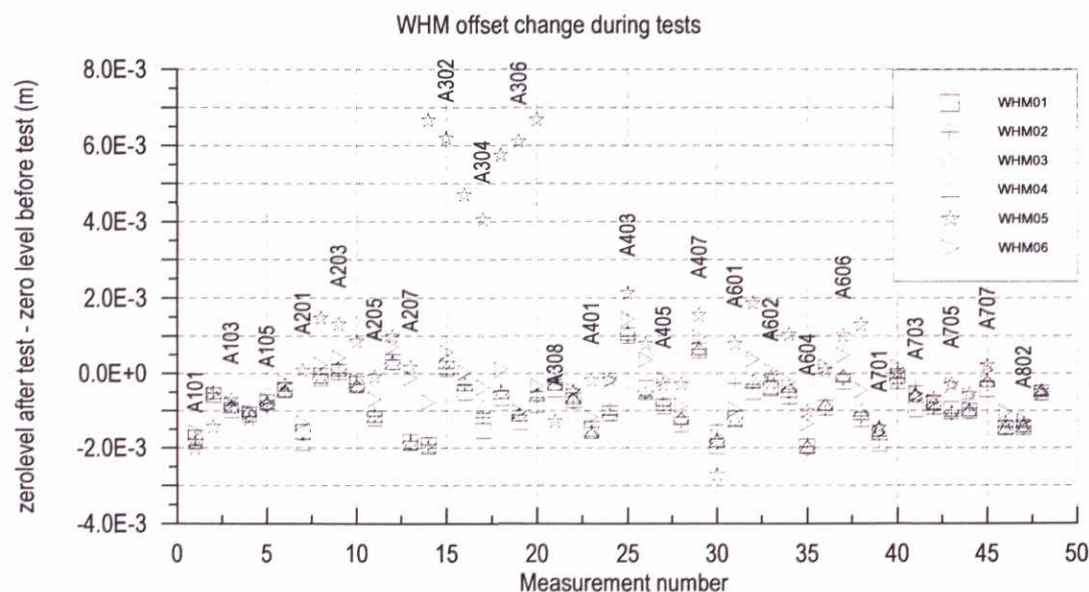


Figure 12 The difference in the still water level before and after each test

In accordance with the above, except for WHM05 in the A3* series, the change in zero level lies in the range of -2 mm to 2 mm, amounting to about 2 mm for the first series on a day (A101, A201, A301, A401, A501, A701 and A801) in which mainly water is withdrawn. Therefore and since the difference in offset during a test is similar for all WHM's, a large part of the offset change is attributed to the deployment of the suction system. As will be discussed below for WHM05 and WHM06 additional factors play a role. To correct the set-up value, we compute the set-up by correcting for the average of the zero levels that were recorded before and after the tests. Table D-39 and Figure 13 show that this significantly reduces the standard deviation of the set-up values; for the first four wave height meters, deployed in every test, the standard deviation reduces with 40%. The lower plot of Figure 13 shows the initial bottom profile together with the single-barred bottom profile obtained after a total wave duration of approximately 30 hours (%A*** and %A904). The error bars in the upper two plots depict twice the standard deviation of the results for the respective location. The uncertainty is only calculated for locations with duplicate measurements. The data points without error bars lack statistics and therefore no statistics are given.

The set-up estimates are higher after correction since on the average more water is withdrawn from the flume during the tests than put back. The WHM at the carriages at $x=20.5$ m (see Table C-33 and Table C-35 for series names) gives a slightly deviating value for the change in zero level, which cannot completely be attributed to the suction system and might originate from a slight lowering of the WHM's on the carriages during the tests in the most energetic regions. For the series 301 through 305 in which wave height meter 5 was deployed at $x=23$ m, a similar but more drastical deviation occurs; the zero level measured after the test drastically increases with respect to the measurements before the

tests. Although the corrected set-up estimates do improve when these values are taken into account, as can be seen from Figure 13, this yet unexplained change in offset should not be trusted. Note that $x=20.5$ m and $x=23$ m are the locations where the highest waves break. At the other locations, the wave height meters on the carriages do not show such differences with the first four WHM's.

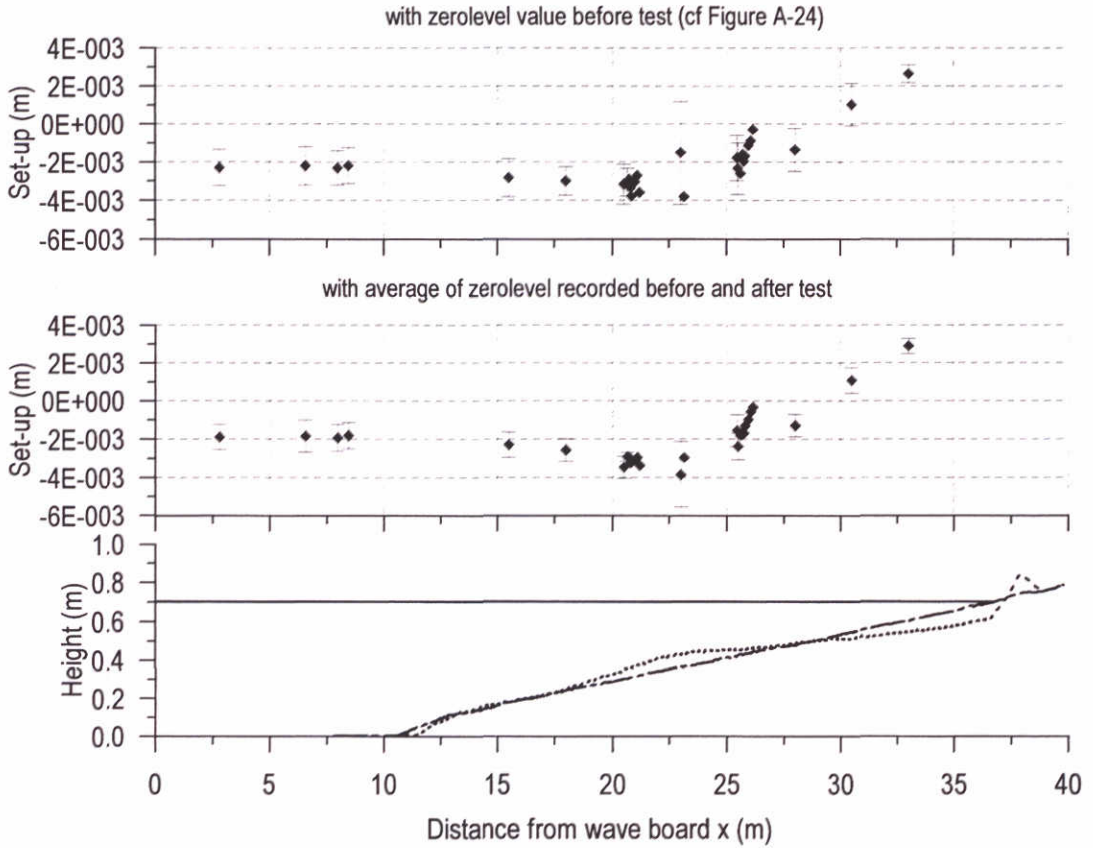


Figure 13 Set-up with zerolevel before test (upper plot) and with average of zerolevel before and after test (middle plot) and initial bed level (%A100) and bed after ~30 hours (%A904) (lower plot). Error bars indicate twice the standard deviation from mean.

Note that the zero-level values in the SEQ files are the zero-levels recorded before the tests. The standard data analysis is performed with those values. The data can be corrected using Table D-40 and Table D-41 which show the zerolevel values before and after the tests.

The bad points in the corrected set-up values defined according to Section 4.5.2 are summarised in Table 19 for the fixed wave height meters WHM01 through WHM04 ($n=48$) and for each x-location along the profile.

Table 19 Outliers in set-up values in A-series

series	outliers (probability to occur)
A204	meancor WHM05 (15%)
A304	meancor WHM01 (7%), meancor WHM03 (38%)
A401	meancor WHM06 (21%)
A802	meancor WHM01 (19%), WHM02 (41%), WHM03 (16%), WHM04 (25%), WHM06 (48%)

The influence of the wandering offset on the oscillatory signal is expected to be limited. The inaccuracy of the order of 1 mm of the instantaneous values is rather small as compared to the oscillation itself.

For series C, the set-up is computed in an identical manner. Table D-43 and Table D-44 shows the zero-level values before and after the tests, whereas the difference between the still water level before and after the tests is shown in Figure 14. This figure shows that, as for series A, the deployment of WHM06 at $x=20.5$ m (C101,C204) and $x=23$ m (c301) gives a zero-level change which does not originate from the change in water level due to the suction system.

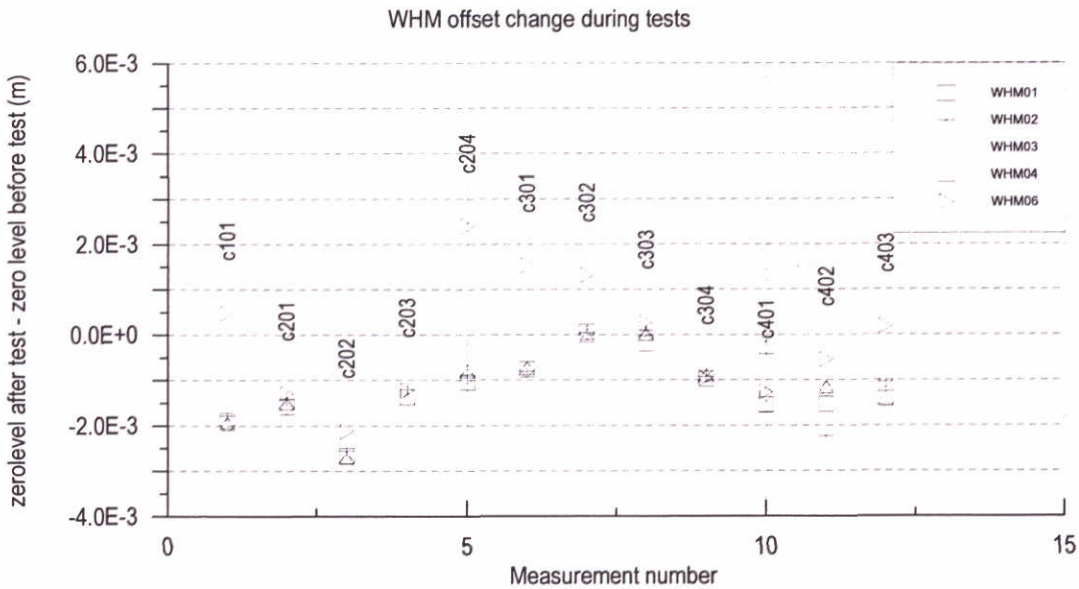


Figure 14 The difference in the still water level before and after each test

By correcting for the change in water level the standard deviation in the measurements is strongly reduced for both series A and C (Table D-39 and Table D-42). When comparing the uncorrected set-up values, we see that the set-up in series C is systematically lower than in series A. After correction this is still the case, although to a lesser extent (Table D-39 and Table D-42). Globally, we have for the first 4 WHM's a set-up which is about 1 mm lower in series C than in series A. The explanation for this might be related to the uneven distribution of the *net* withdrawal in time by the regime of putting back the buckets. This regime can be expected to be different in series A and C. In series C, the duration of the tests is twice as long and seven instead of four suction tubes are used. When using the average value of the zero-level before and after the test, we assume that on average the

buckets are put back half-way the test duration. As compared to series A, in Series C a larger percentage of the withdrawn water was put back during the actual test series. However, in series C a large amount of buckets needed to be handled with fewer people than in series A. It can therefore be expected that the putting back of water into the flume is biased towards the end of the test duration. If we assume that due to this different scheme, the buckets in series C are put back for the larger part at the second half of the test, the set-up would be underestimated by using the average value of the zero-level before and after the test. A better representation might then be for instance one third of the zero level after and before the test. This would result in higher set-up values.

Summarising we find that by correcting the set-up values by using the average value of the zero-level before and after the test, we reduce the internal error in both series A and series C. However, the difference in set-up between series A and C of ~ 1 mm indicates that an external uncertainty of ~ 1 mm is still present, which is related to the measurement duration and the scheme of bucket handling.

Oscillation

The mean and twice the standard deviation of the standard deviation, skewness and kurtosis of the oscillatory signal of the WHM's are shown in Figure 15.

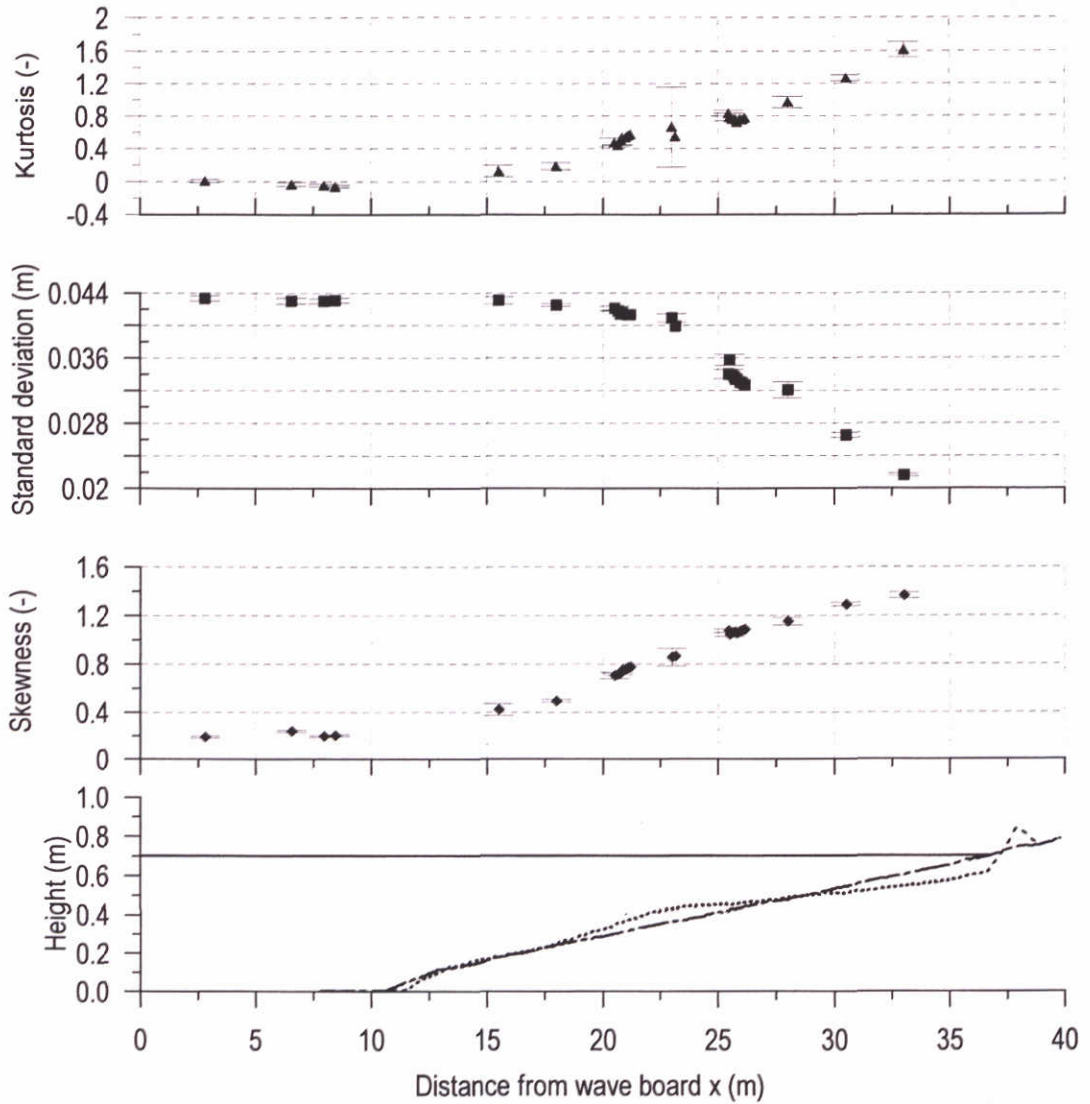


Figure 15 Kurtosis (first plot), standard deviation (second), skewness (third plot) and initial bed level (%A100) and bed after ~30 hours (%A904) (fourth plot) for surface elevation signal of series A. Error bars indicate twice the standard deviation of data.

Despite the changing bed profile, the standard deviation of these parameters is remarkably small. It can be concluded that variability of the *total* oscillatory surface elevation signal during the complete series A, especially that due to the changing bottom profile, is limited. Although the variations are small, a consistent pattern can be found. This can be seen in Figure A-26, which shows the variation of the zeroth spectral moment m_0 (see Table 14) of the surface elevation spectra, for the complete frequency band and for the high-frequency part only. The plots in Figure A-26 show the time-variation (between the various series) at $x = 20.5$ m, 23 m, 25.5 m and $x = 28$ m, respectively. In the data at 25.5 m, also the A70* series ($x = 25.46$ m) are taken into account. The plots show that in time the spectral energy content m_0 decreases, which can be attributed to the seaward shift of the breaker point as a result of the bar development. Therefore, variations in time are mainly noticeable for the stations landward of the breaker bar: $x = 25.5$ and 28 m. At the horizontal part of the flume and the stations on the profile before initial breaking, the high-frequent energy content is less variable. However, some variability is introduced in the low-frequency component, as will be shown in

Section 4.5.3. This variability hardly shows in Figure 15, since the energy content in the low frequency part of the spectrum is very small compared to the high-frequency energy content. The following parameters were defined as outliers (Table 20):

Table 20 Outliers in A-series: standard deviation, skewness and kurtosis of surface elevation

series	outliers (probability to occur)
A101	skewness WHM01 (27%), kurtosis WHM04 (23%)
A102	skewness WHM04 (14%)
A305	skewness WHM05 (13%) and kurtosis WHM05 (11%)
A308	skewness WHM05 (37%) and kurtosis WHM05 (35%)
A406	stdev WHM01 (7%), WHM02 (45%), WHM03 (40%), WHM04 (13%), WHM05 (21%)
A602	stdev WHM03 (43%), stdev WHM04 (13%)
A705	kurtosis WHM02 (25%)
A801	kurtosis WHM02 (24%)

The reason of the deviations in the series in Table 20 could partly be detected. On visual inspection, WHM05 in measurement #A305 appeared to malfunction between 370 and 377 s, possibly due to intense wave breaking. For series A406 and A602, the standard deviation computed from the time series deviates from the value of $\sqrt{m_0}$ as determined from spectral analysis. This indicates that the distribution of the surface elevation deviates from a Gaussian distribution. In the respective series, the wave board was in its maximum position during about 10 sec. This is the result of the reflection compensation and might explain the deviating standard deviation in those series. The same holds, to a lesser extent, for series A403 and A301, although it does not show in the standard deviation.

In series C, the following parameters were rejected on Chauvenet's criterion with a probability to occur smaller than 50% (Table 21):

Table 21 Outliers in C-series: standard deviation, skewness and kurtosis of surface elevation

series	outliers (probability to occur)
C101	skewness WHM01 (41%), skewness WHM03 (47%)
C203	stdev WHM04 (46%) and meancor WHM05 (11%)
C204	skewness WHM02 (47%) , meancor WHM04 (49%)

4.5.3 Long waves

Figure 16 shows the cross-correlation coefficient between the low-pass filtered surface elevation and the wave envelope as well as the long wave energy. The wave envelope is derived through high-pass filtering, squaring, de-meaning, and low-pass filtering of the elevation signal. The deviating value at $x=23$ m is a result of the failure of the WHM05 in A305 during a short part of the test duration (see Section 4.5.2). The variations in the cross-correlation coefficient between long wave surface elevation and wave envelope can for the greater part be explained from an increase of free long waves reflected from the beach as a

result of the changing bottom profile. This can be seen from Figure 16 where the correlation coefficient and the long wave energy m_0 for the fourth WHM are shown for all tests in chronological order.

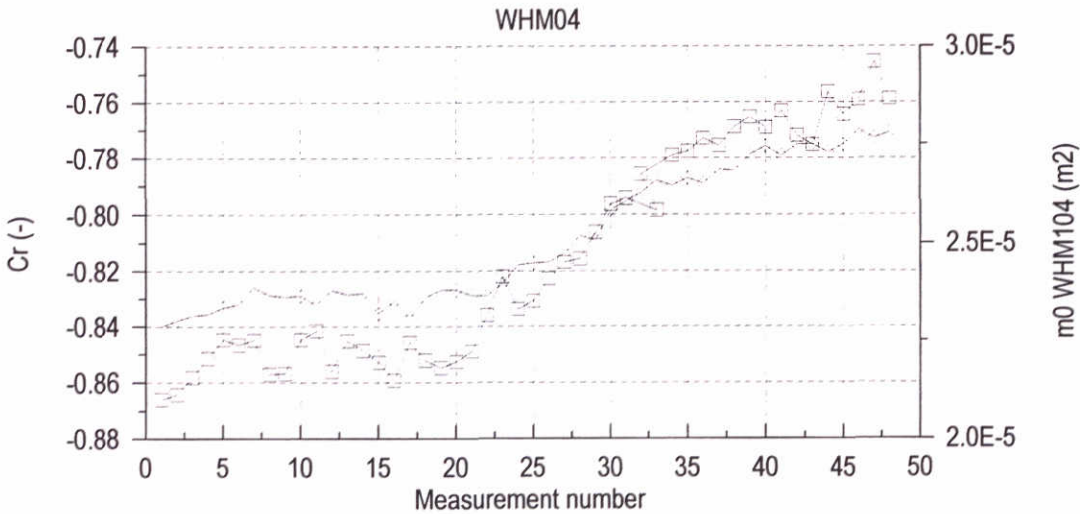


Figure 16 Development of cross-correlation coefficient between long wave surface elevation and wave envelope (squares) and low wave energy (triangles) in time for WHM04

Due to the increase of free long wave energy (as a result of the changing bottom profile) some variability in the conditions is introduced.

4.6 Concentration

4.6.1 Visual inspection of time-series

Here we distinguish between the analogue output range, which is equal or larger than 10 V depending on the applied zero-shift (see Section 3.3.2) and the validity range. If the output exceeds the analogue output range, the time-series are clipped to a maximum for a certain portion of the complete time-series. The validity range refers to the fact that at an output signal of approximately 10 V above the zero-level, the input signal is reduced to ~ 1 mV which can be regarded as noise. The maximum voltage range in which accurate concentration measurements can be made is therefore 10 V. Although due to the zero-level shift the voltage range could be larger than 10 V, the measurements with peaks exceeding this range should be considered with care.

On visual inspection, it was found that in some concentration time-series the signal of the OPCON exceeded the analogue output range during a certain portion of the complete time-series (see Table 22). The result is that the measured time series are clipped. Depending on the applied zero-shift, there were also series which were not clipped but in which the output voltage range exceeded 10 V. This happened in a few series in which rather high concentrations occur (Table 22).

Table 22 Outliers in concentration measurements

Series name	Instrument name	finding
A201	OPC01	Out of analogue output range for a few peaks
A401	OPC02	Out of validity range for a few peaks
A601	OPC01	Signal breakdown during 14 s
A601	OPC02	Out of validity range for a few peaks
A611	OPC02	Out of validity range for a few peaks
A603	OPC02	Out of validity range for a few peaks
A603	OPC02	Out of validity range for a few peaks
A605	OPC02	Out of validity range for a few peaks
A606	OPC02	Out of validity range for a few peaks
A607	OPC02	Out of validity range for a few peaks
A801	OPC02	Out of validity range for a few peaks

In the results discussed in the next section, those series have not been excluded because the exceedance of the output or validity range did only occur for a very limited part of the time series such that the effect on the time-averaged quantities is estimated to be limited.

4.6.2 Results

Figure A-27 through Figure A-32 show some time-averaged quantities of the concentration data for series A and C. Note that the results shown are not corrected for grain-size or density. For the series A data, which are adjusted for the effect of grain-size on the OPCON one is referred to Bosboom et al. (1999). The median diameters of the suspended material that are needed to correct for the grain-size effect are given in Part I (Koomans and Bosboom, 2000).

Figure A-27 through Figure A-30 show the mean concentration and the standard deviation of the total, low-pass and high-pass filtered concentration signals respectively for the eight locations along the profile. During the 48 half hour measurements several point measurements were repeated in order to assess the repeatability of the measurements. Variations can occur both as a result of changes in the conditions at the specific location along the profile due to the changing bottom profile and as a result of changes induced by variations in the positioning of the instruments with respect to the ripples. Generally, the agreement between the time-averaged quantities of repetitive measurements is satisfactory. It can be seen that both the high and low frequency part of the concentration signal are significant, the latter showing a stronger vertical gradient in the standard deviation. Low-frequency oscillations in the concentration signal could be induced not only by low-frequency wave groups but by ripple migration as well.

The correlation measurements A501_OPC02, A70*_OPC0* and A60*_OPC02 performed at 1 cm above the ripple tops are not included in the Figure A-27 through Figure A-30. These measurements are included in Figure A-31 though, which shows the mean concentration and the standard deviation of the total, low-pass and high-pass filtered concentration signals respectively for all measurements performed at 1 cm above the ripple tops. Figure A-32 is a comparable figure for series C in which measurements were performed at 3 cm above the ripple tops only.

4.6.3 Comparison with suction system

Since the OPCON calibration is dependent on grain-size, for each measurement the OPCON calibration needs to be corrected for the effect of the difference in grain-size as collected with the suction system in the respective measurement and the grain-size used in the calibration measurements. Based on a series of OPCON calibrations performed with varying grain-sizes in a representative range, the multiplication factor for the concentrations determined using the calibration for the bed material is roughly estimated as $D_{50}/D_{50,bed}$ with $D_{50,bed} = 129 \mu m$ (see Section 3.3.2). To check the grain size correction to the OPCON calibration, the mean concentrations are calculated with and without the corrections and results are compared with the measurements of the suction system (with the averaged results of the suction tubes on d- en w- side).

Figure 17 compares the thus determined mean concentrations from the OPCON with the corresponding values determined from the suction system with the trapping efficiency $\alpha = 0.77$ (following Bosman (1984), see Part I, Koomans and Bosboom, 2000). The dotted line is the linear fit $y = 1.02x$ through the data points ($R^2 = 0.95$). The solid line is the line of perfect agreement $y = x$. The agreement is good, especially considering the uncertainties in for example the OPCON calibration and the dependency of the calibration on the grain-size as well as the uncertainties in the trapping efficiency and the error caused by the volume measurements of the sampled sediment. Without correction for the grain-size the deviation from the line of perfect agreement is significantly larger (Figure 18). Here we have for the linear fit through the origin $y = 0.82x$ ($R^2 = 0.96$) and thus on average 20% lower values for the mean concentration from the suction system as compared to the OPCON measurements.

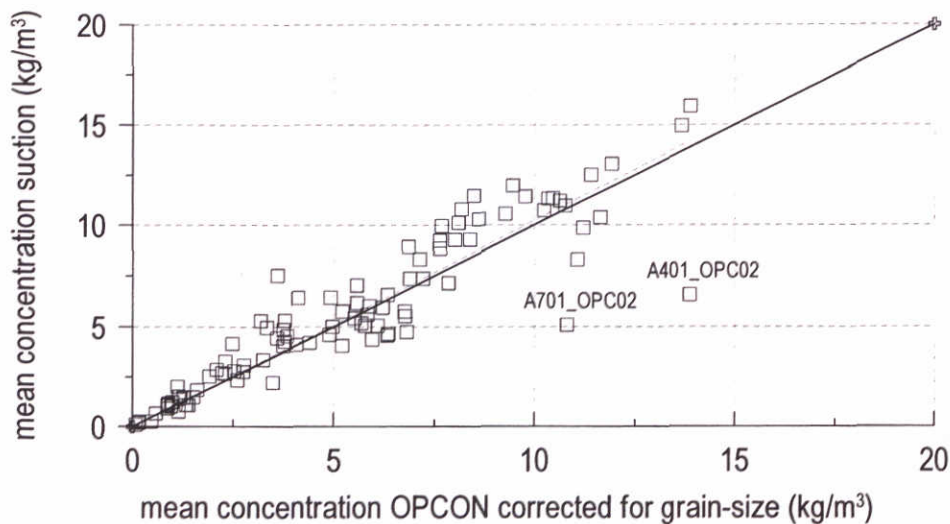


Figure 17 Comparison between mean concentration measured with the OPCON (corrected for grain-size) and determined from the suction system with $\alpha = 0.77$ for all measurements in series A

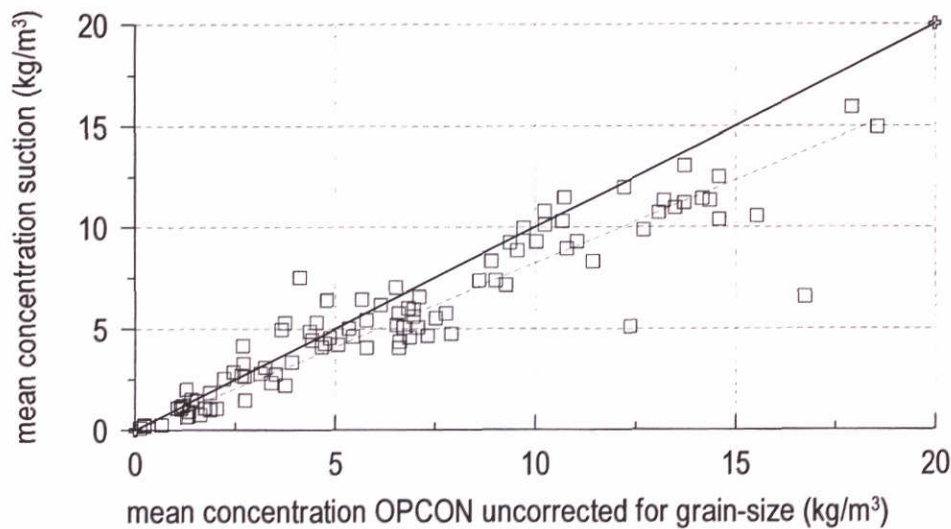


Figure 18 Comparison between mean concentration measured with the OPCON (uncorrected for grain-size) and determined from the suction system with $\alpha = 0.77$ for all measurements in series A

Two out of 96 data points in Figure 17 are significantly further from the line of perfect agreement than the other data points. For these series (see Table 23) the OpCon result is significantly higher than the suction system.

Table 23 Outliers in comparison between suction and Opcon measurements

Series name	Instrument name	finding
A401	OPC02	Concentrations by OpCon larger than by suction
A701	OPC02	Concentrations by OpCon larger than by suction

For A701_OPC02 it is likely that the Opcon series gives unrealistic results; the concentration by Opcon 2 in A701 is not in line with the Opcon and suction measurements in A70* for which the conditions are comparable to A701. The concentration by suction in A701 OpCon 2 is comparable with the concentrations in series A70*. No repetitive measurements are available to judge the concentration measurements of series A401.

4.7 Velocity

4.7.1 ADV files

Besides sampling and storage of the ADV signals by AUKE-PC via three analogue outputs, the recorded signals are also stored directly by the ADV data acquisition system. Although the time-synchronisation with the other data is lost in this case, these files contain useful information on the quality of the data, i.e. correlation and signal to noise ratio. The files can be viewed and processed using a viewer and postprocessing programme like WinADV which is public domain software. The file names of the ADV file start with the test name (for instance A101 or C204) and have the extension .ADV

Phase differences

In the analysis of the ADV data we mainly used the data sampled by AUKE-PC. Inspection of some of the ADV files showed that the data storage by the ADV acquisition system occasionally lags behind the data sampling. In those series, large spikes, not present in the AUKE-PC data, are present in the ADV data. Apparently, the local data storage of the ADV data occasionally failed (see for instance A305, carriage 1 and 2, from about 550 s onwards). When using the ADV files one should therefore carefully compare the data in the ADV files with the data sampled and stored by AUKE-PC to analyse whether for the specific series phase differences and spikes are introduced in the ADV files due to the local data storage.

Data quality

The correlation parameter can be thought of as a quality parameter for the velocity data. A correlation score is calculated for each sample stored in the ADV file, for each of the three signal beams; values are expressed in percent, with 100 being a perfect correlation. Correlations of 70 to 100 percent are typically considered good. Low correlation values may indicate problems related to turbulence, signal strength (low Signal-To-Noise Ratio, see below), scatterer density, excessive air bubbles, or problems with the probe itself.

The Signal-To-Noise Ratio (SNR) is the ratio of signal strength to the background acoustic noise level inherent in the ADV instrument. The values are given in dB relative to the noise level. For measuring oscillating velocities, the signal-to-noise ratio should be consistently above 15 dB. Low signal-to-noise ratios usually are caused by a low concentration of scatterers in the sample volume.

Typical examples of the correlation and SNR in the present experiments is given in Figure A-33 and Figure A-34. The figures show the data from carriage 1 and 2 of series A305, respectively. In the series shown in Figure A-33 ($x=23$ m, $z=9$ cm), the correlation is very high in general. We find however, a sharp decrease in correlation around 430 s, which results in a noisy velocity signal. This decrease does not seem to have any connection with either the velocity amplitude or gradient or the concentration signal. The figure also shows a rather high Signal to Noise ratio, indicating that enough scatterers are available in the water (suspended sediments).

Figure A-34 shows a rather different pattern ($x=30.5$, $z=0.5$ m). The maximum onshore velocity is of the same order of magnitude as in Figure A-33, but the velocity signal is more asymmetric. The main difference is the proximity to the bed and therefore the rather high sediment concentrations, which are an order of magnitude larger than in Figure A-33. This results in even higher SNR values. The correlation (averaged over the three beams) however drops regularly from 90% to values below 70%. A rather strong pattern can be seen; the correlation values are low during isolated events, when the velocity and concentration signals show maxima. It might be that the ADV poorly deals with either the turbulence or sediment concentration related to (sediment-laden) vortices being ejected in the flow. Note that the occurrence of suspension events rather than the magnitude of the concentrations seem to result in the drops in correlation. The low correlation events does not result in unacceptably noisy velocity signals.

For A305.ADV the local storage of velocity values failed (from 550 s onwards). From 550 s onwards, spikes and phase differences are introduced in the ADV file A305, which are not found in the AUKE-PC files. The quality parameters (correlation and SNR) are still high in the part of the series where local storage of velocity values failed. We can therefore use the ADV quality parameters to get a general idea of the quality of all series. When filtering the samples using a criterion that the correlation should be higher than 70 we find that 99.6 and 94 percent of the samples fulfil this requirement, for carriages 1 and 2 of series A305, respectively.

For the other tests in series A, the quality of the series is shown in Figure A-35. The time-averaged correlation, averaged over the three beams is indicated by the squares. The correlation values are generally higher than 85. The percentage good (%) is indicated in the figure by rounds. It refers to the percentage of the samples fulfilling the requirement that the correlation score is higher than 70% and the Signal-To-Noise Ratio > 15 dB. The lowest values on correlation and percentage good are found for the A101 through A104 series, for which a 6 mm sampling volume and a 10 cm/s velocity range was chosen, instead of a 9 mm sampling volume and a 30 cm/s velocity range.

As argued above, differences in the quality of the ADV data in the various series are likely to be related to either the turbulence or sediment concentration related to (sediment-laden) vortices being ejected in the flow from the rippled bed. From Figure 19, it can be seen that close to the bed the percentage good and the average correlation score are generally lower, than further from the bed (especially above ~3 cm) the quality of the ADV data is very high. No obvious relation was found between the time-mean concentration and the data quality.

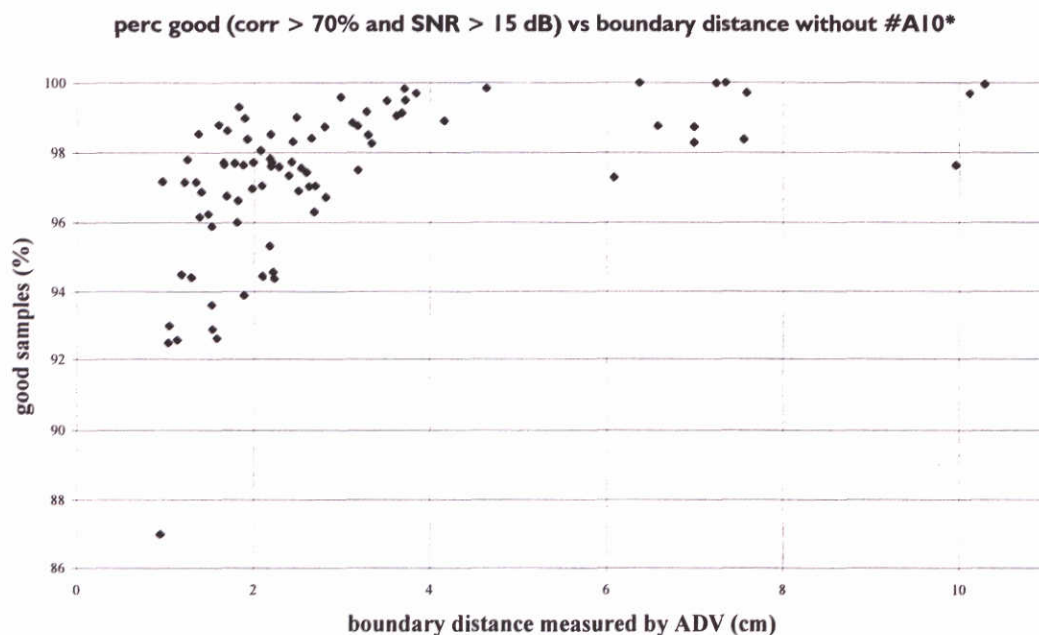


Figure 19 Percentage of samples with correlation > 70% and SNR > 15 Db as a function of the distance from the bed as measured by the ADV.

For the C-series, Table 24 shows the averaged quality parameters. The values are sufficiently high. Note that all measurements in the C-series were performed at a relatively high level above the bed ($z = 3$ cm). For series C101, an ADV-file of only 400 s was recorded. An error was found when trying to read ADV-file of series C403. In this test, also the AUKE-PC files showed a malfunctioning ADV (see 4.7.2).

	Perc good (%)	Average correlation (%)	Average SNR (dB)
c201	96	89	43
c202	100	95	38
c204	99	94	41
c301	100	94	42
c302	99	92	42
c303	98	91	42
c304	98	90	41
c402	98	93	40
c403	97	91	43

Table 24 Quality of ADV signals in C-series: Percentage good (%), averaged correlation (%) and SNR (dB)

4.7.2 Spike detection filter

In our analysis we have mainly used the AUKE-PC files, which were first filtered in order to remove any spikes on the velocity signal. The velocity-spike filter attempts to identify individual velocity readings in the time series that exhibit consecutive large and opposite changes in velocity direction and magnitude relative to adjacent velocity data. The differences are compared to a user-specified threshold. This filter was developed by the New Zealand Institute for Water and Atmospheric Research and used in WinADV in a slightly modified version. Here we have implemented the spike detection filter following the WinADV version. This filter is well suited to data sets that have good signal-to-noise ratios, but suffer from low correlation scores due to turbulence. The filter is implemented in Matlab as follows:

Given three adjacent velocity measurements at sample numbers $n-1$, n , and $n+1$:

$$(u, v, w)_{n-1}; (u, v, w)_n; (u, v, w)_{n+1}$$

For each component, compute the two accelerations. For the u -component this reads:

$$A_{1,u} \frac{(u_n - u_{n-1})}{\Delta t}; A_{2,u} \frac{(u_{n+1} - u_n)}{\Delta t}$$

Take the difference between them to obtain the change in acceleration ΔA_u from sample $n-1$ to sample $n+1$. If they are of opposite signs, then they indicate a spike and their magnitudes will be additive in the subtraction process. If the two accelerations are of the same sign, then they tend to cancel one another out in the subtraction process because the two accelerations were similar and do not indicate a "spike", but rather a relatively uniform acceleration.

These calculations are repeated for each velocity component. Then these acceleration-change components are used to compute a scalar change in acceleration:

$$\Delta A = \sqrt{\Delta A_u^2 + \Delta A_v^2 + \Delta A_w^2}$$

If ΔA exceeds the threshold specified by the user then sample n is a spike and should be removed from the data set. The threshold was determined iteratively at $0.2g$, with the gravitational acceleration. With this threshold we were able to remove the majority of the spikes in the series with lower correlation parameters, whereas instantaneous values and the time-mean parameters (mean, standard deviation) in the series with very low percentages of spikes remained unaffected. We typically detect a few percent of the total samples as spikes, with a maximum up to 10%. The effect of the spike filtering on the time-mean parameters of the series is limited; even in the case of 10% spikes, the effect on mean and standard deviation of the series is $\sim 1-4\%$.

In the C-series low percentages of spikes are found (in the range of 1 to 7%), with the exception of #C401 in vertical 1 (30%). On further inspection, it was found that for #C401_ADV01, the ADV malfunctioned, possibly due to insufficient water depth.

The velocity related A***.DAT and .SEQ files which are the basis of the AUKE-PC analysis are not directly obtained from the raw data files but from files named Z***.DAT and .SEQ. The raw data are first filtered with the spike detection filter. These filtered data are stored in the Z***.DAT and .SEQ files. In converting the Z*** files to the A*** files, the calibration correction for ADV02 is taken into account.

4.7.3 Results

Velocity profiles

Some characteristics of the vertical velocity profiles in series A are shown in Figure A-36 through Figure A-39. Note that for the position shoreward of the breaker bar crest ($x = 25.5\text{ m}$), in this figure the A70* series ($x = 25.46\text{ m}$) are not taken into account. Figure A-36 and Figure A-37 show the vertical profiles of undertow and the standard deviation of the horizontal velocity signal, respectively. The increase in standard deviation of the velocity signal towards the bed, is likely to be related to the increased turbulence in the wave boundary layer. The results at $x = 20.5\text{ m}$ consists of data from carriage 1 in the A20*, A40* and A60* series. For this location some variability in surface elevation (Figure A-26) and velocity data can be found between repetitive tests, but is not as clear as for instance $x = 28\text{ m}$: two points in that vertical show a consistently lower standard deviation than the other points. These points correspond to runs A308 and A309, for which also the energy content of the surface elevation is lower than for the other series (A20*), due to variation in bed level. For results on the standard deviation of the low-pass filtered and de-meanned velocity and high-pass filtered velocity signal, respectively one is referred to Bosboom et al. (1999).

Figure A-38 and Figure A-39 show the vertical profiles of mean and standard deviation of the vertical velocity signal, respectively. Figure A-38 shows that a non-zero mean vertical velocity is found. This will be treated in the section below.

Scatterers and vertical velocities

In the experiments we systematically found a downward time-mean velocity of maximum 1 cm/s, whilst one might expect a zero time-mean velocity. A possible reason for deviations from zero may be the existence of large-scale turbulent structures in cross-wise direction of the flume. Next, horizontal gradients in hydrodynamic conditions or the sloping bed (or, equivalently, instrument tilt) could attribute to a time-mean nonzero velocity. However, when estimating the magnitude of the velocities introduced by horizontal gradients in wave energy due to wave breaking, we arrived at values of maximum ~ 1 mm/s, which is an order of magnitude smaller than the measured time-mean vertical velocities. Also the slope of the bed or instrument tilt is not large enough to explain the vertical velocities: we measured above 4 cm from the bed vertical velocities in the order of $1/10$ of the u -velocity, and closer to the bed $1/20$ of the u -velocity. The global slope of the bed however varies from $1/40$ to $1/140$, only getting as steep as $1/25$ on the seaward slope of the breaker bar. The effect of settling velocity (~ 1 cm/s) could also attribute to the measured time-mean velocities. Particles in the flow reflect acoustic signals back to the probe receivers. The ADV probe actually measures the velocity of the scatterers in the flow. Microbubbles of air can be effective scatterers. In our experiments however, the sediments suspended in the flow act as scatterers as well. This means that we are measuring scatterer/sediment velocity instead of water velocity. In horizontal directions the sediment velocity may be assumed equal to the water velocity. In vertical direction however, we have to take the sediment settling velocity into account. At the moment this effect seems the most likely explanation for the nonzero time-mean vertical velocities. In Figure 20, the measured time-mean velocities (series A) are shown versus the sediment settling velocities of the corresponding sediment samples obtained by the suction system. It can be seen that on the basis of this figure, no conclusive relationship can be found between the time-mean vertical velocities and the settling velocities. The figure shows vertical velocities which are generally smaller or equal to the settling velocity. However, the vertical velocities and the settling velocity are of the same order of magnitude. Besides, since the sediments are not the only scatterers in the flow, it could be expected that the measured vertical velocities can reach values up to the settling velocity, but are generally smaller than the settling velocity, especially when large amounts of other scatters are present, such as air bubbles or the very fine material in the flow. Besides, the amount of suspended sediment in the flow, is highly variable during the wave half-hours.

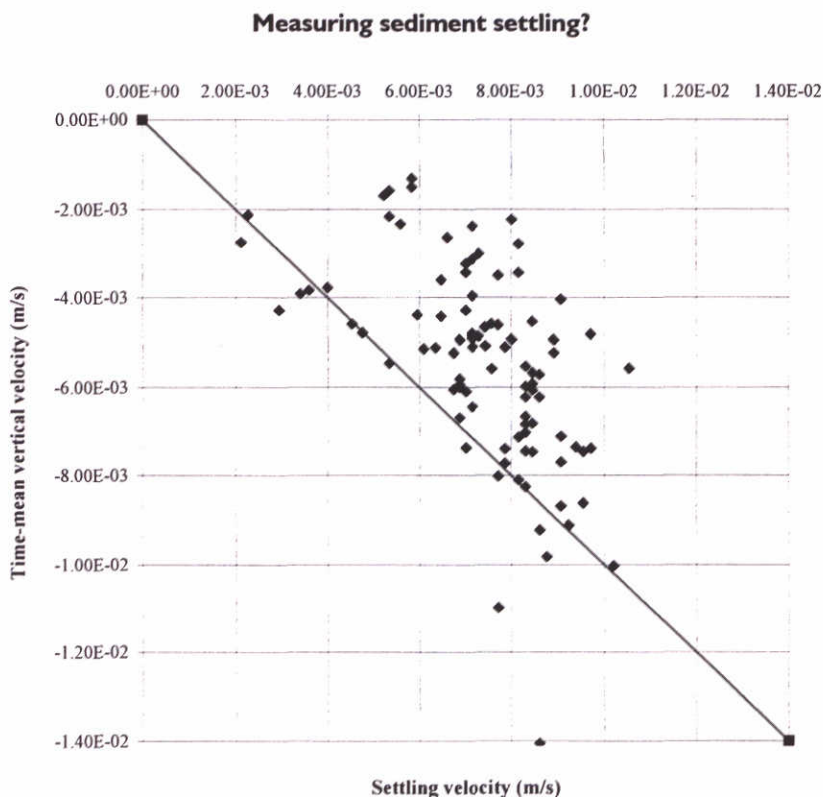


Figure 20 Time-mean vertical velocity versus settling velocity

Variation along flume

Some characteristic time-averaged quantities are given in Figure A-40 through Figure A-43 as a function of the position along the flume. For these figures, the choice was made to use the signals recorded at 3 cm above the ripple crests, since for that elevation data are available in both series A and C. Figure A-40 and Figure A-42 show the mean and standard deviation of the horizontal and vertical velocity for series A and C, respectively. The mean velocity (upper plot) is primarily due to the undertow, induced by wave breaking and can be seen to become larger in magnitude throughout the surf zone. In Figure A-41 and Figure A-43, the horizontal velocity moments according to Section 4.4.2 (Table 16 and Table 17) are shown for series A and C, respectively. It can be seen that the results of series A and C compare well. For more in depth information about the velocity moments and their relevance to cross-shore sediment transport, one is referred to Bosboom et al. (1999).

4.8 Sediment fluxes

In Figure A-44 and Figure A-45 time-averaged sediment fluxes are shown at 1 and 3 cm above the ripple tops for series A and C, respectively. In the figures, a distinction is made between total fluxes and mean flow, long wave and short wave related fluxes defined according to Section 4.4.4 (Table 18). In Figure A-46 through Figure A-49 the sediment flux profiles are shown, for total, high-frequency, low-frequency and current-related fluxes, respectively. All figures, clearly show the variability in the results in 'repetitive tests'.

The detailed treatment of the results on sediment fluxes is not the subject of this data report (see Bosboom et al., 1999 for that). However, the comparison between net transport rates derived from profile deformation and from integration of the net flux profiles of series A, may yield important information about validity of the data. Therefore, this comparison is shown here (Figure A-50). In this figure, we see besides sediment transport rates, the time mean load. *Note that for this figure, the effect of grain-diameter on the OpCon calibration is taken into account, as opposed to the other results in this report.*

In order to obtain the time-mean load along the profile, the time-mean concentration profiles are integrated over depth (see Figure A-50 upper plot). On visual inspection of the mean concentration profiles, it appeared that all but the profiles for the two most shoreward stations are closed well. The load might therefore be somewhat underestimated for these two stations. It can be seen that the load increases as the wave shoal, reaching a maximum around the top of the bar where the highest waves are breaking, from where on, despite the increased turbulence in the surf zone, the load decreases with decreasing wave height.

Net transport rates have been inferred from profile deformation by applying the continuity equation for the sediment volume assuming the porosity of the bed material to be constant (see Part I, Koomans and Bosboom, 2000). The thus derived transport rates are shown in Figure A-50 (second plot, drawn line) for which the measured bottom profiles after about 8 and 26 hours respectively were used. In addition, the time-averaged transport rate has been computed as the time- and depth-averaged sediment flux, given by:

$$\langle q \rangle = \frac{1}{(t_2 - t_1)} \int_{t_1}^{t_2} \int_{z_b}^{z_s} u(x, z, t) c_v(x, z, t) dz dt,$$

where z_s is formally the water level and practically the elevation of the highest measuring point, u the horizontal velocity and c_v the volume concentration of sediment. Figure A-50 shows, besides the net transport rate inferred from profile deformation, the transport rates computed from integration of the fluxes. The agreement between the two is striking; apparently we are able to account for the majority of the transport when using the measured suspended sediment fluxes. Note that for the two most shoreward measuring locations the concentration does not completely vanish for the highest measuring point, such that we can expect that at those locations the transport rates inferred from the flux profiles underestimate the actual transport rates. This however cannot explain the shift in the maximum transport, which for the transport rates inferred from the flux profiles occurs at deeper water. The total flux from the flux profiles can be decomposed into mean flow related, long wave related, and short wave related transport. The respective contributions to the net transport rates are shown in the third plot of Figure A-50. It can be seen that the mean flow related transport is the most significant component for the larger part of the profile, especially in the outer breaker zone where the wave-generated undertow is combined with a high suspended load. Seaward of the point of initial breaking however, the small but dominant short wave related transport results in a small onshore transport. It can be concluded that outside the breaker zone the prediction of the transport direction by any transport formulation is critically dependent on the proper representation of relatively small terms.

5 Conclusions and recommendations

The data presented in this report were obtained and analysed within the framework of the EU-sponsored MAST-III SAFE project. The measurements of hydrodynamics, suspended sediment concentrations, sediment transport and radiometry were carried out on a natural 2DV beach under erosive conditions in WL|DELFT HYDRAULICS' Scheldt flume. Besides dune sand (series A), also various mixtures of dune sand and heavy minerals were used to investigate selective transport phenomena of minerals with a different density (series B through D). Time-mean sediment concentrations, radiometry (bed composition), bed profile evolution (data report part I: Time-averaged measurements (Koomans and Bosboom, 2000) and time-dependent measurements (surface elevations and time-dependent velocities and sediment concentrations at one elevation above the bed; data report part II: Time-dependent measurements (Bosboom and Koomans, 2000) were measured for all mixtures.

Random waves were generated by a wave board equipped with an active wave absorption system (Klopman, 1995), such that at the same time waves were generated and reflected waves were absorbed. The latter prevented the re-reflection of free, long waves travelling offshore towards the wave board. The incident wave conditions at deep water (water depth $h = 0.7$ m) and geometry are $H_{m0} = 0.17$ m and a peak period $T_p = 2$ s.

The following instruments were deployed for time-averaged and time-dependent measurements: transverse suction system, wave height meters (WHM), Optical concentration meter (OPC), Acoustic Doppler Velocity meter (ADV). Most of the instruments that were operated during the runs were situated on a measurement carriage. Since the general objectives of the A and C series differed, special assemblies were used for each experiment.

The free surface elevation, with respect to still water level was recorded continuously with wave height meters (WHM). Four resistance-type twin-wire WHM's were placed in the model at the following locations. The locations were chosen such that in principle the incoming bound, incoming free, the reflected free and reflected bound components may be separated. Besides the four wave gauges at a fixed position, two wave gauges were located on the measurement carriages.

During the operation quantities were measured by a number of instruments attached to two movable carriages. Moreover, four wave-gauges at a fixed position throughout the experimental programme measured the water elevation. The instruments on the carriage measured at a fixed horizontal and vertical position for about half an hour and were then moved to other locations. During each wave half-hour, exactly the same steering signal was used. The aim of this procedure was to use subsequent measurements to resolve the conditions at several locations at the profile and several distances from the bed, as if the measurements were made simultaneously. In order to assess this assumption of repeatability of the conditions, several point measurements were repeated. Variations can occur both as a result of changes in the conditions at the specific location along the profile due to the changing bottom profile and as a result of changes induced by variations in the positioning of the

instruments with respect to the ripples. From the comparisons made in these reports it appears that the variations in the time-mean parameters are small.

In Series A, the focus was on the collection of instantaneous velocity and concentration data at several locations along the beach profile and for varying distances from the sandy bed. The set-up of the measurement programme was so as to enable the identification of the spatial correlation (in both horizontal and vertical direction) of concentration, the time-dependent near-bottom response of the concentration to water velocity and the contribution of the various velocity components to the sediment fluxes. Series A consisted globally of two parts. The first part aimed at collecting data at various heights above the bed at eight selected horizontal positions ranging from the shoreline up to the toe of the profile. In the second part of series A, the focus was on horizontal correlation measurements. In those series the elevation of the instruments was 1 cm above the ripple crests. The first carriage was located in the same vertical (same x-position) during all half-hour tests, whereas the second carriage was moved after every half-hour. Carriage 2 was first placed 15 cm onshore from carriage 1 and the final position was 70 cm from carriage 1. This procedure was performed at two locations at the profile.

Series B focused on the selective transport of placers of Zircon. Thin layers of Zircon were placed at several x-positions on the single-barred final profile of series A. In these experiments only the sediment profile and composition was measured.

The C-series aimed at measurements of selective transport processes. The series started again from a 1 in 40 beach, in which the upper 10 cm of the bed consisted of a mixture of 60% sand and 40% Zircon by mass. During runs hydrodynamic parameters and sediment concentrations were recorded; in between the runs, profile and sediment composition were measured.

The objective of the D-series was to test a new device to record "friction" sound. These experiments were carried out with still water on the end profile of Series C.

At specific time intervals (mostly the end of the day) profile measurements were conducted by an automatic sounding system. From these profiles, sediment transport rates could be inferred, such that the measurements can be used for sediment transport model and morphodynamic model verifications.

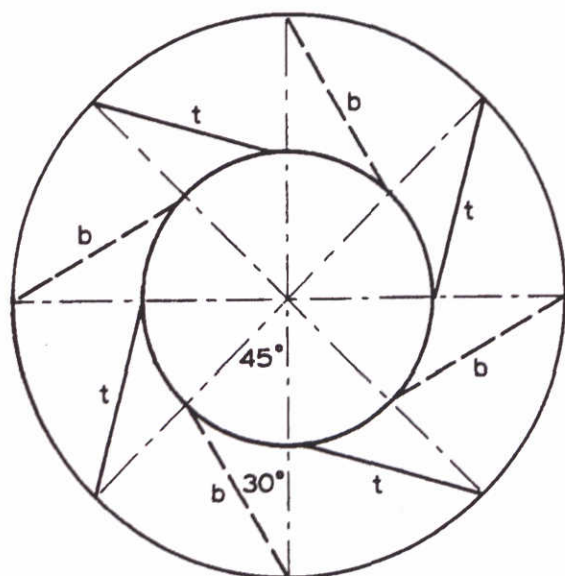
In the presented reports attention was paid to the calibration and validation of the measurements. A first analysis of the time-dependent results (Bosboom *et al.*, 1999) aimed at identifying the relative importance of mean flow, long and short waves to the net sediment fluxes and transport. The recommended next steps are the actual in-depth analysis of the sediment response, the horizontal and vertical structure of velocity, concentration and sediment fluxes. Also parts of the time-averaged measurements are analysed (Koomans *et al.*, 1999) with attention to the distribution of the heavy mineral concentrations. Future research on the effects of density gradation will focus on the transport mechanisms and transport modes of the different minerals and will aim to describe the processes responsible for heavy mineral placer formation. The experiments to test a new instrument to determine

median grain size from measured “friction” sound are analysed in depth and will be published.

References

- Bosboom, J., R.L. Koomans and A.J.H.M. Reniers (1999): Laboratory Experiments on Suspended Sediment Concentration and Fluxes, *Proceedings Coastal Sediments 1999*, Long Island, USA : 179-194.
- Bosman, J.J. (1981). Optical measurements for sediment concentration, Statistical aspects of particle observation. Report on investigation R716, part IV., WL/Delft HYDRAULICS
- Bosman, J.J. (1984). Calibration of optical systems for sediment concentration measurements, Report on investigation R716, part V., WL/Delft HYDRAULICS
- Bosman, J.J. et al. (1987). Sediment concentration measurements by transverse suction. *Coastal Eng.*, Vol. 11: 353-370
- Dean, R.G. and Dalrymple, R.A. (1984). Water wave mechanics for engineers and scientists. Advanced series on Ocean Engineering, Volume 2. World Scientific Singapore: 353 pp.
- Katopodi et al. (1994). Intra-wave sediment transport in an oscillatory flow superimposed on a mean current. Data report H1684.33, WL/Delft HYDRAULICS
- Klopman, G. (1995). Active wave absorption, Digital control systems for wave channels based on linear wave-theory. Report on desk study, Part II. Report H1222, WL/Delft HYDRAULICS
- Klopman, G. (1998). Personal communication
- Koomans, R.L., J. Bosboom, R.J. de Meijer and L.B. Venema (1999): Effects of Density on Cross-Shore Sediment Transport, *Proceedings Coastal Sediments 1999*, Long Island, USA : 313-324.
- Koomans, R.L. and J. Bosboom (2000): Laboratory experiments on sediment dynamics and density gradation: Part I, time-averaged measurements.
- Roelvink and Stive (1989), Bar-generating offshore flow mechanisms on a beach. *Journal of Geophysical Research*, Vol. 94, No. C4, pp: 4785-4800.
- Venema, L.B., de Meijer, R.J., van Os, B. and Gieske, J.M. (1999), In-situ characterisation of coastal and river sediment. COPEDEC 99, 1 (Ed. By G.P. Mocke), Cape Town, South Africa: 324-334

A Figures

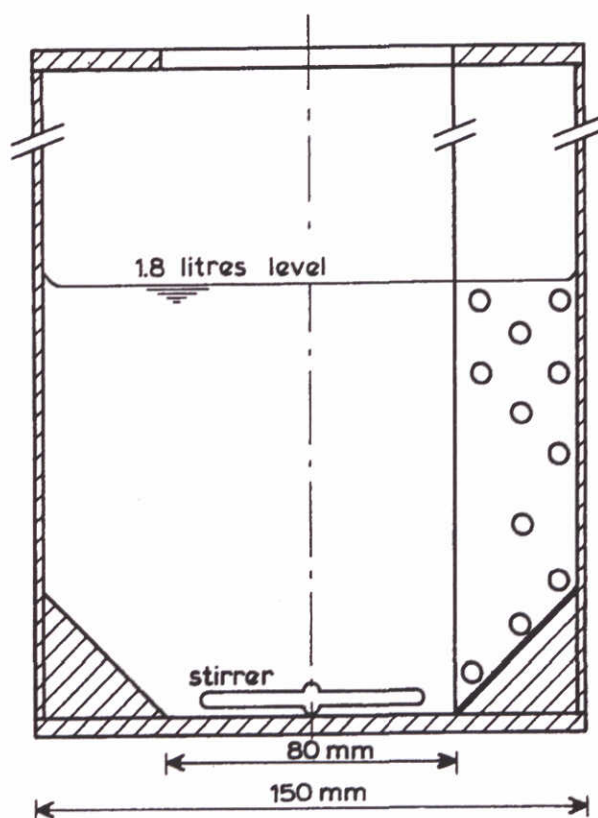


partitions :

b = bottom

t = top

TOP AND BOTTOM
HORIZONTAL CROSS -SECTION



330 mm

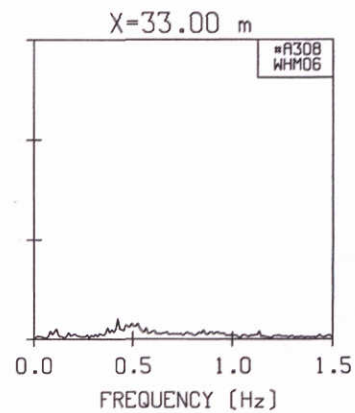
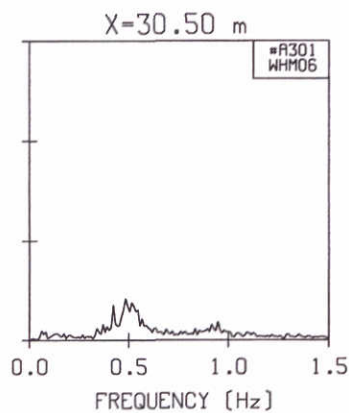
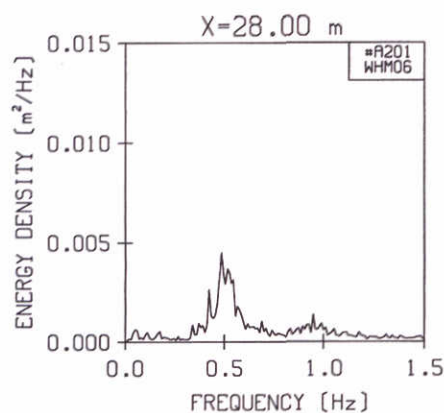
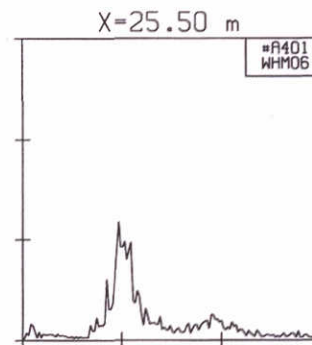
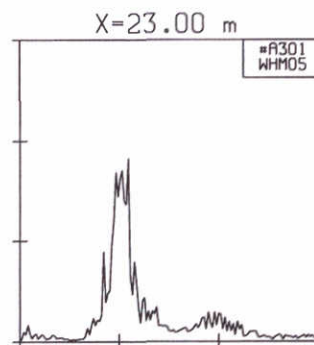
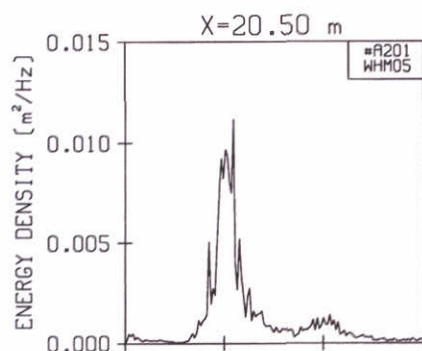
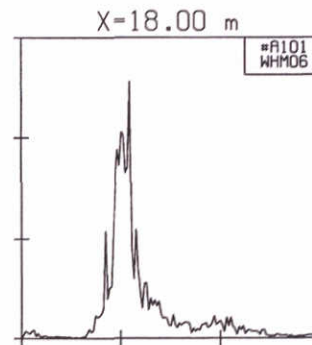
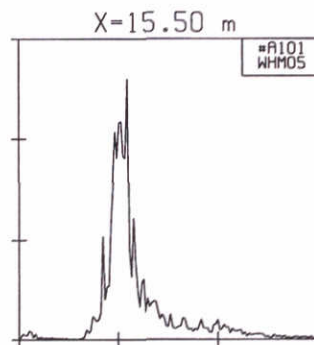
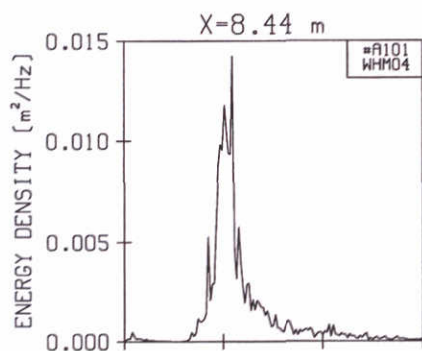
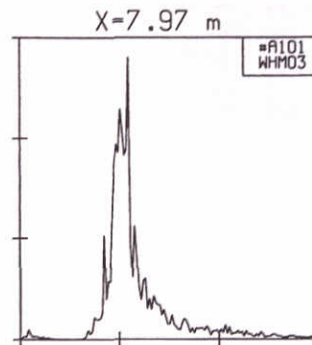
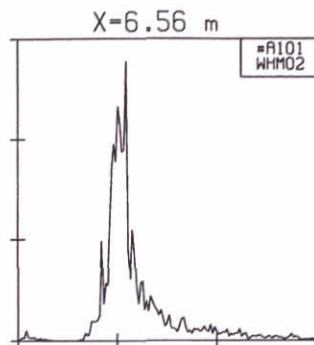
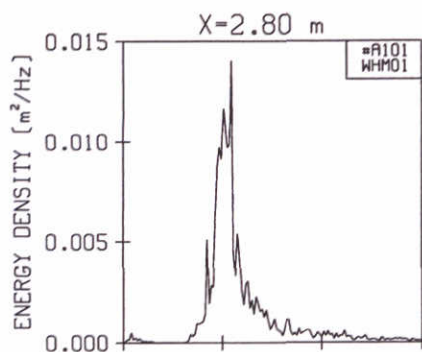
VERTICAL CROSS - SECTION

SCHEMATIC DRAWINGS OF SUSPENSION VESSEL

WL|DELFT HYDRAULICS

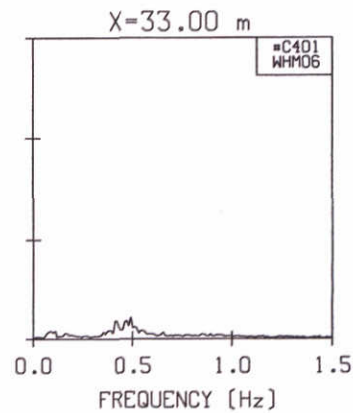
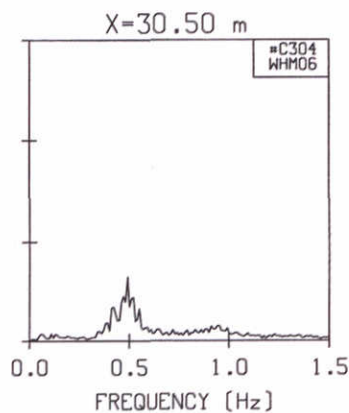
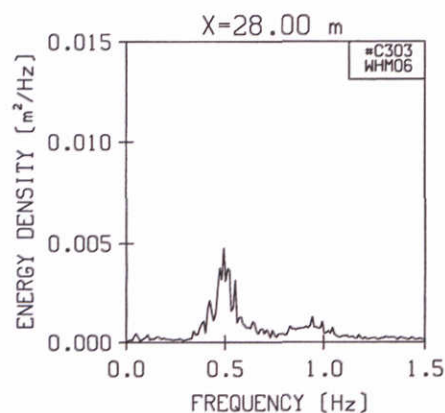
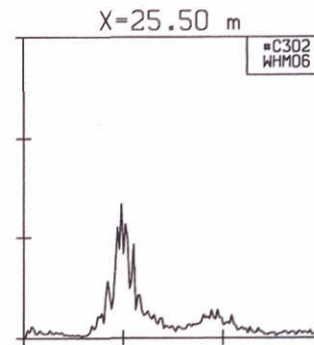
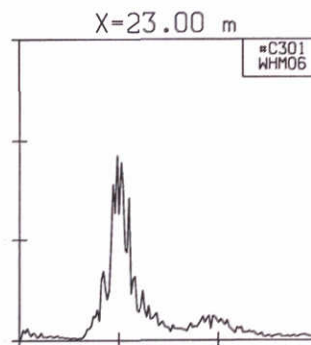
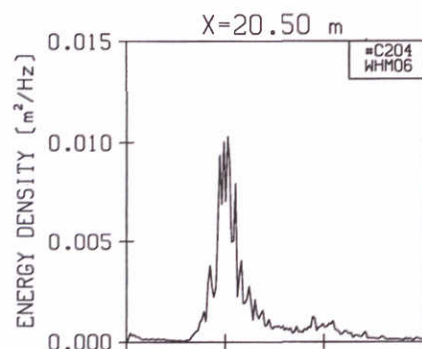
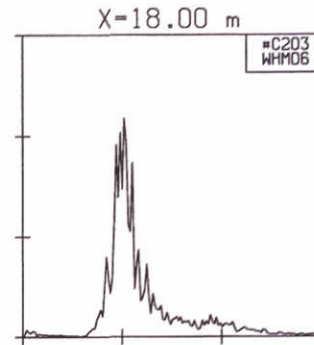
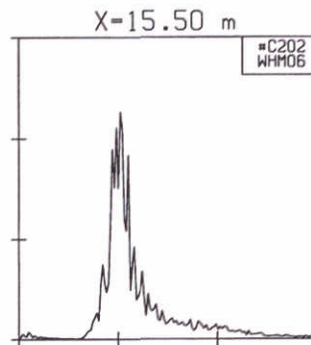
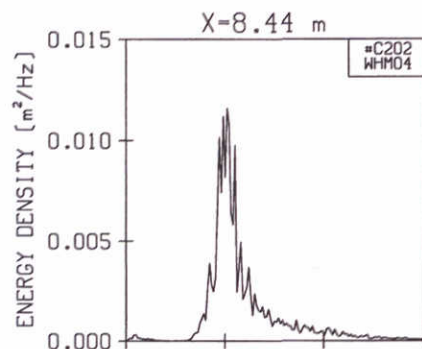
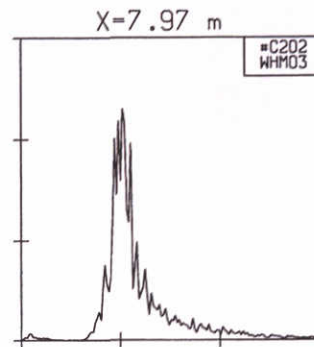
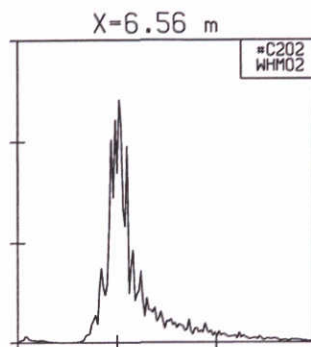
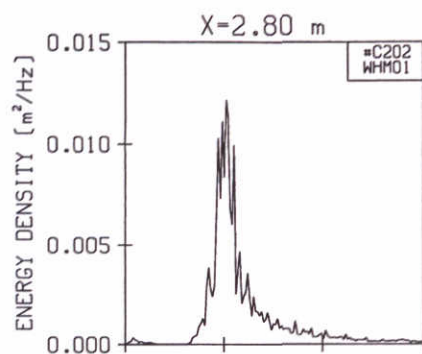
H 2305

FIG. A21



SURFACE ELEVATION SPECTRA

SERIE-A



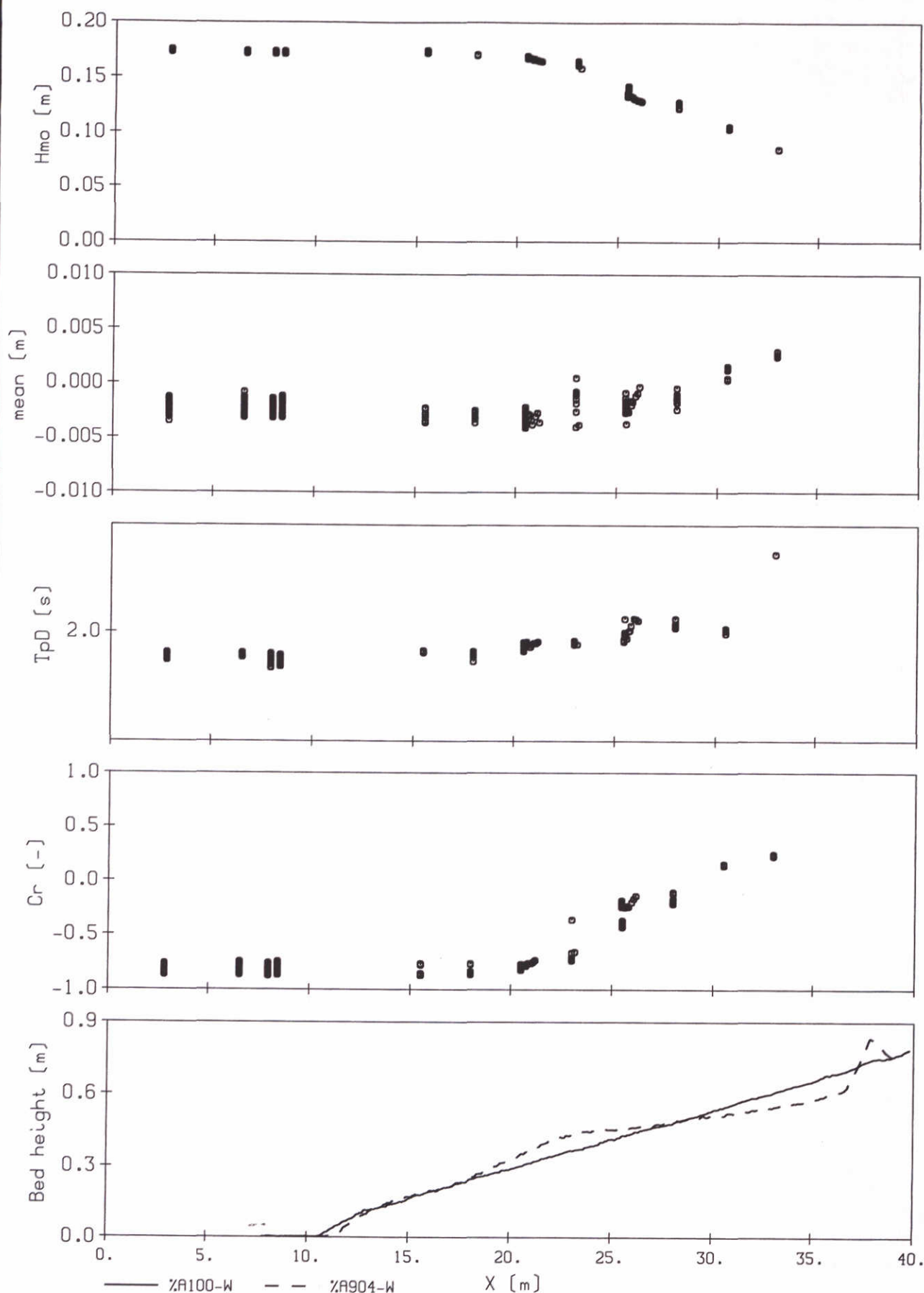
SURFACE ELEVATION SPECTRA

SERIE-C

WL | DELFT HYDRAULICS

H2305.70

FIG. A23



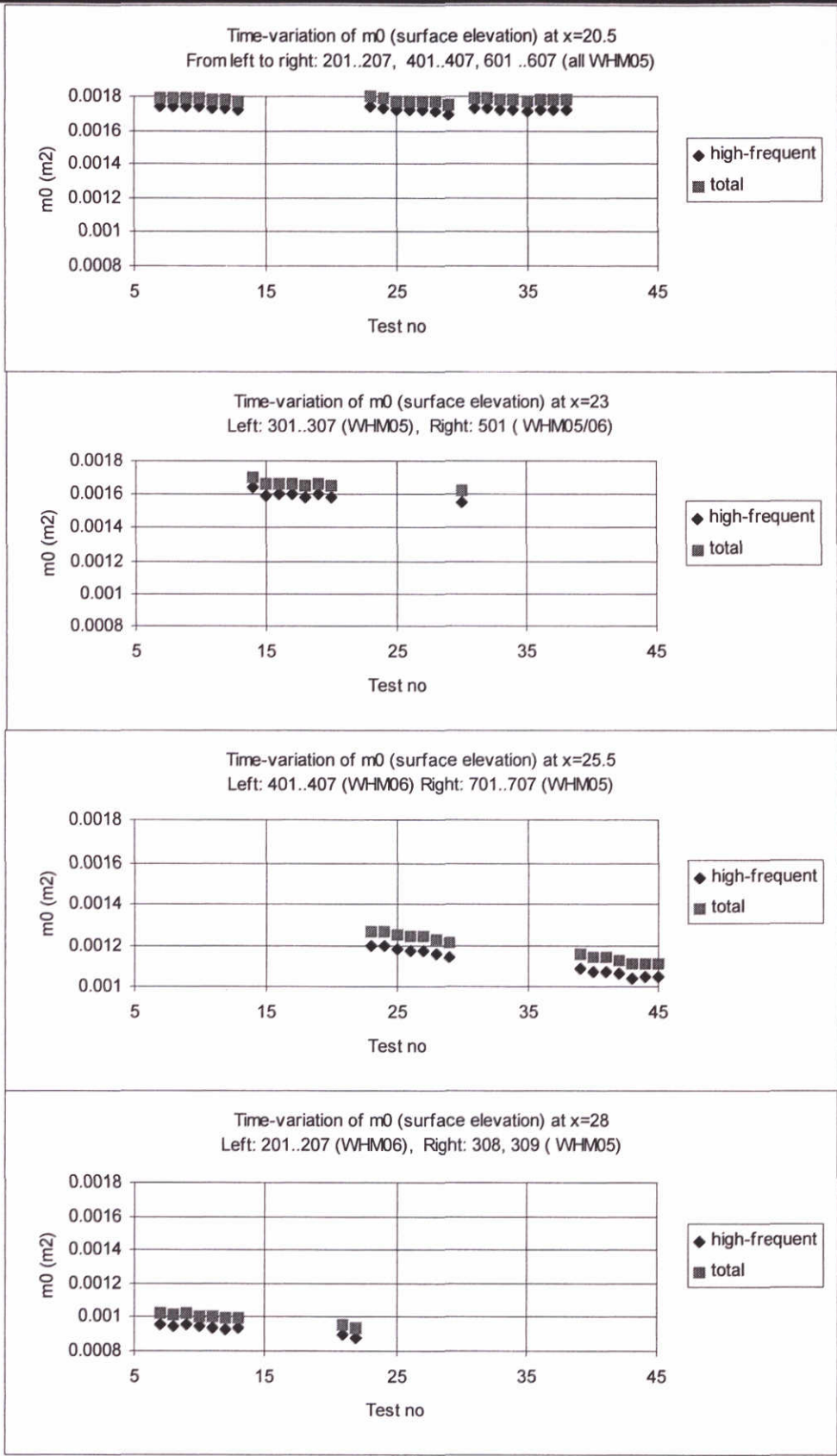
INTEGRAL SURFACE ELEVATION DATA
(UNSELECTED AND UNCORRECTED)

SERIE-A

WL | DELFT HYDRAULICS

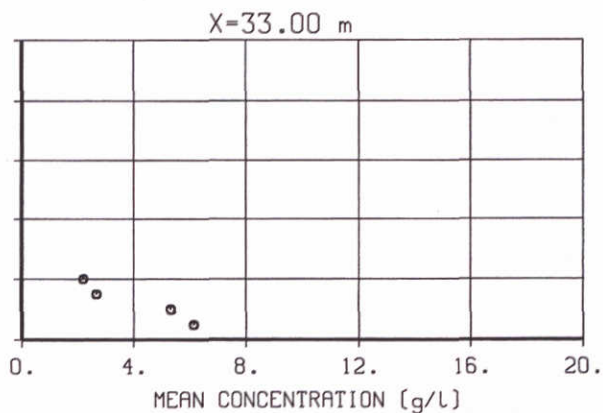
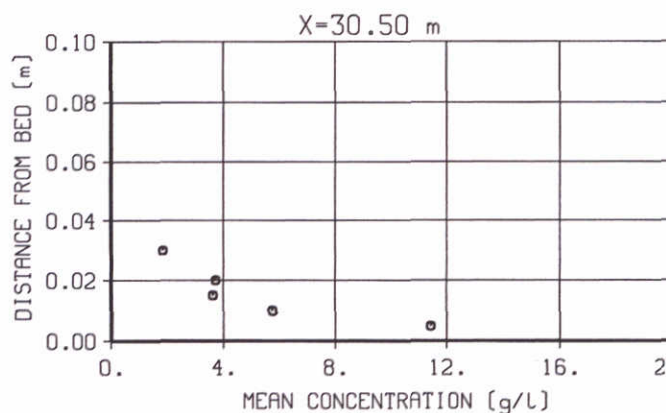
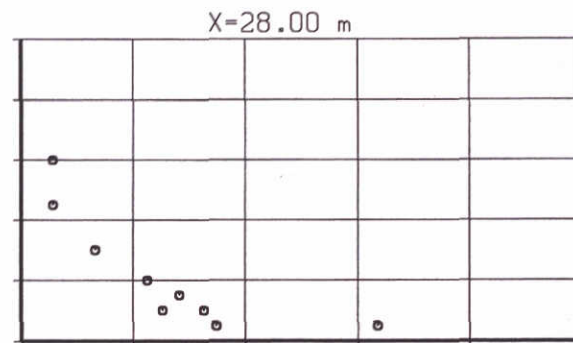
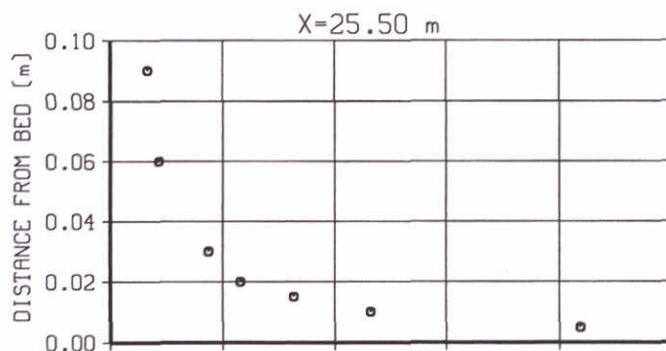
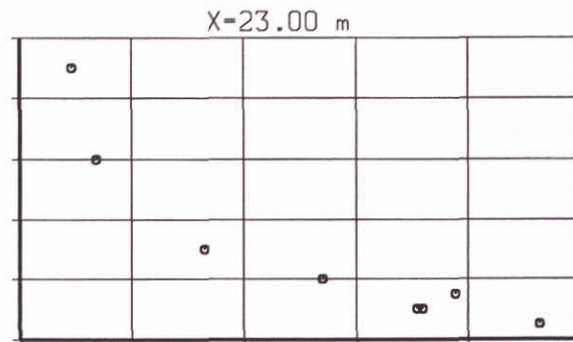
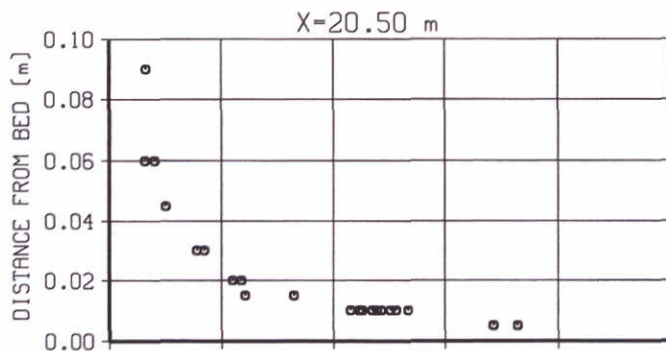
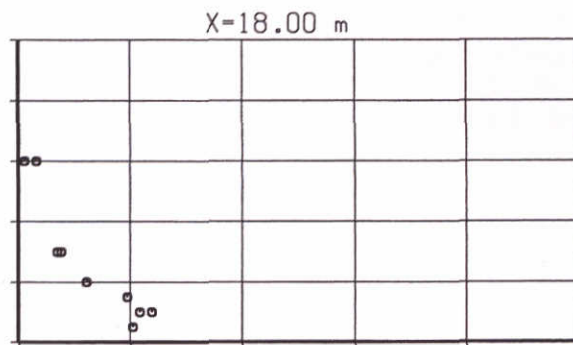
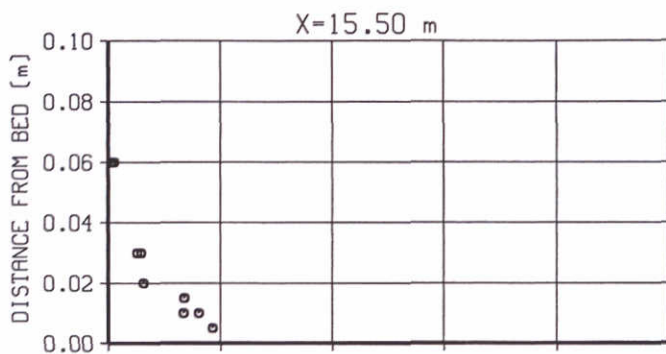
H2305.70

FIG. A24



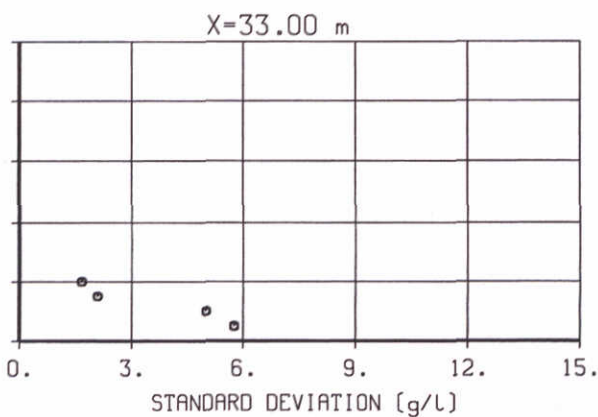
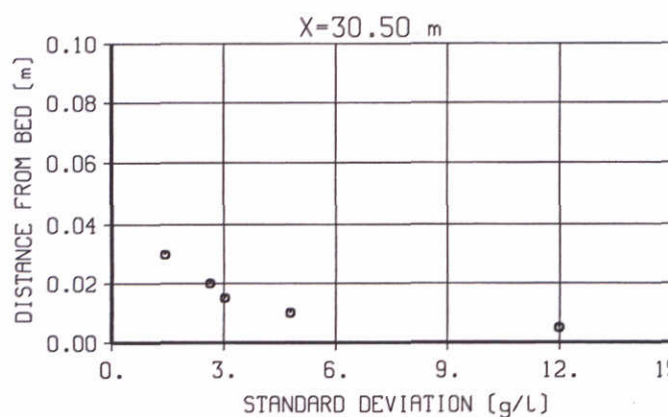
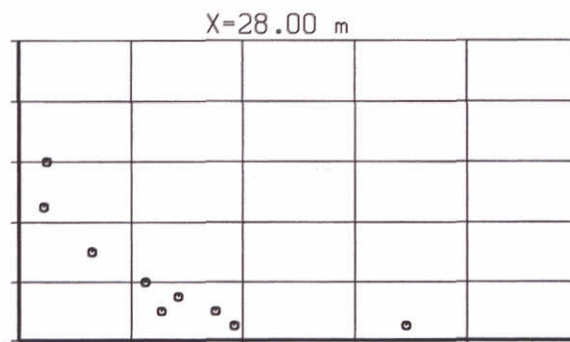
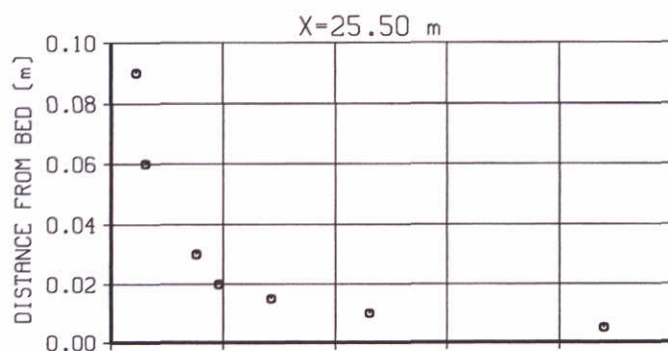
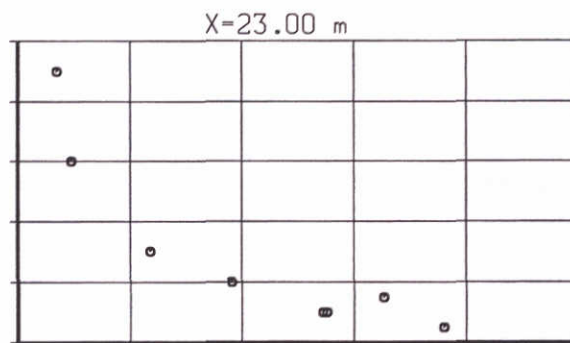
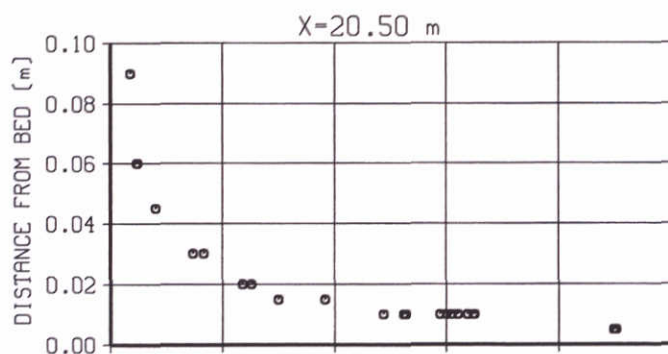
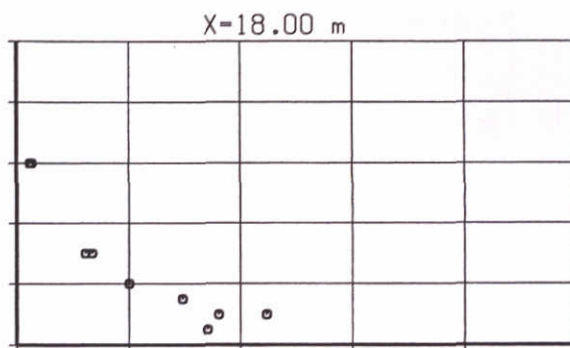
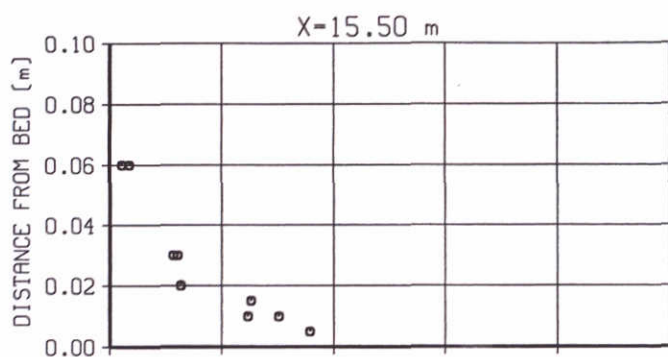
Time-variation in m_0 of surface elevation spectra

Series A



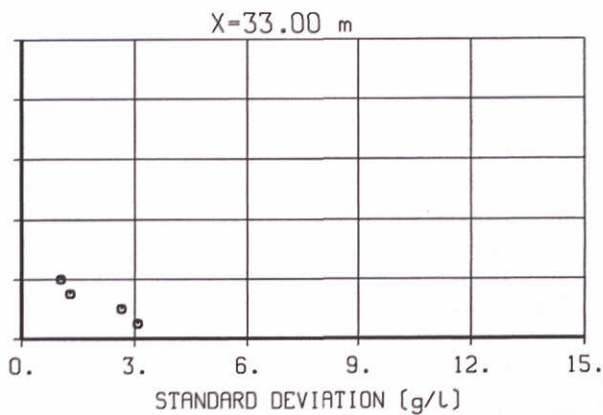
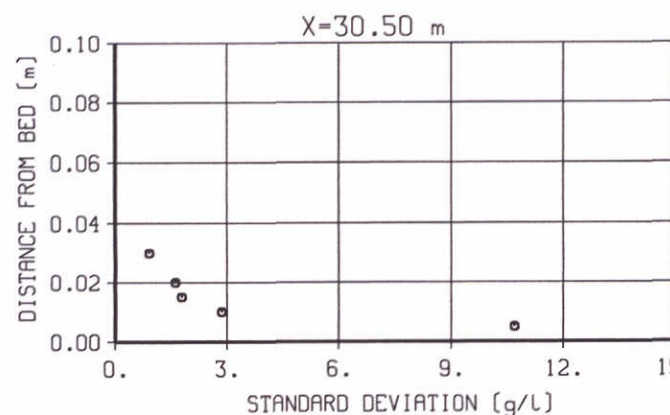
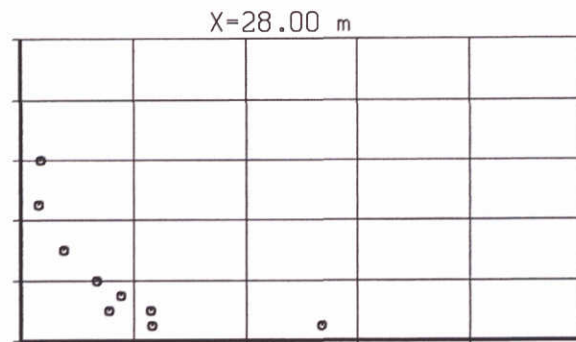
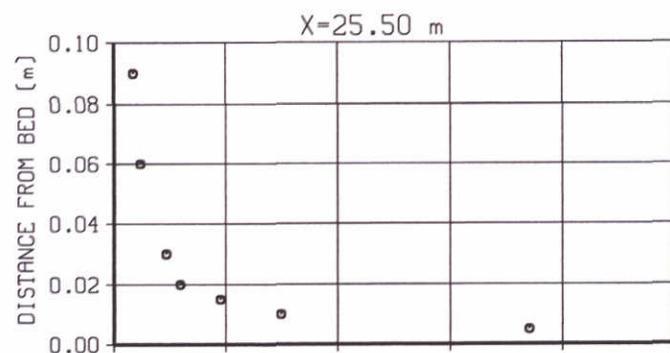
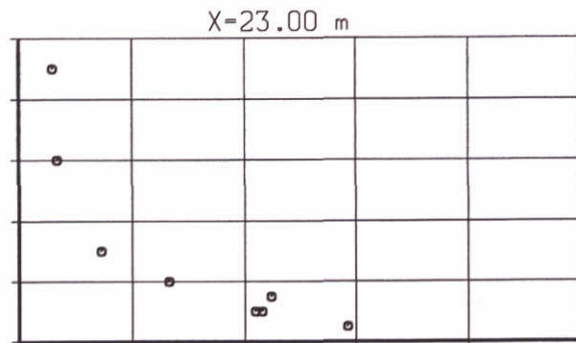
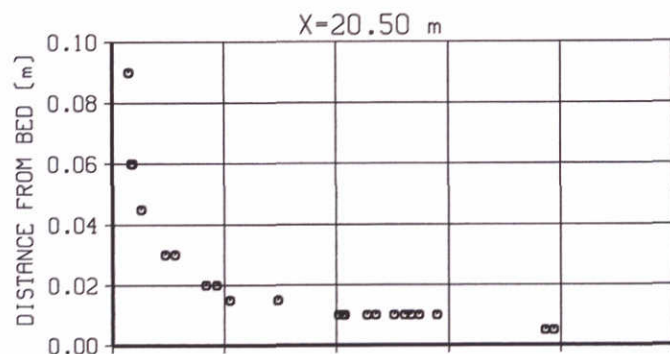
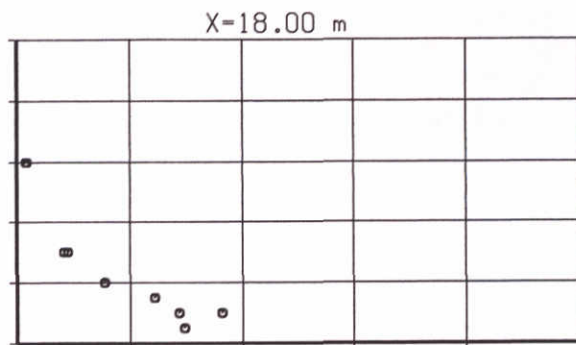
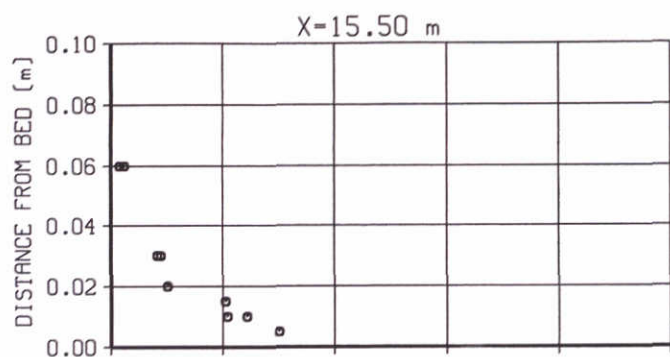
MEAN CONCENTRATION MEASURED BY OPCON
WITHOUT GRAIN-SIZE CORRECTION

SERIE-A



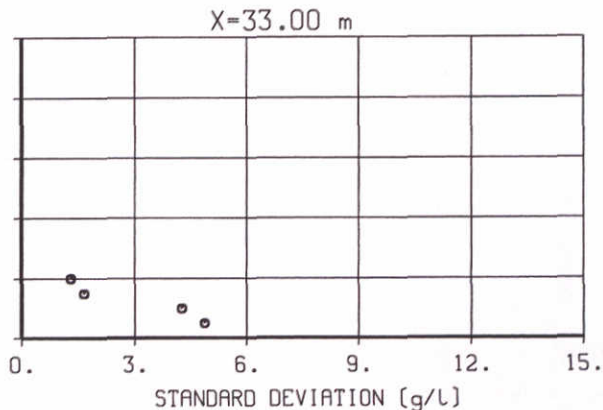
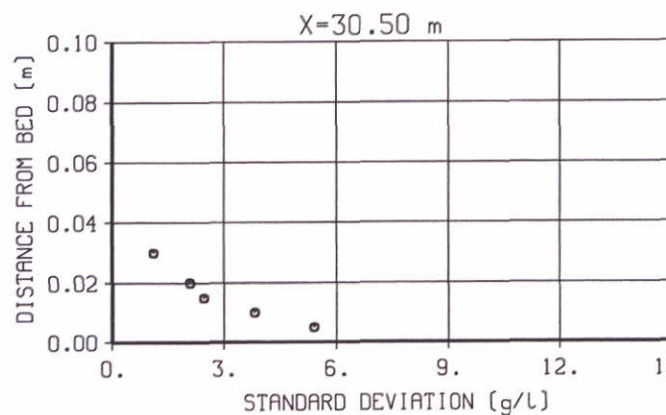
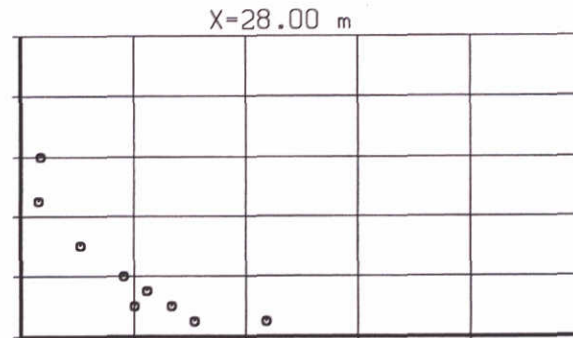
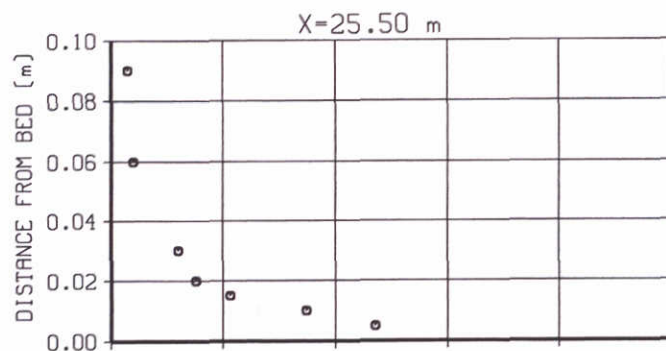
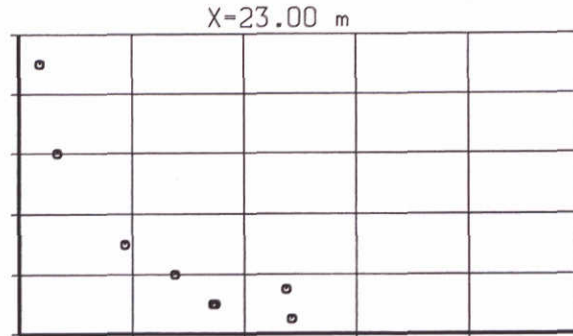
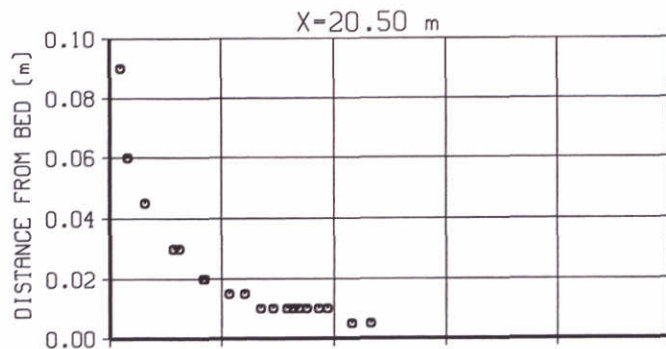
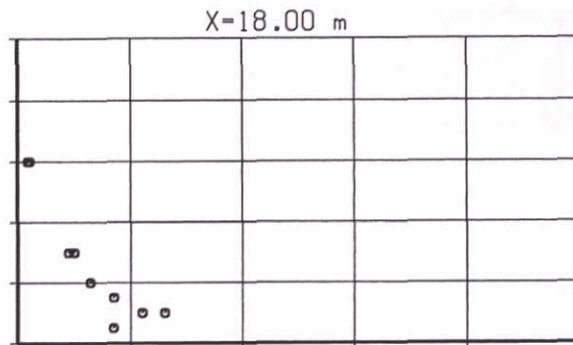
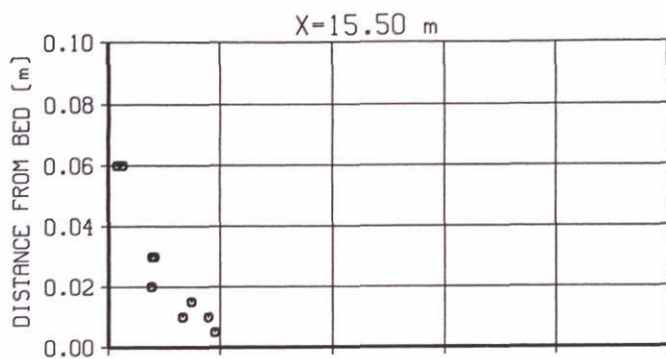
STANDARD DEVIATION OF OPCON SIGNAL
WITHOUT GRAIN-SIZE CORRECTION

SERIE-A



STANDARD DEVIATION OF
LOW-PASS FILTERED OPCON SIGNAL
WITHOUT GRAIN-SIZE CORRECTION

SERIE-A



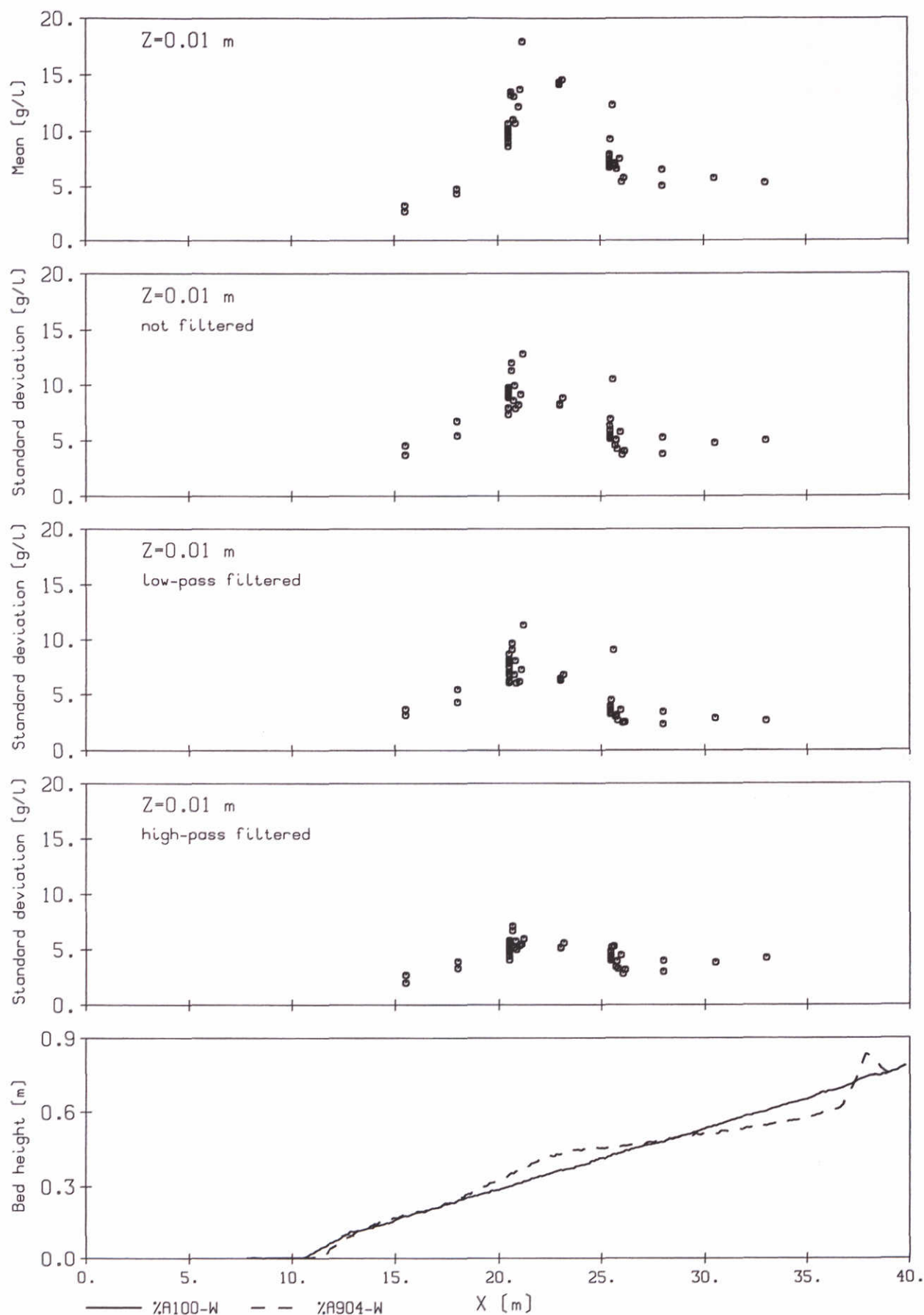
STANDARD DEVIATION OF
HIGH-PASS FILTERED OPCON SIGNAL
WITHOUT GRAIN-SIZE CORRECTION

SERIE-A

WL | DELFT HYDRAULICS

H2305.70

FIG. A30



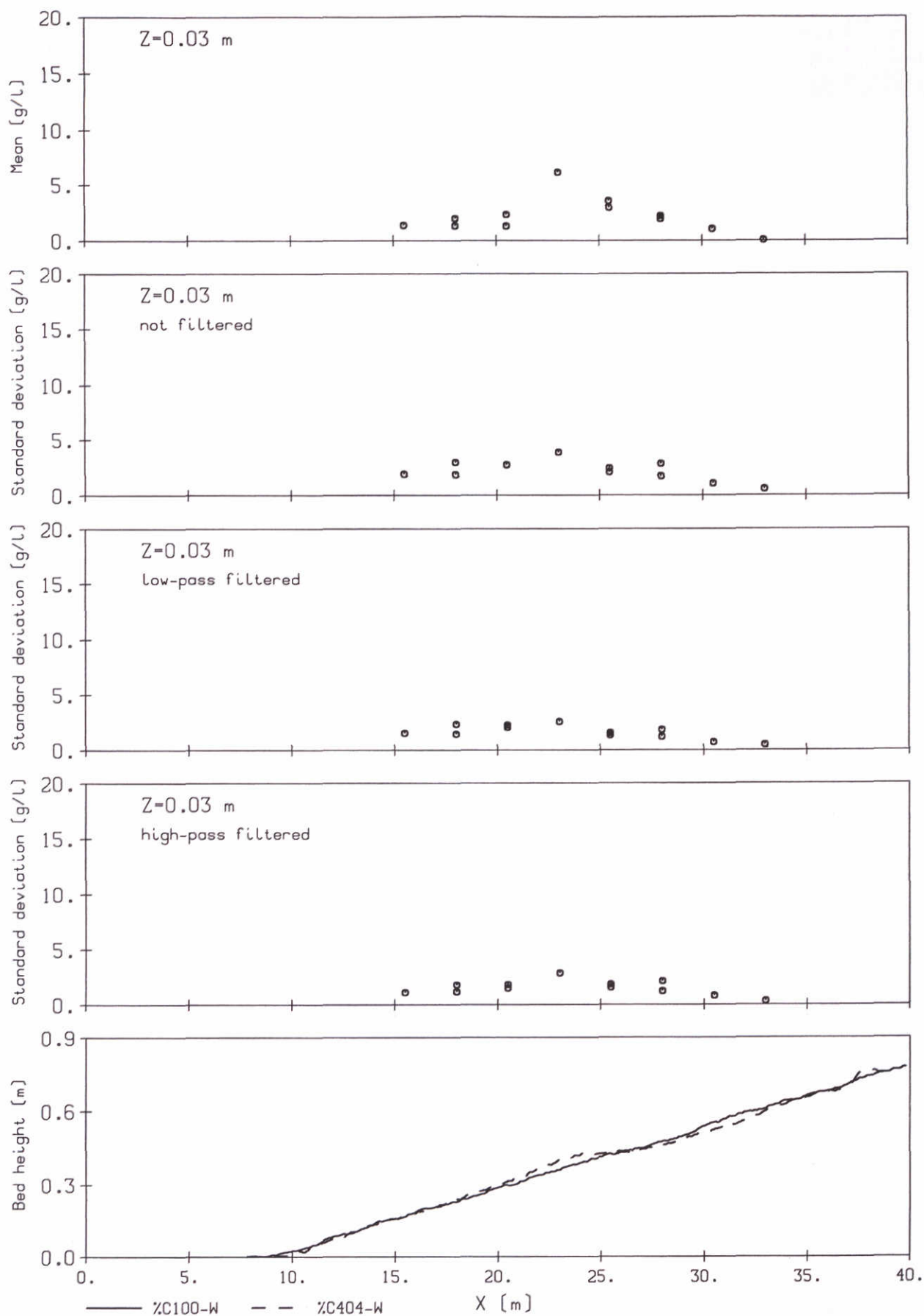
CONCENTRATION DATA

SERIE-A

WL | DELFT HYDRAULICS

H2305.70

FIG. A31



CONCENTRATION DATA

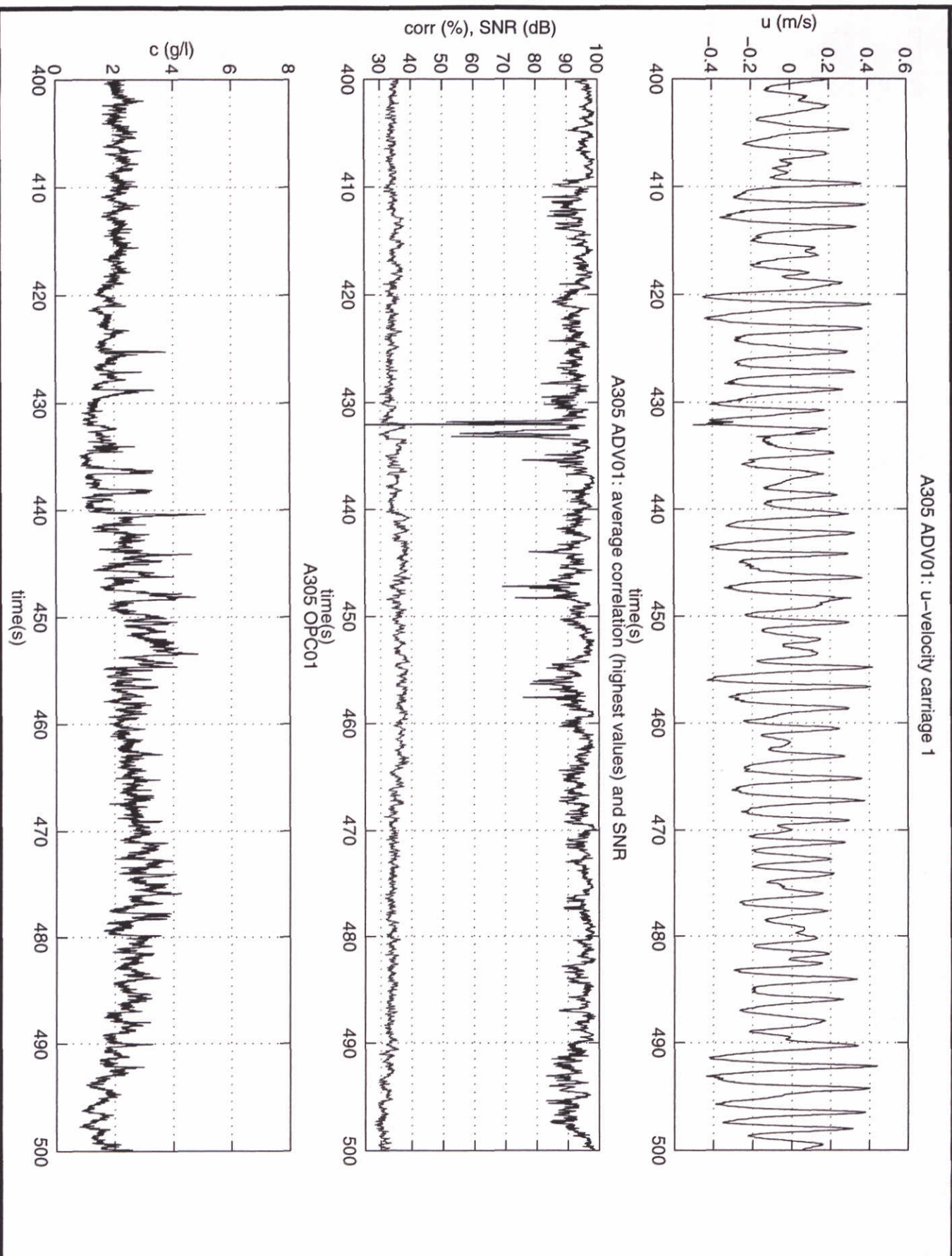
WITHOUT GRAIN-SIZE AND DENSITY CORRECTION

SERIE-C

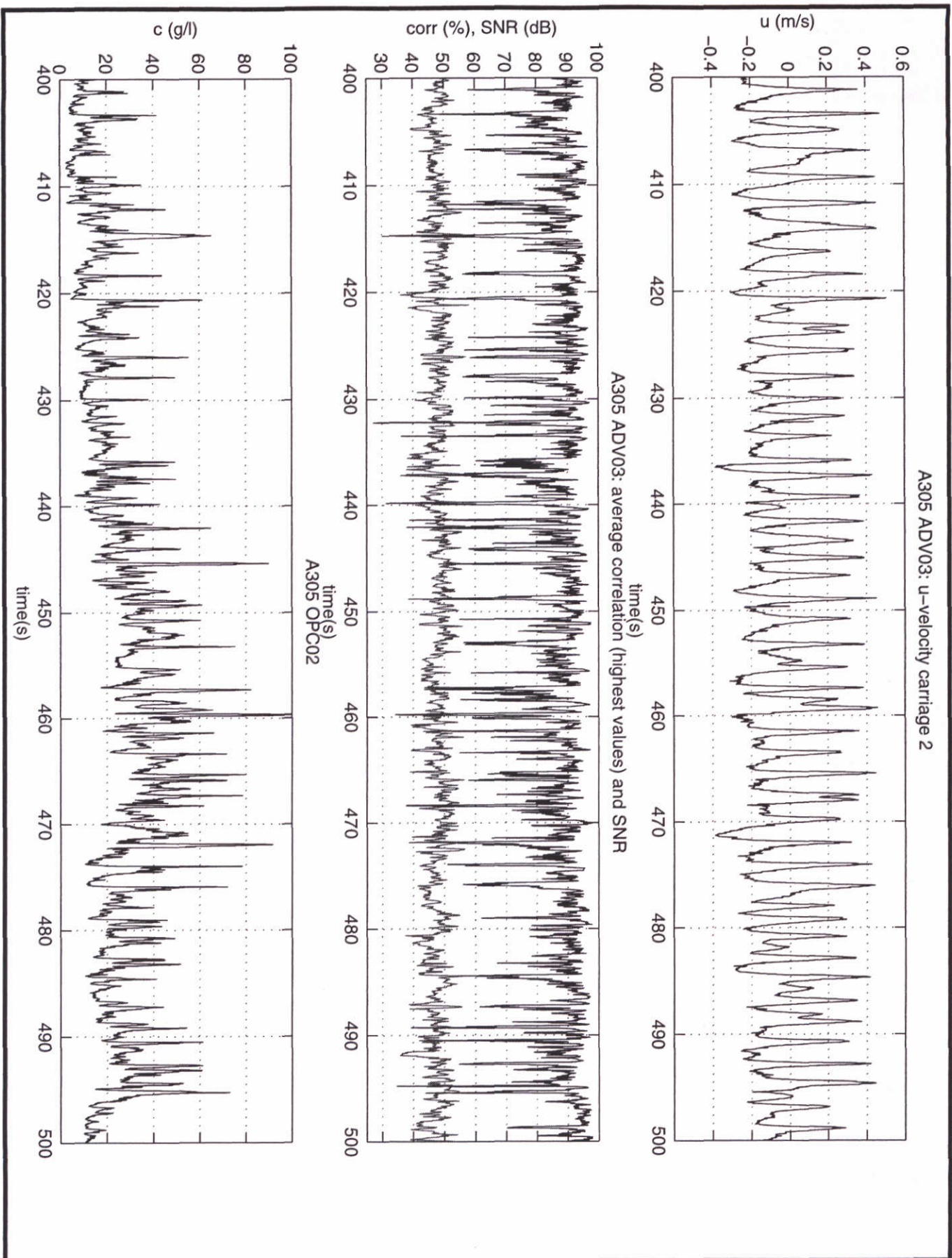
WL | DELFT HYDRAULICS

H2305.70

FIG. A32

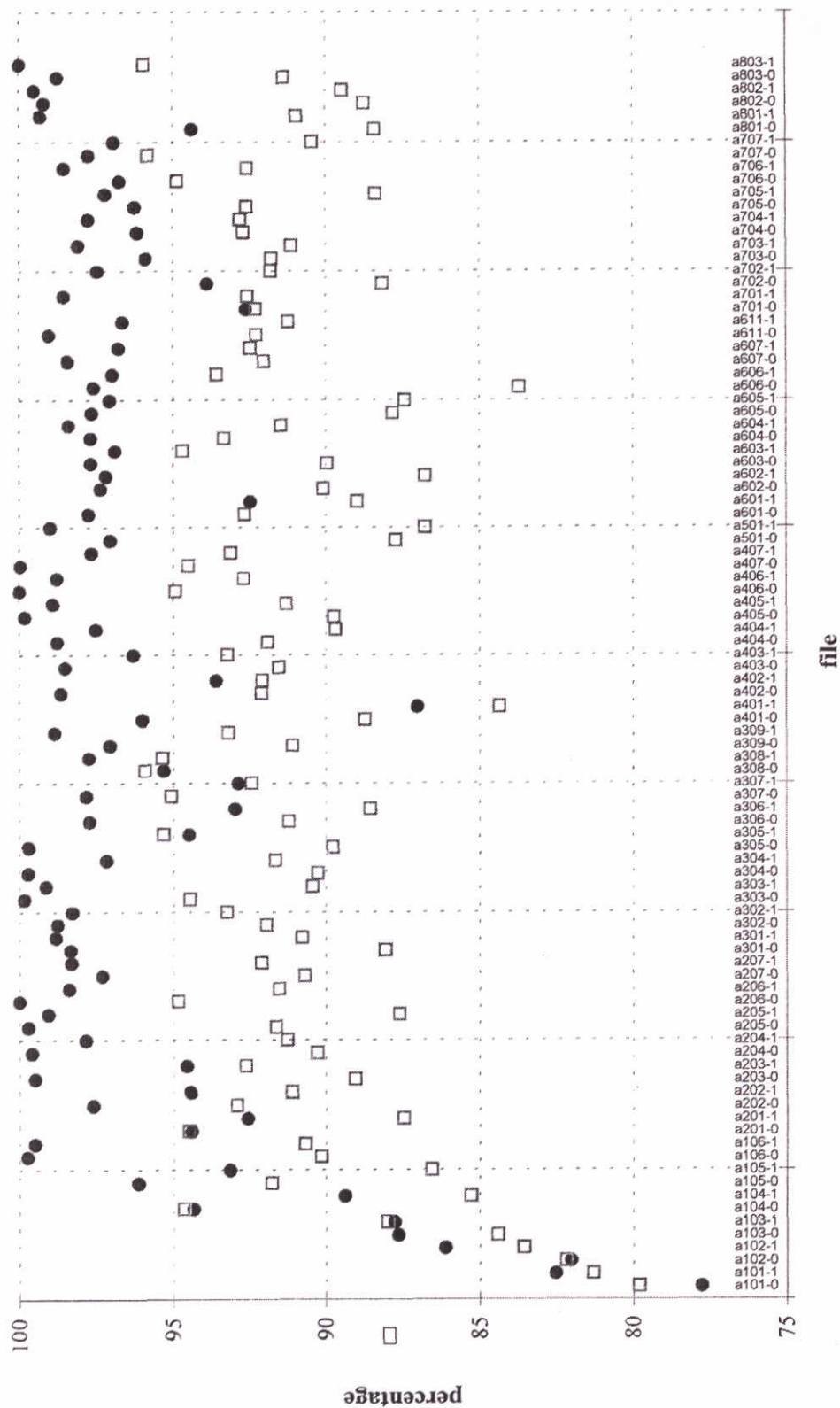


Horizontal velocity, correlation and SNR, and sediment concentration for A305 carriage 1 (x=23 m, z=9 cm)

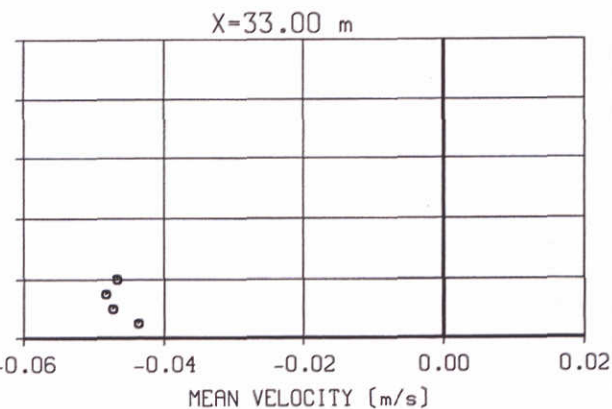
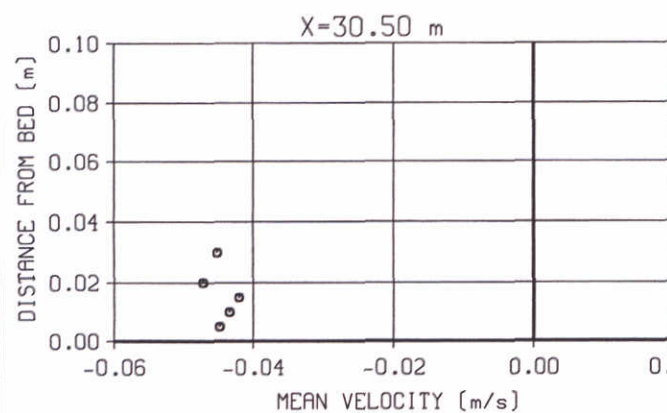
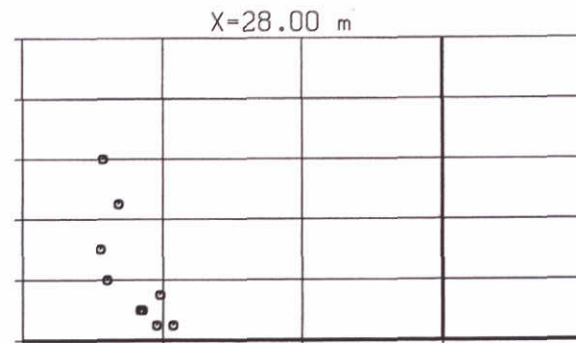
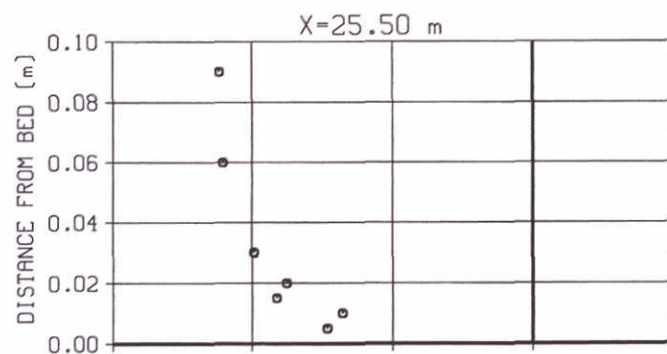
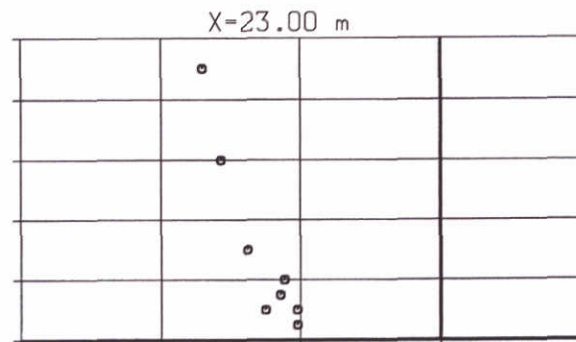
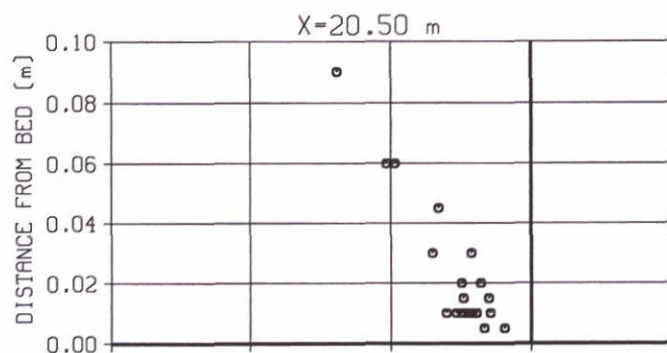
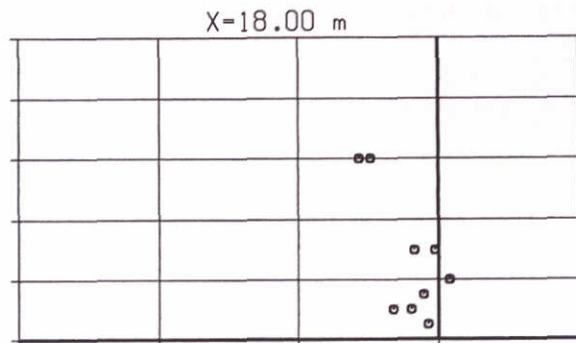
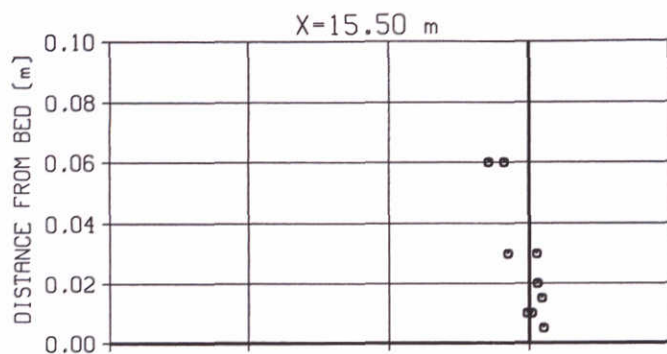


Horizontal velocity, correlation and SNR, and sediment concentration for A305 carriage 2 (x=30.5 m, z=0.5 cm)		
	WL DELFT HYDRAULICS	<div>H 2305</div> <div>FIG. A34</div>

Percentage good (% of time-series with corr > 70% & SNR > 15 dB) and time-averaged correlation (%)

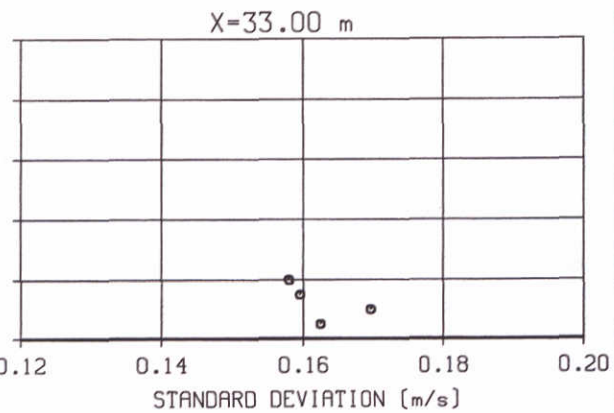
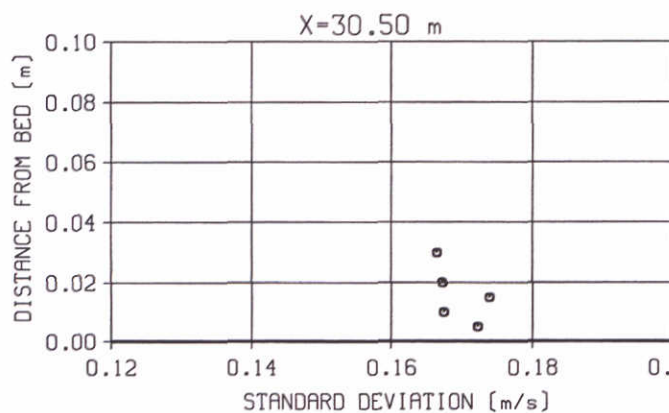
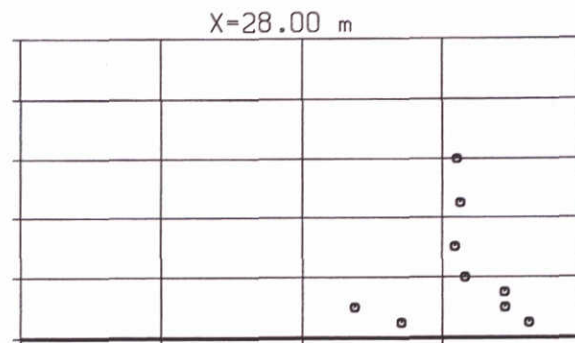
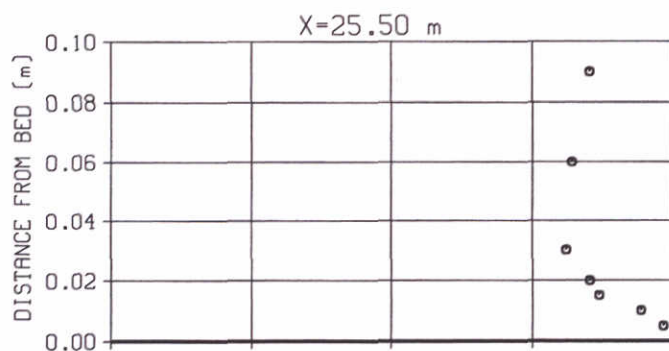
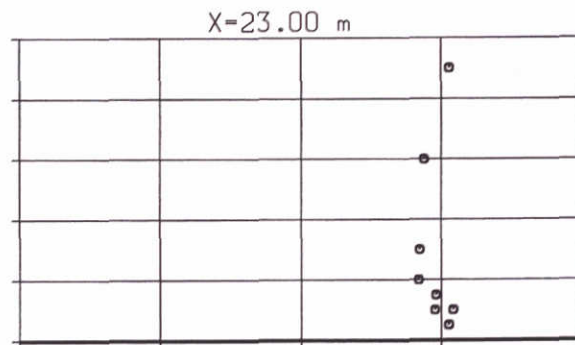
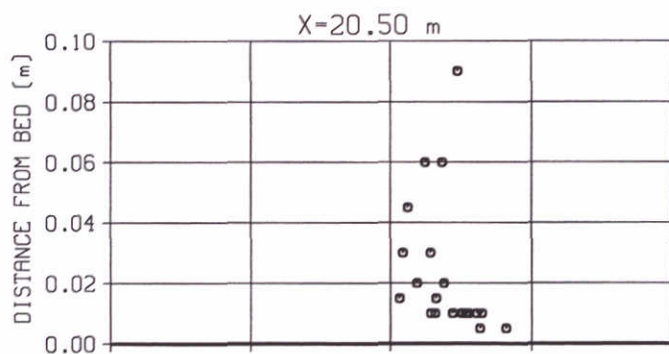
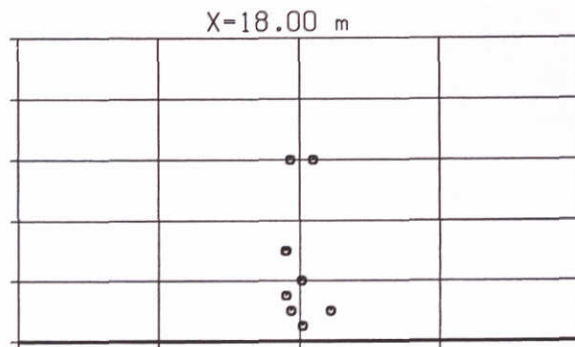
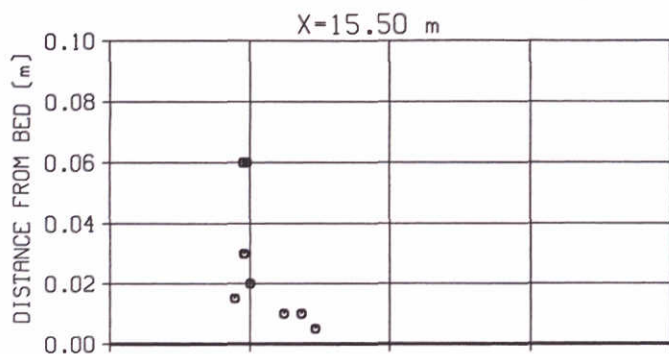


Quality of ADV signals in A-series. Rounds: percentage good (%) and squares: time-averaged correlation (%)



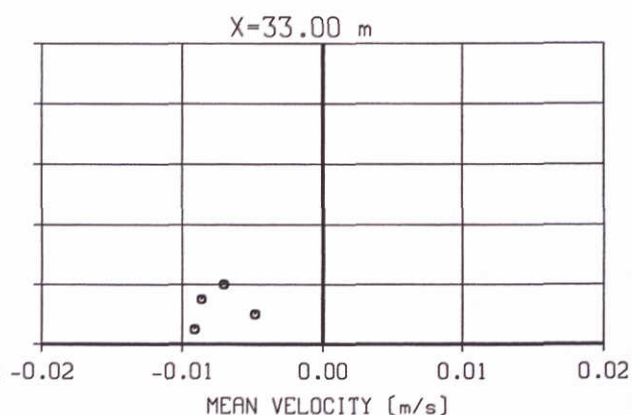
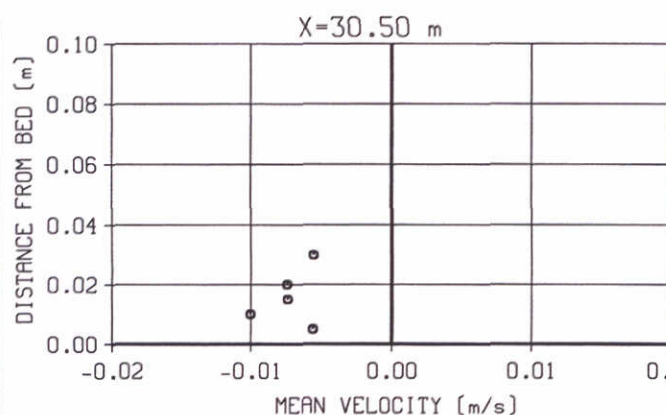
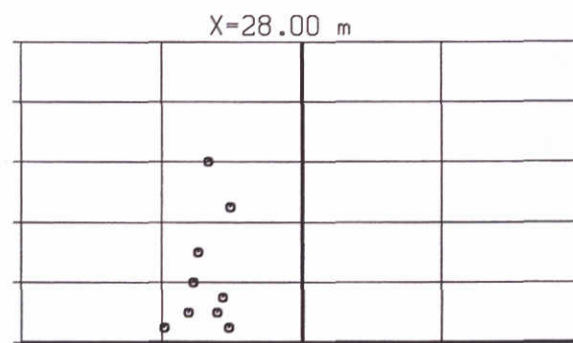
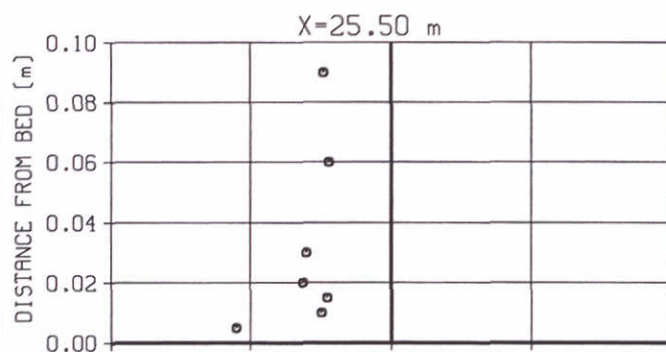
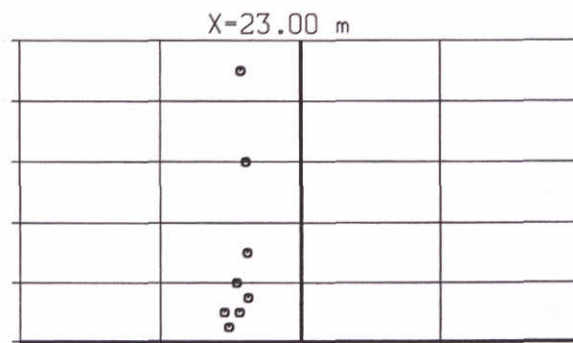
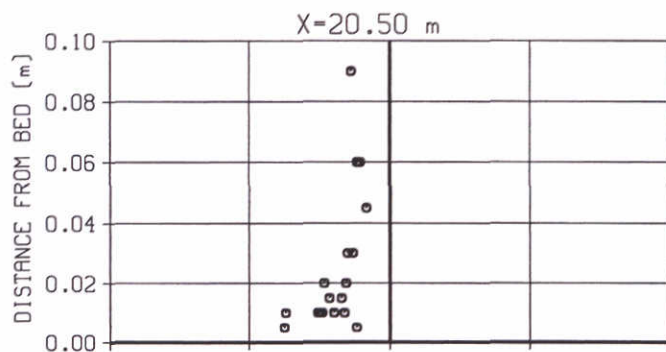
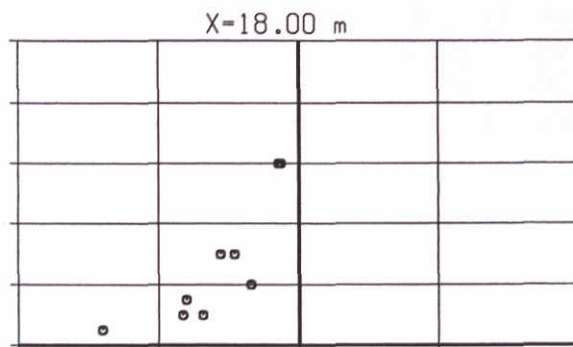
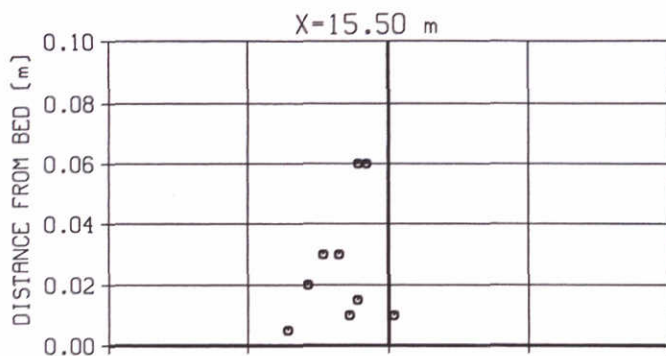
MEAN HORIZONTAL VELOCITY

SERIE-A



STANDARD DEVIATION OF HORIZONTAL VELOCITY SIGNAL

SERIE-A



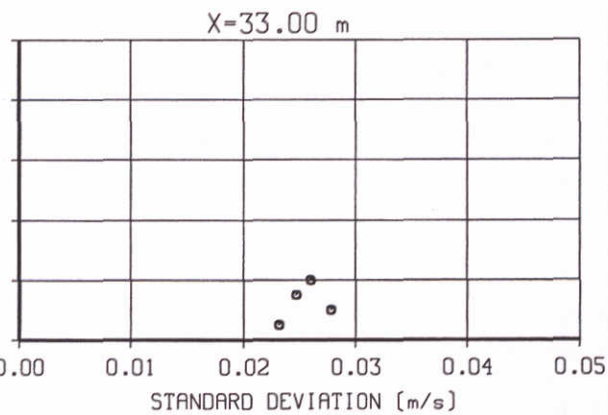
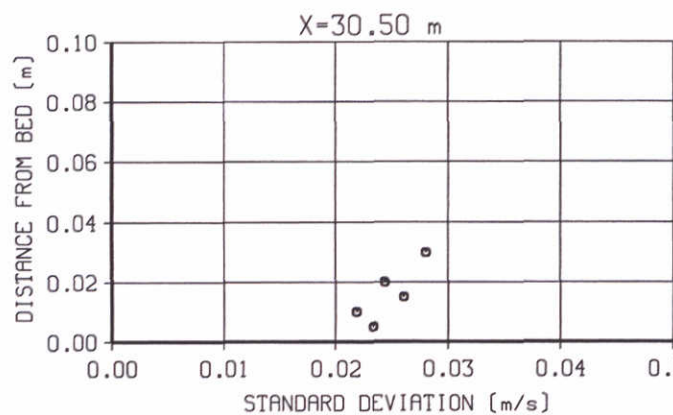
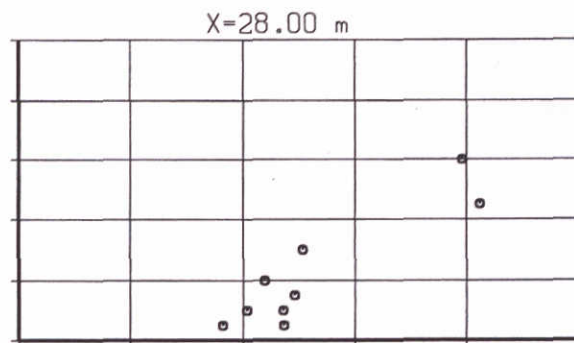
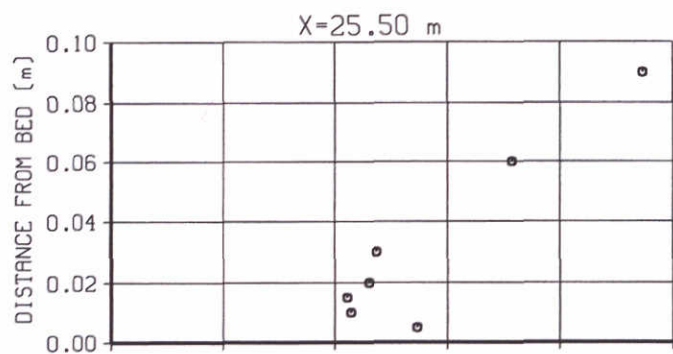
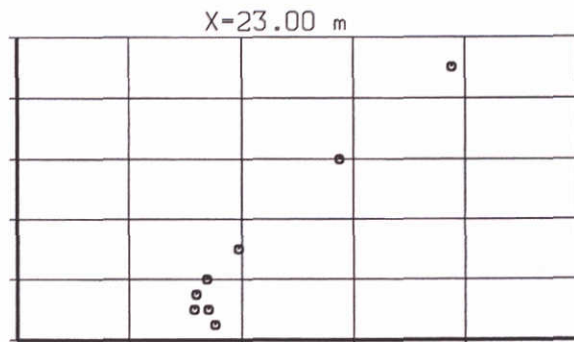
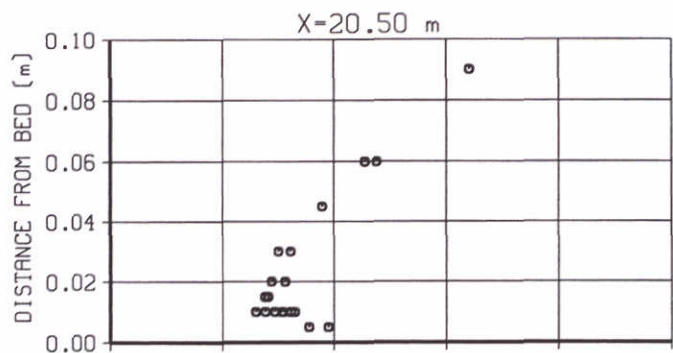
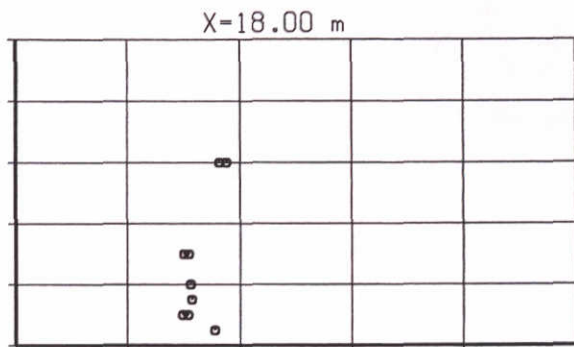
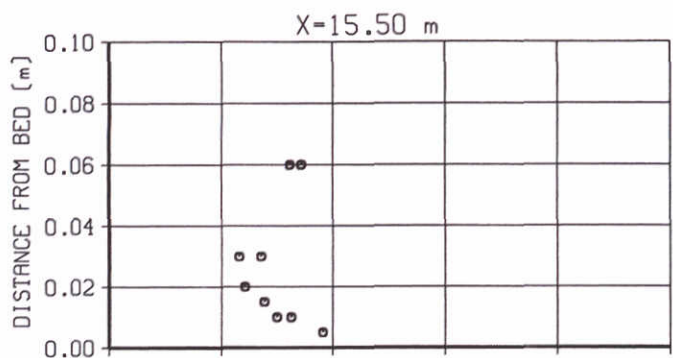
MEAN VERTICAL VELOCITY

SERIE-A

WL | DELFT HYDRAULICS

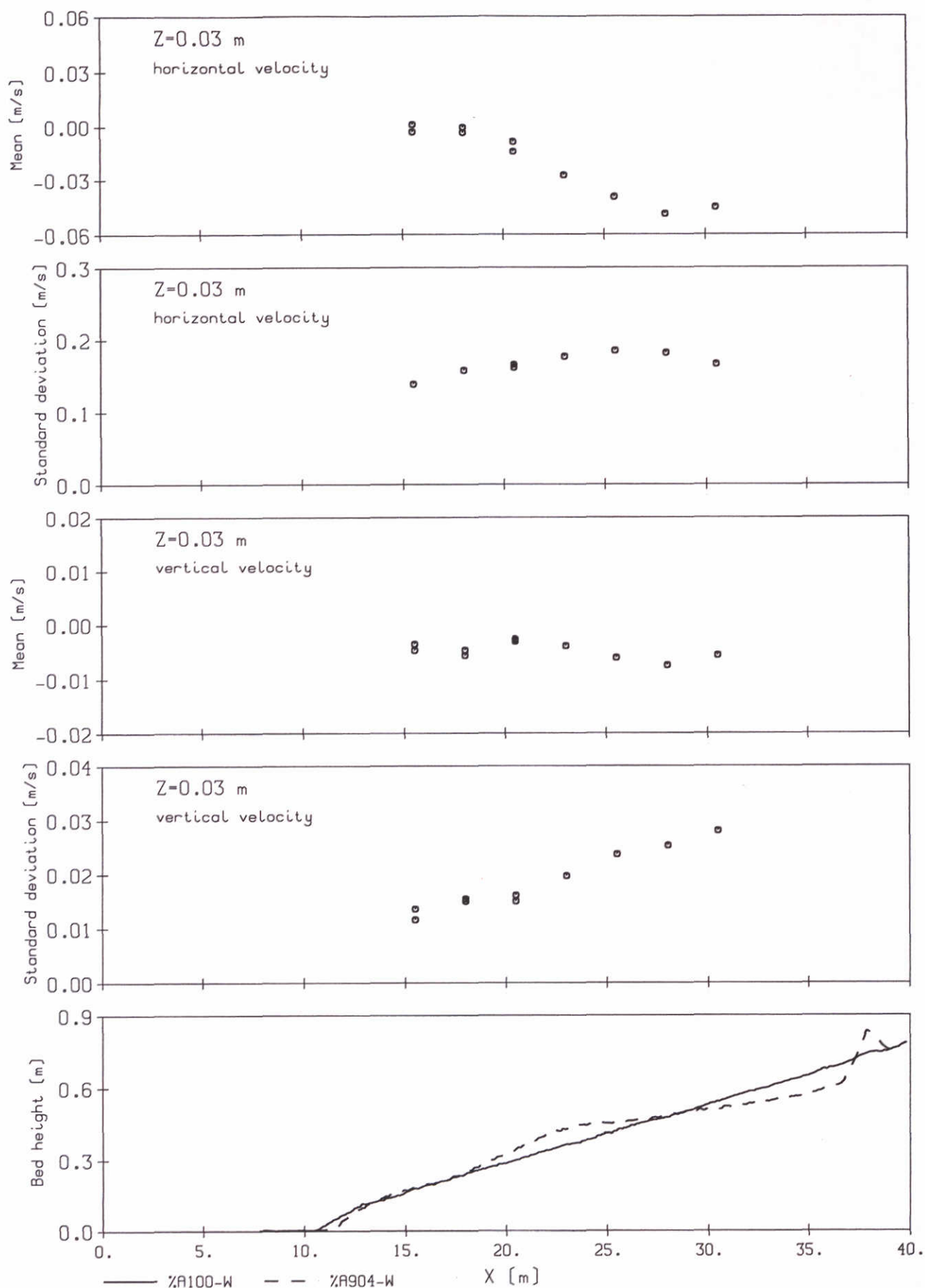
H2305.70

FIG. A38



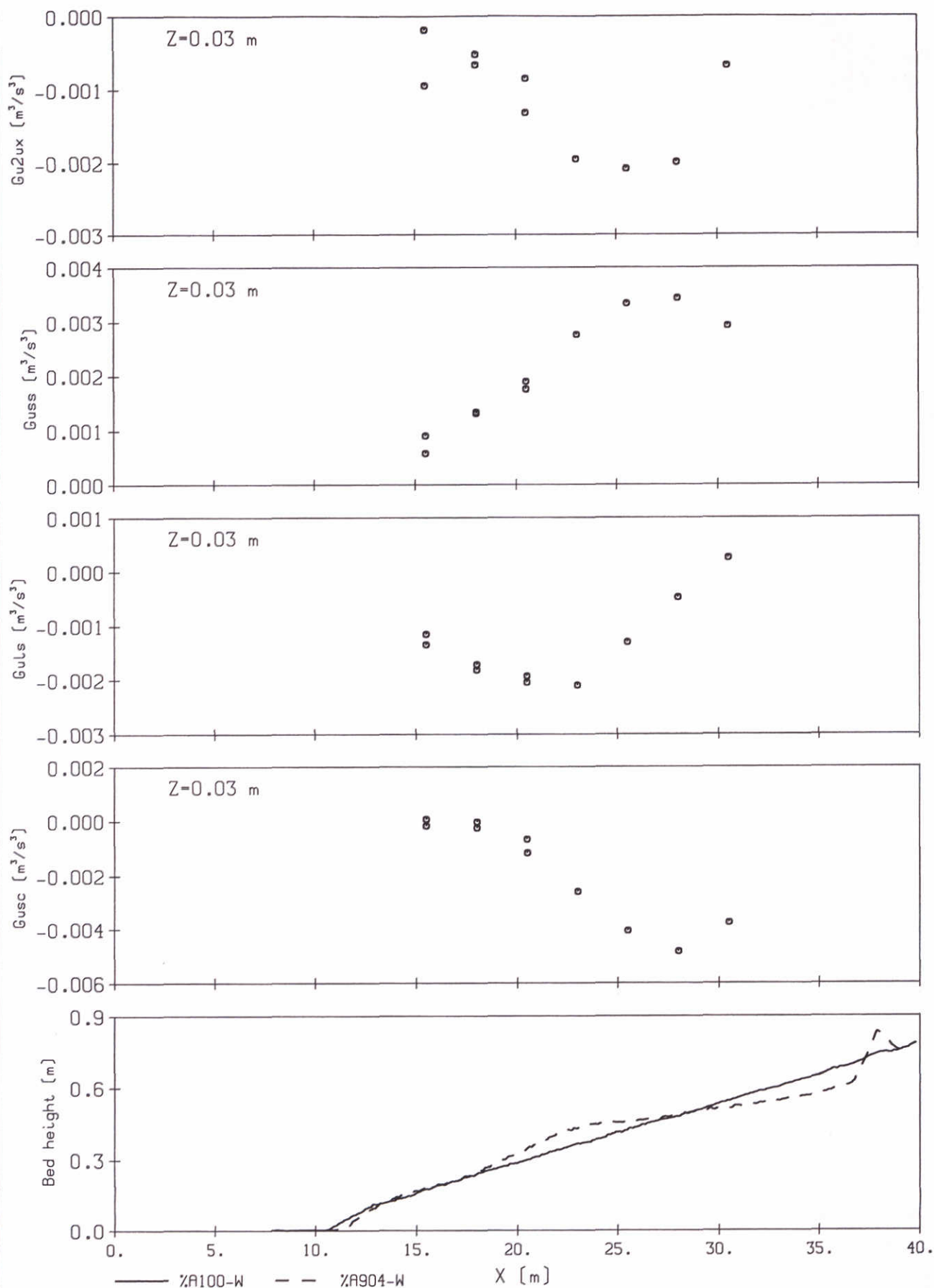
STANDARD DEVIATION OF VERTICAL VELOCITY SIGNAL

SERIE-A



VELOCITY DATA

SERIE-A



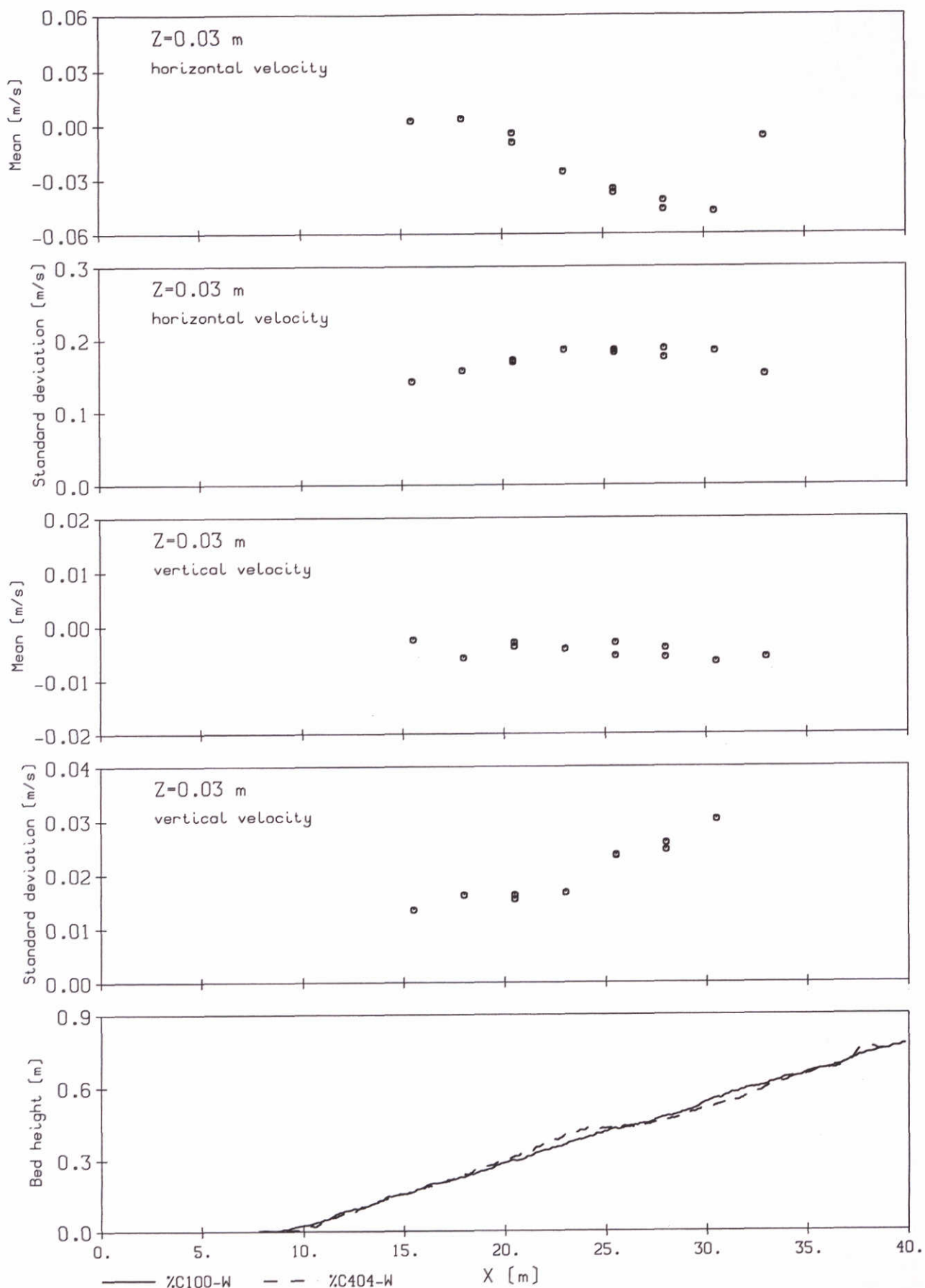
HORIZONTAL VELOCITY MOMENTS

SERIE-A

WL | DELFT HYDRAULICS

H2305.70

FIG. A41



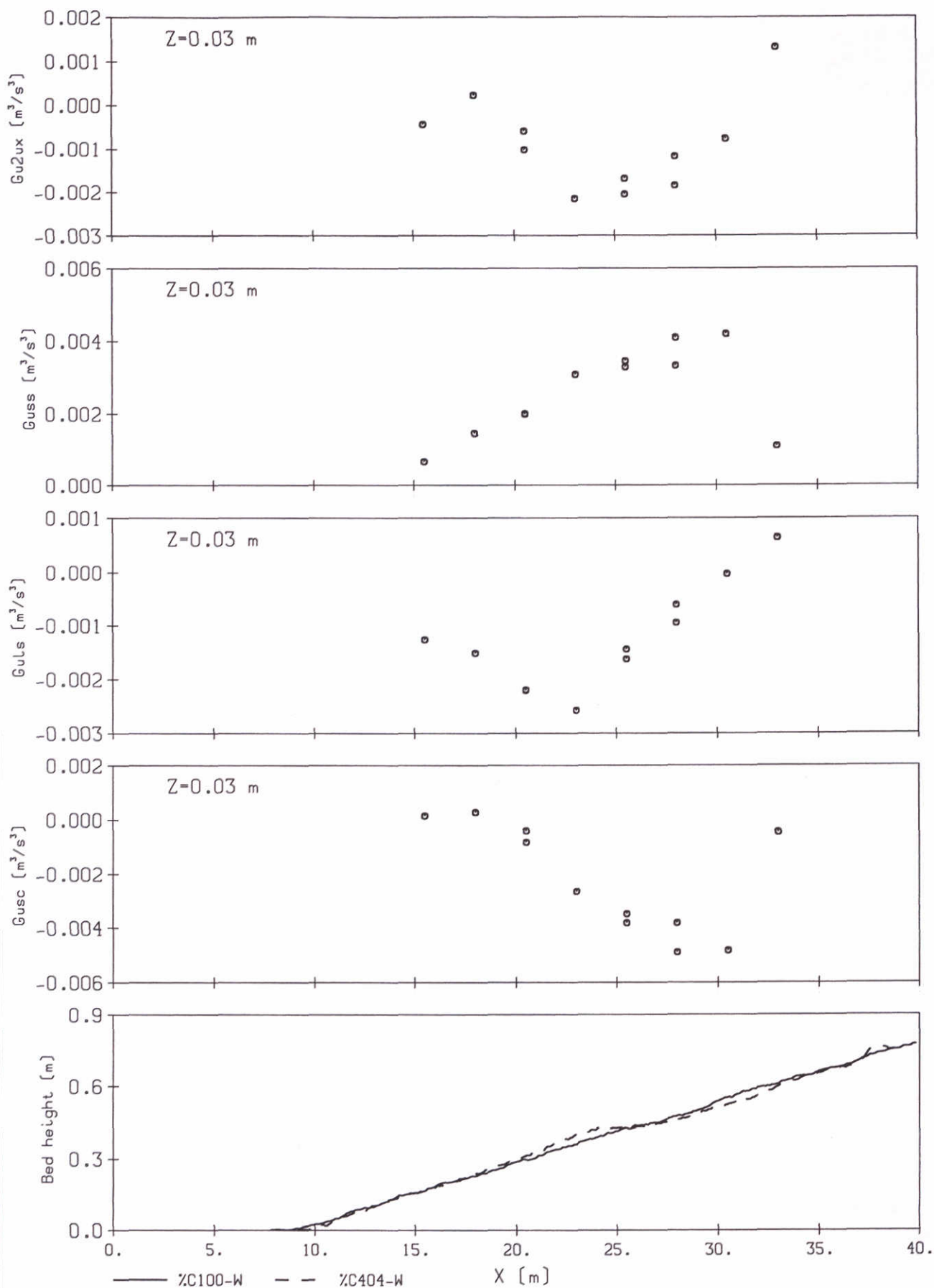
VELOCITY DATA

SERIE-C

WL | DELFT HYDRAULICS

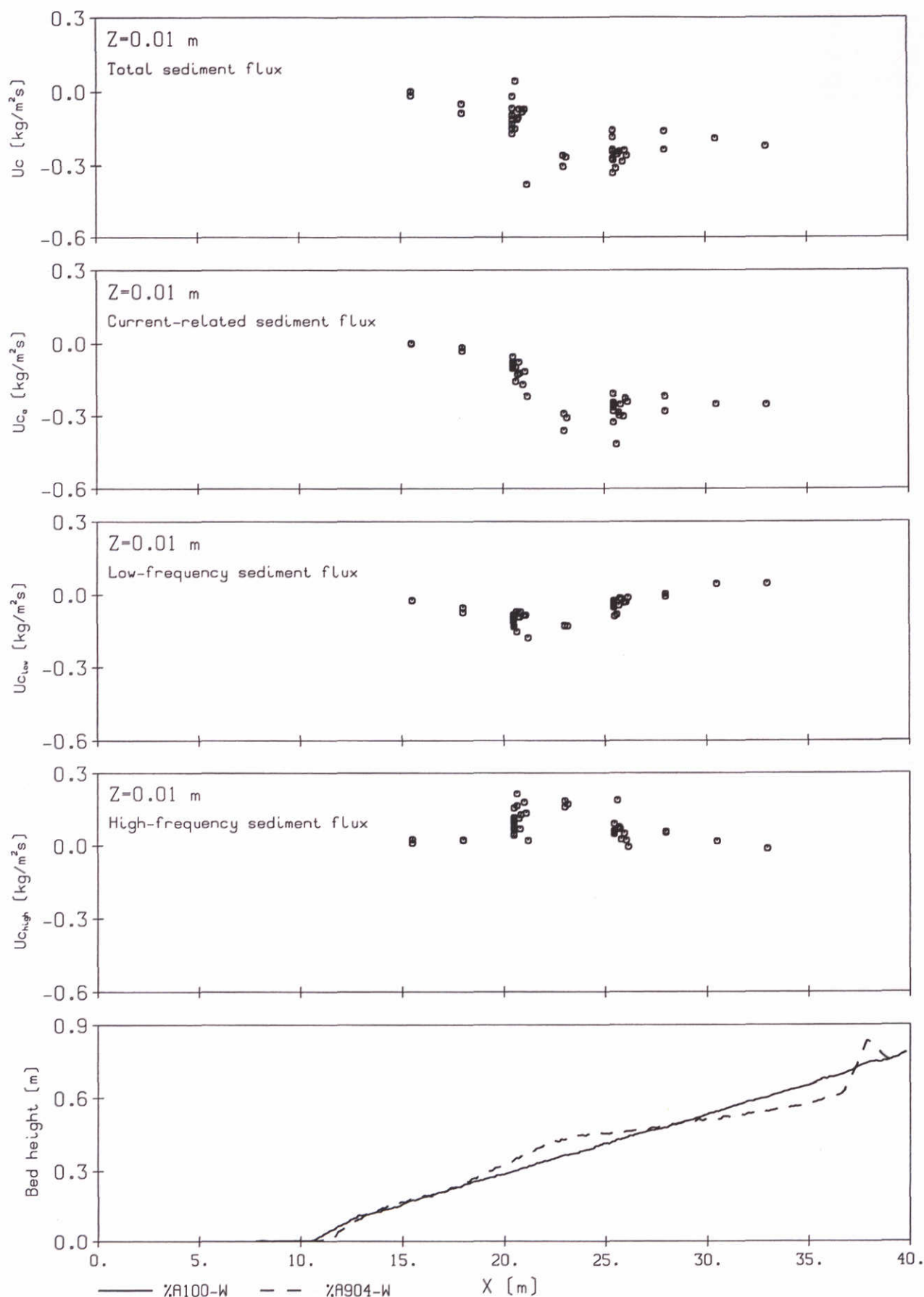
H2305.70

FIG. A42



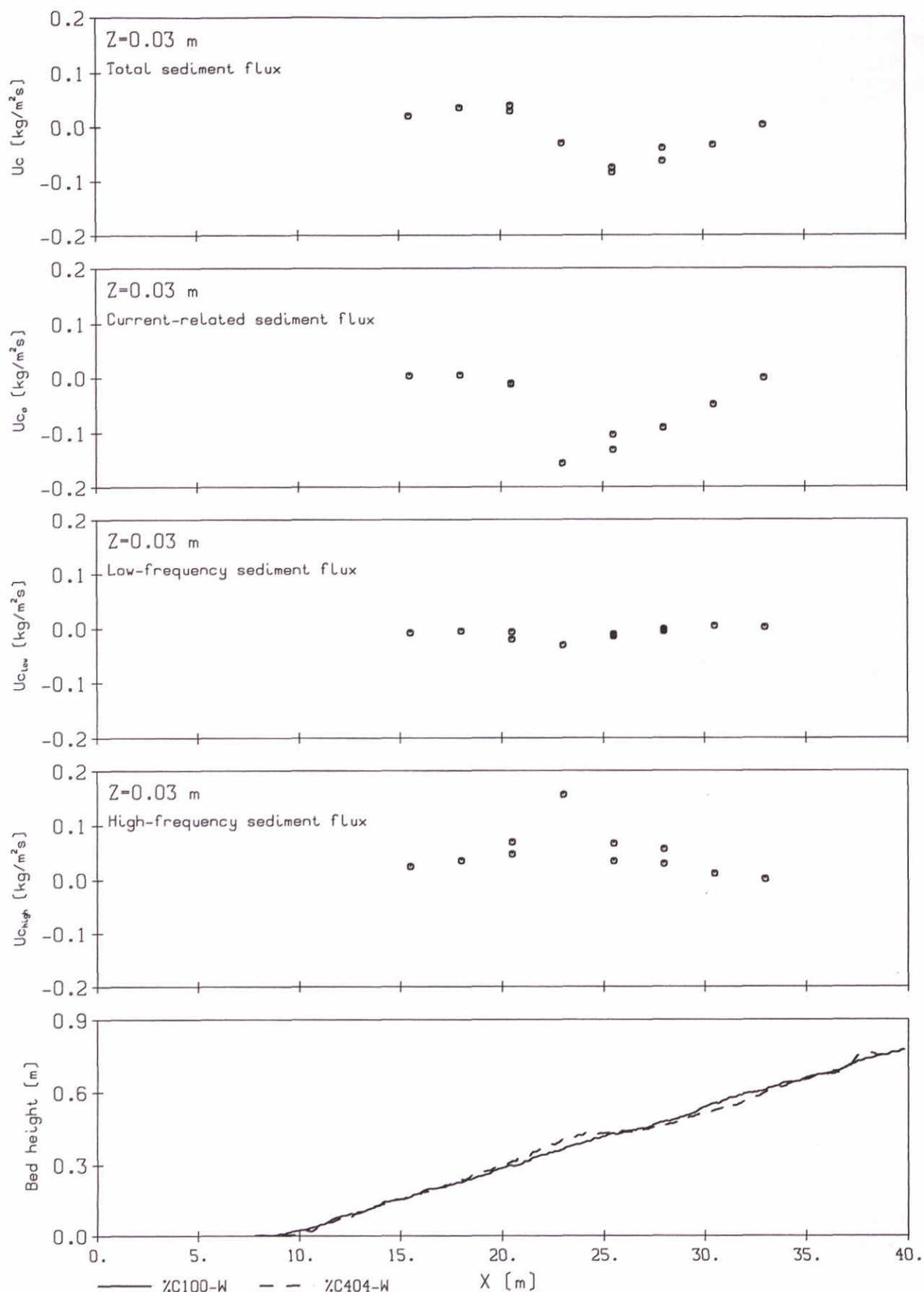
HORIZONTAL VELOCITY MOMENTS

SERIE-C



SEDIMENT FLUX

SERIE-A



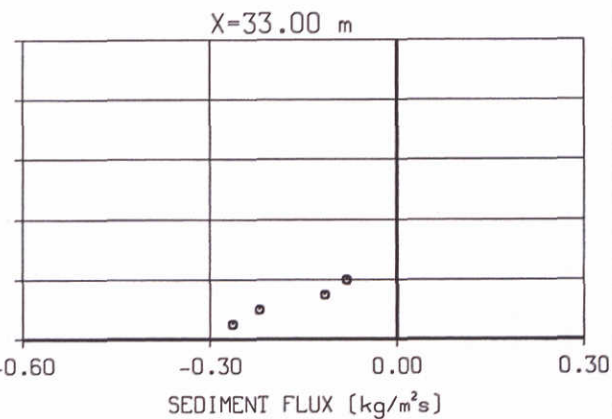
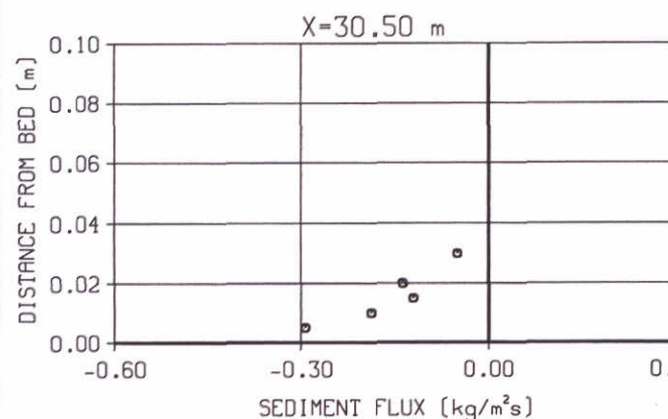
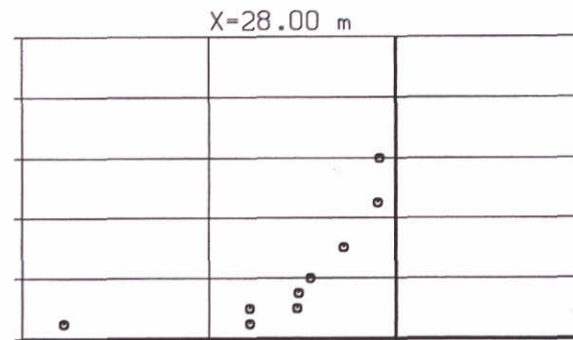
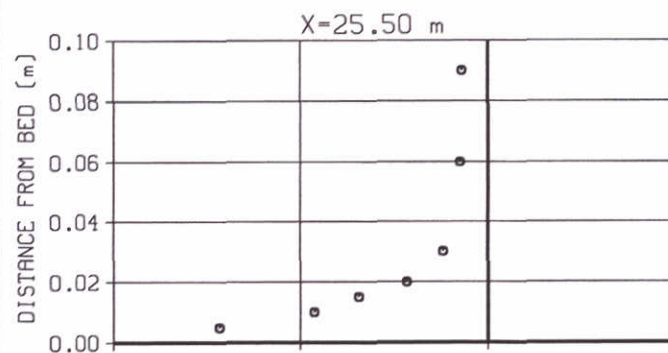
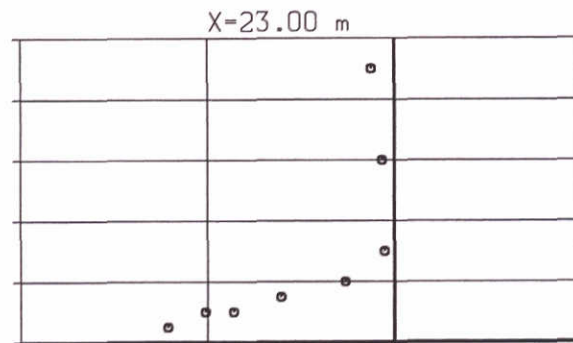
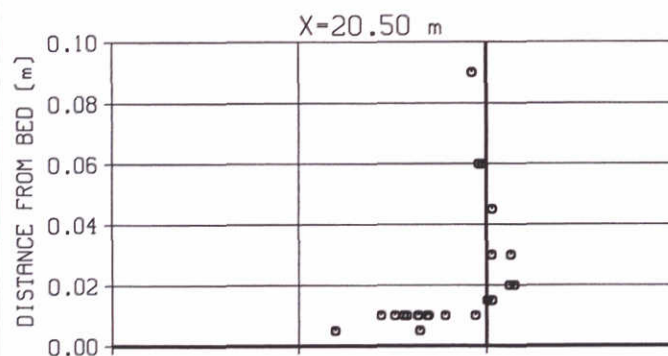
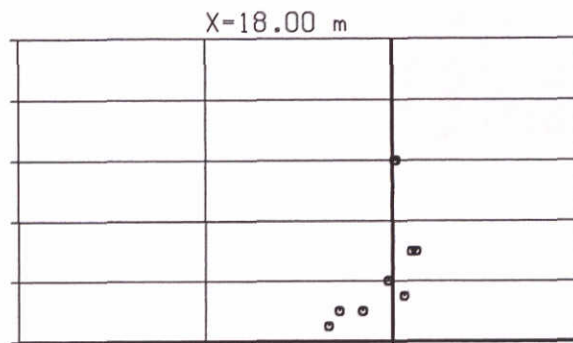
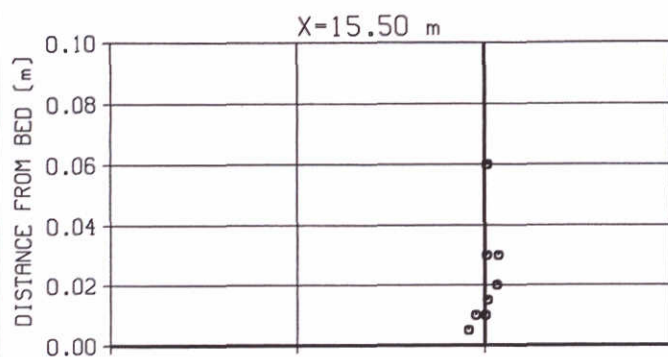
SEDIMENT FLUX

SERIE-C

WL | DELFT HYDRAULICS

H2305.70

FIG. A45



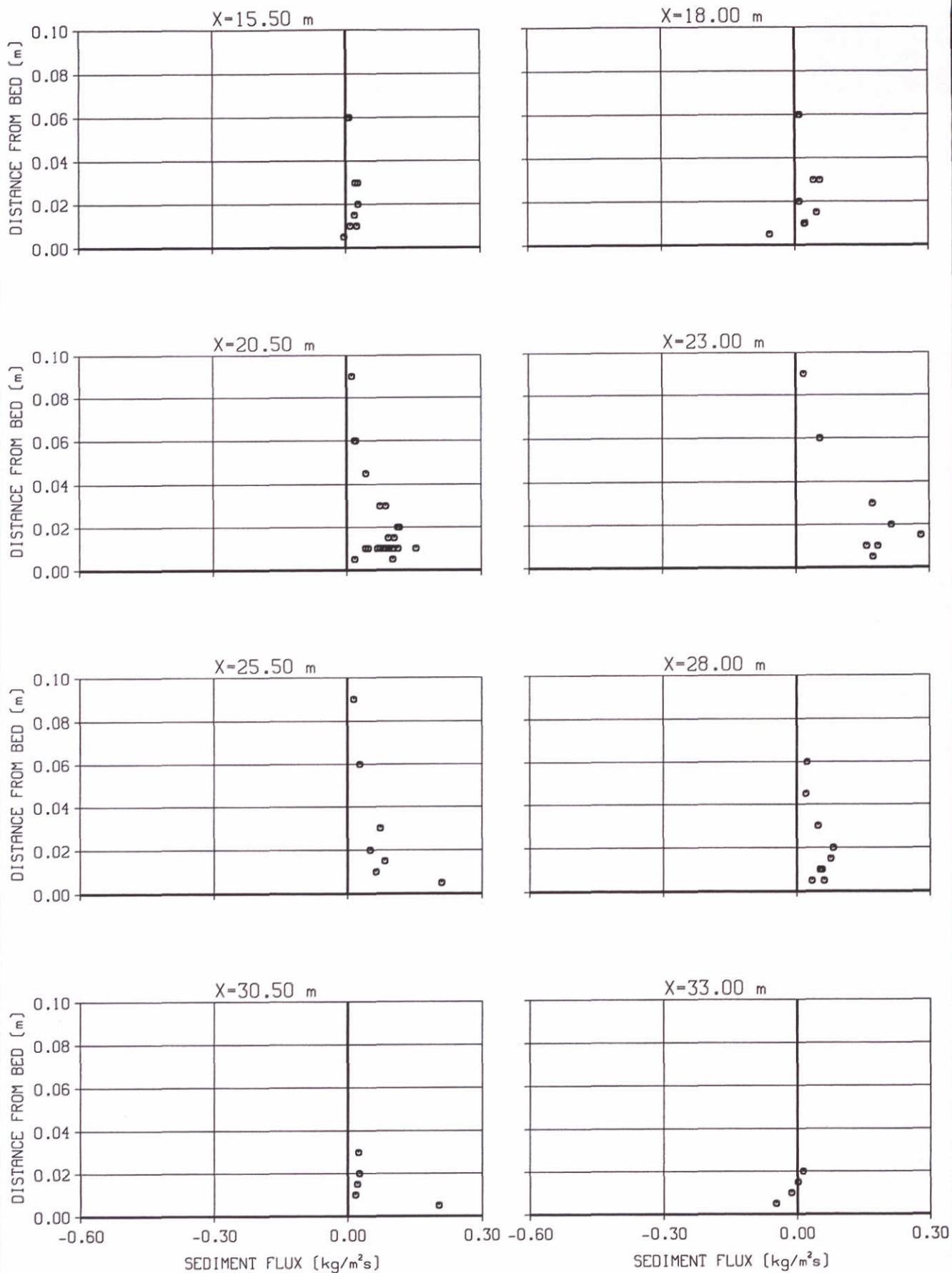
TOTAL SEDIMENT FLUX

SERIE-A

WL | DELFT HYDRAULICS

H2305.70

FIG. A46



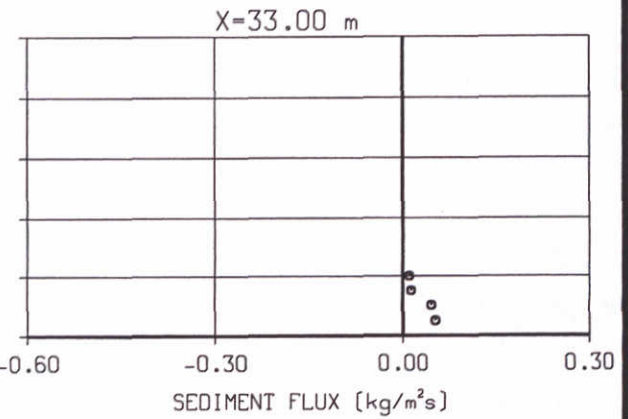
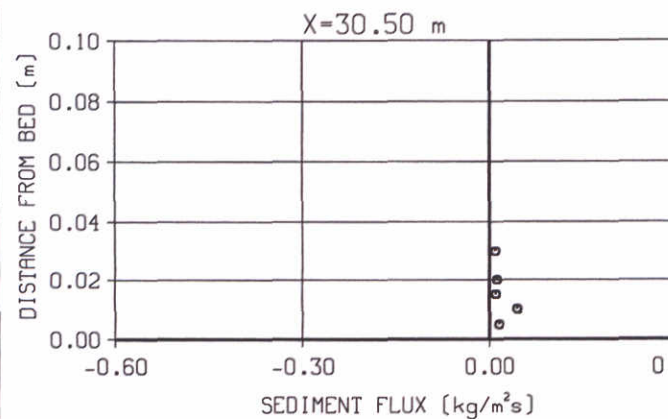
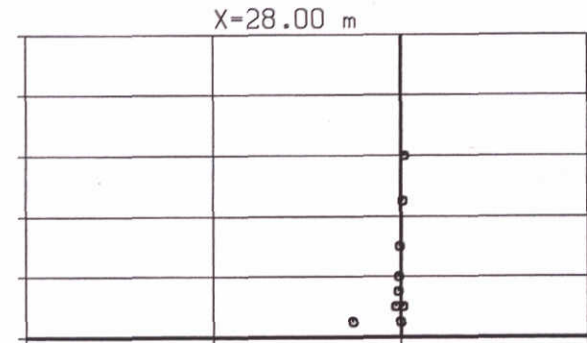
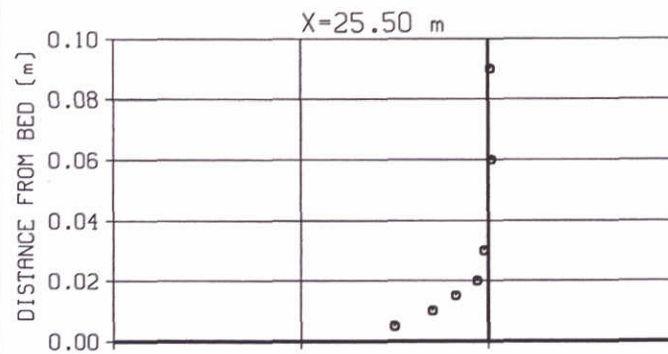
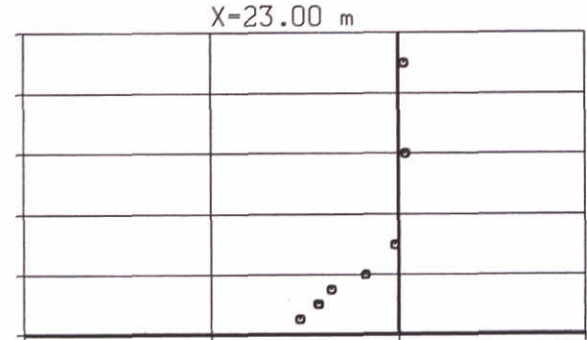
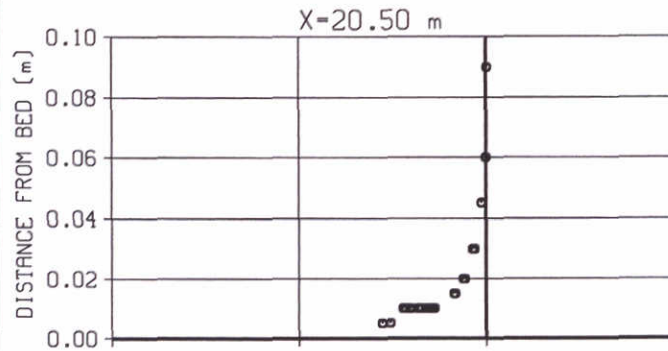
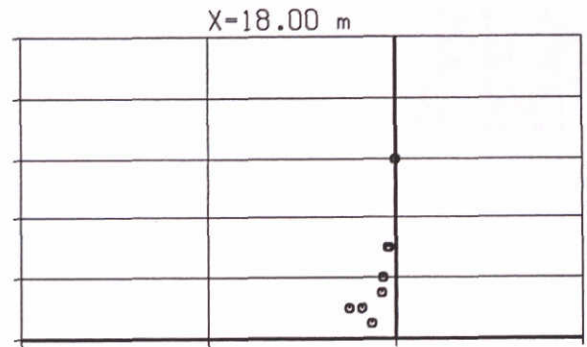
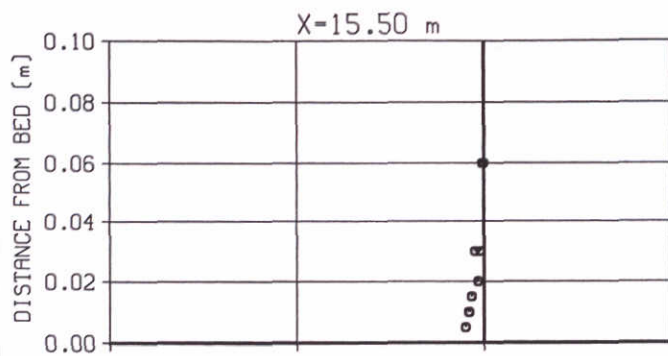
HIGH-FREQUENCY SEDIMENT FLUX

SERIE-A

WL | DELFT HYDRAULICS

H2305.70

FIG. A47



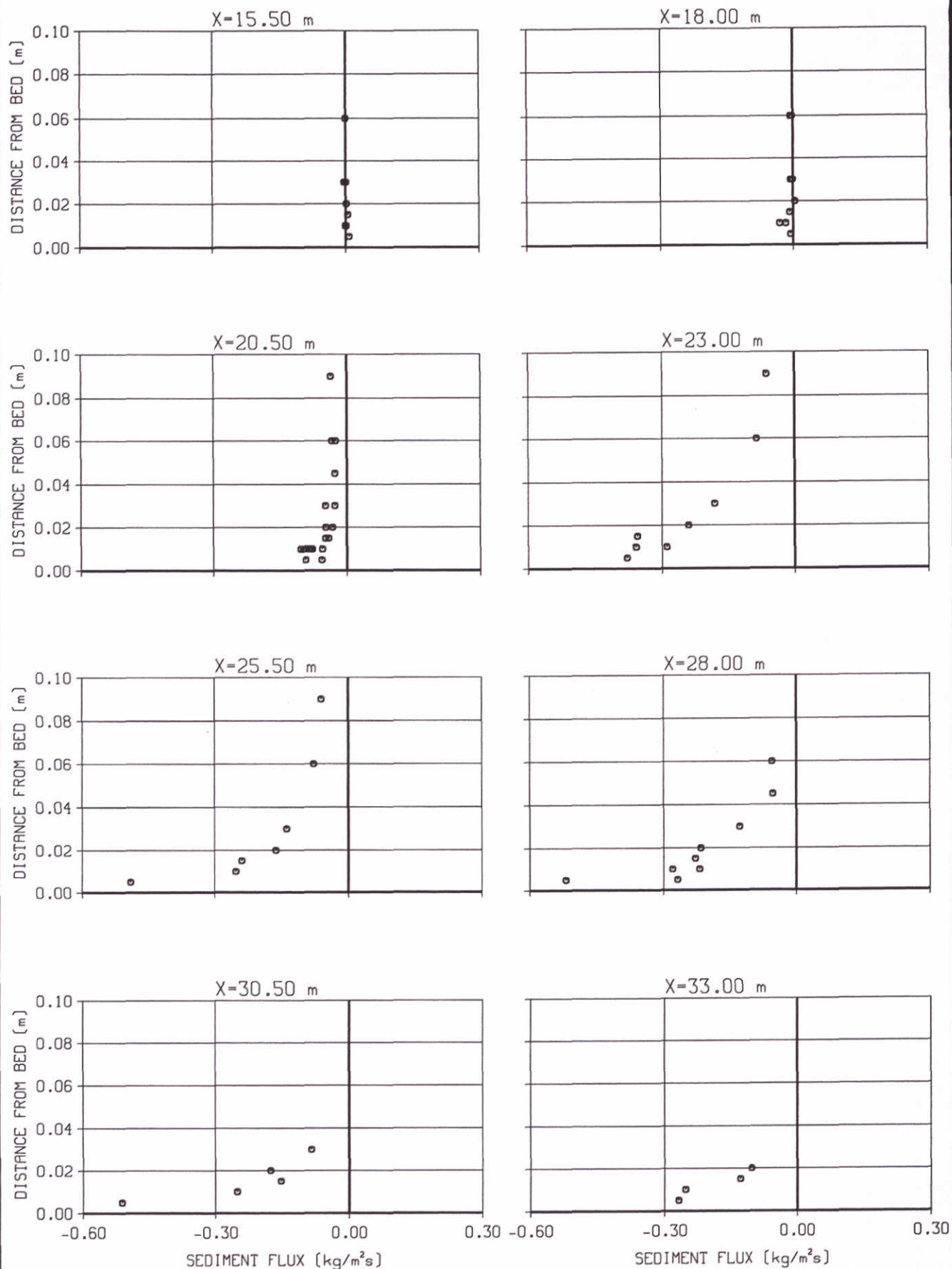
LOW-FREQUENCY SEDIMENT FLUX

SERIE-A

WL | DELFT HYDRAULICS

H2305.70

FIG. A48



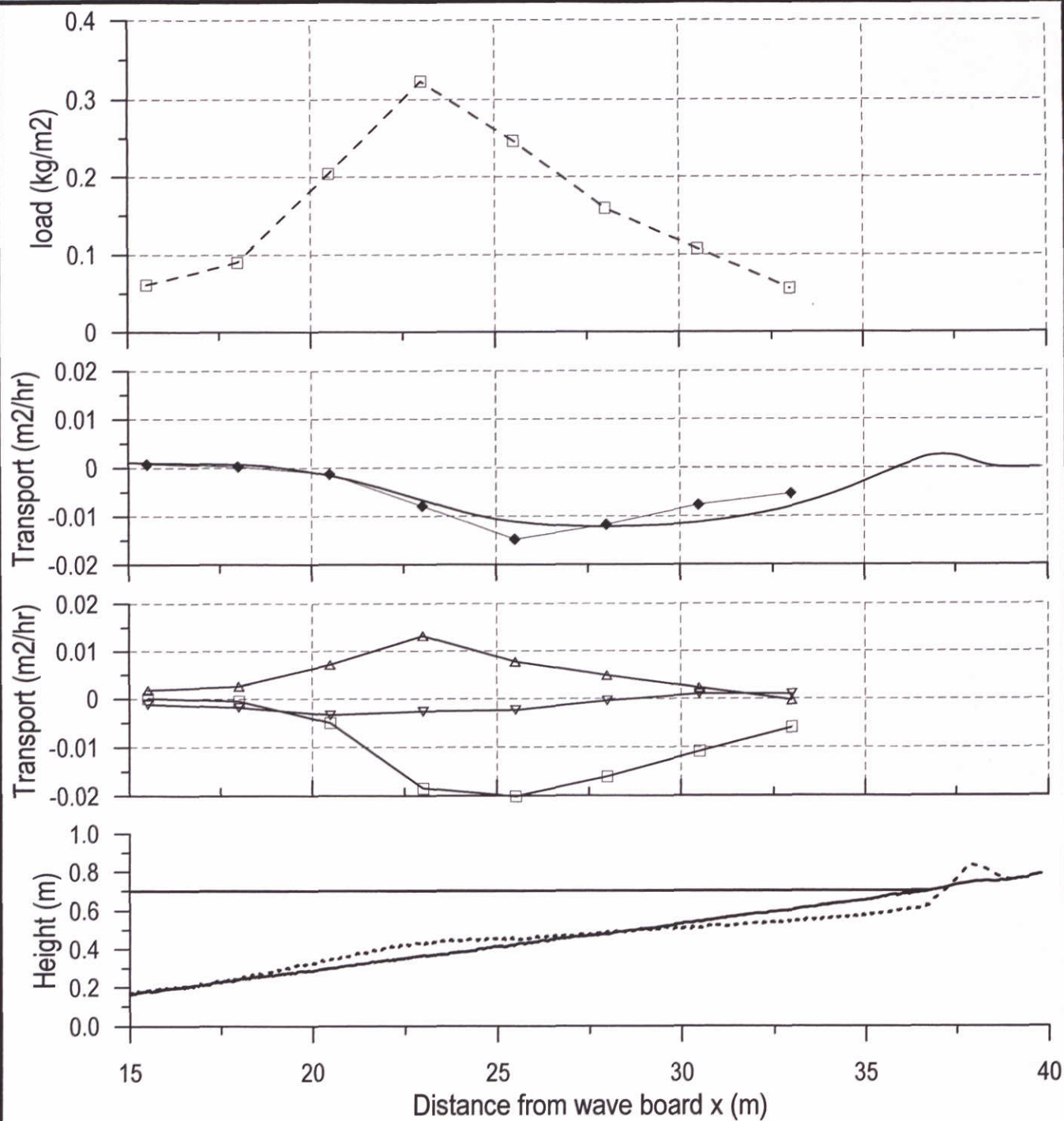
CURRENT-RELATED SEDIMENT FLUX

SERIE-A

WL | DELFT HYDRAULICS

H2305.70

FIG. A49



Transport from flux profiles in third plot: decomposed in short wave contribution (triangle up), long wave contribution (triangle down) and mean flow (square)

Time-mean load (upper plot), sediment transport (second plot) derived from profile deformation (line) and from flux profiles (diamond) and initial bed and bed after 30 hours (lower plot)

B Scheldt flume

Wave flume "Scheldegoot"

The "Scheldegoot" facility of DELFT HYDRAULICS is a wave flume with a wave maker capable of generating both periodic and random waves. The translation/rotation ratio for the wave board motion is adjustable. The wave generator is equipped with a patented device to prevent reflection against the wave board and also to avoid undesired long-periodical waves. At the back of the flume a second wave board is installed for active wave absorption.

For wave board control, data acquisition and data processing DELFT HYDRAULICS' time-series generating and processing package AUKE/pc is used. Wave board control for random second-order waves is available. The flume is equipped with a pump system enabling the simulation of currents, so that the combination of waves and current can be studied too.

relevant data:

wave flume

- length: 55 m
- width: 1 m
- height: 1.2 m.

wave maker

- width: 1 m
- height: 1.2 m
- minimum water depth 0.25 m
- maximum water depth 1.0 m
- cradle-type wave board
- hydraulically driven system
- control signal is a digitized time series.

wave characteristics

- wave frequencies between 0 and 2 Hz
- maximum wave height $H_{\max} = 0.4$ m for $f = 0.5$ Hz
- maximum significant wave height $H_s > 0.25$ m for $T_p = 1.9$ s
- wave damping: spending beach.

pump capacity

- maximum pump capacity 120 l/s.



C Measurement programme

A-series

Series A consisted globally of two parts. The first part aimed at collecting data at various heights above the bed at eight selected horizontal positions ranging from the shoreline up to the toe of the profile (Table C-25).

Table C-25 Positions of the measuring verticals

Vertical	x-position (m)
1	33
2	30.5
3	28
4	25.5
5	23
6	20.5
7	18
8	15.5

In the first part of series A, consecutive half-hour measurements were made at the x-locations in Table C-25 at different heights above the ripple crests. In the second part of series A, the focus was on horizontal correlation measurements. In those series the elevation of the instruments was 1cm above the ripple crests. The first carriage was located in the same vertical (same x-position) during all half-hour tests, whereas the second carriage was moved after every half-hour. Carriage 2 was first placed 15 cm onshore from carriage 1 and the final position was 70 cm from carriage 1. This procedure was performed in both vertical 4 and 6. The positions of the carriages in the correlation measurements is given in Table C-26:

Table C-26 Positions of carriage 2 in the correlation measurements and distance of carriage 2 landwards of carriage 1.

Vertical	x-position (m)	$x_{\text{car2}} - x_{\text{car1}}$
4a	25.65	0.15
4b	25.75	0.25
4c	25.8	0.30
4d	25.85	0.35
4e	26	0.50
4f	26.1	0.60
4g	26.2	0.70
Vertical	x-position (m)	$x_{\text{car2}} - x_{\text{car1}}$
6a	20.65	0.15
6b	20.75	0.25
6c	20.8	0.30
6d	20.85	0.35
6e	21	0.50
6f	21.1	0.60
6g	21.2	0.70

Table C-27 Positions of the carriages during each half-hour run of series A (in chronological order)

Series name	carriage 1		carriage 2		remarks
	vertical	height (cm above bed)	height (cm above bed)	vertical	
%A100					profile
A101	8	0.5	0.5	7	⁶⁷
A102	8	1	1	7	⁶⁷
A103	8	1.5	1.5	7	⁶⁷
A104	8	2	2	7	⁶⁷
A105	8	3	3	7	⁶
A106	8	6	6	7	⁶
%a106					⁸
A201	6	0.5	0.5	3	
A202	6	1	1	3	
A203	6	1.5	1.5	3	
A204	6	2	2	3	
A205	6	3	3	3	
A206	6	6	6	3	
A207	6	4.5	4.5	3	
%a207					profile
A301	5	1.5	1.5	2	
A302	5	2	2	2	
A303	5	3	3	2	
A304	5	6	1	2	
A305	5	9	0.5	2	⁹
A306	5	0.5	0.5	1	
A307	5	1	1	1	
A308	3	0.5	1.5	1	
A309	3	1	2	1	
%a309					profile
A401	6	0.5	0.5 ¹⁰	4	
A402	6	1	1	4	
A403	6	1.5	1.5	4	
A404	6	2	2	4	
A405	6	3	3	4	
A406	6	6	6	4	
A407	6	9	9	4	
%a407					profile
A501	5	1	1	5a	
A601	6	1	1 ¹⁰	6a	¹¹

⁶ Due to velocity range of 10cm/s instead of 30 cm/s ADV1 and ADV2 signals contain spikes which can partly be removed by further post-processing

⁷ Sampling volume ADV 6 mm instead of 9 mm

⁸ signal OPC01 and OPC02 out of (analogue output) range; percentages of time need to be assessed

⁹ ADV01 a few moments close to water surface

¹⁰ OpCon signal range larger than 10 V; further inspection on validity of peaks is necessary

¹¹ OPC01 signal not complete

Series name	carriage 1		carriage 2		remarks
	vertical	height (cm above bed)	height (cm above bed)	vertical	
A611	6	1	1 ¹⁰	6a	
A602	6	1	1	6b	
A603	6	1	1 ¹⁰	6c	
A604	6	1	1	6d	
A605	6	1	1 ¹⁰	6e	
A606	6	1	1 ¹⁰	6f	
A607	6	1	1 ¹⁰	6g	
%a607					profile
A701	4	1	1	4a	¹²
A702	4	1	1	4b	
A703	4	1	1	4c	
A704	4	1	1	4d	
A705	4	1	1	4e	
A706	4	1	1	4f	
A707	4	1	1	4g	
%a707					
A801	8	1	1 ¹⁰	7	
A802	8	3	3	7	
A803	8	6	6	7	
A901					video
A902					video
A903					video
A904					video
%a904					profile

Table C-28 Measured vertical positions, name of the series and carriage number for vertical 1

Vertical	height (cm above bed)	series name	carriage
1	0.5	A306	2
1	1	A307	2
1	1.5	A308	2
1	2	A309	2

¹² Series A7* 4 cm offshore from vertical 4

Table C-29: Measured vertical positions, name of the series and carriage number for vertical 2

Vertical	height (cm above bed)	series name	carriage
2	0.5	A305	2
2	1	A304	2
2	1.5	A301	2
2	2	A302	2
2	3	A303	2

Table C-30 Measured vertical positions, name of the series and carriage number for vertical 3

Vertical	height (cm above bed)	series name	carriage
3	0.5	A308	1
3	0.5	A201	2
3	1	A309	1
3	1	A202	2
3	1.5	A203	2
3	2	A204	2
3	3	A205	2
3	4.5	A207	2
3	6	A206	2

Table C-31 Measured vertical positions, name of the series and carriage number for vertical 4

Vertical	height (cm above bed)	series name	carriage
4	0.5	A401	2
4	1	A402	2
4	1	A701 ¹²	1
4	1	A702	1
4	1	A703	1
4	1	A704	1
4	1	A705	1
4	1	A706	1
4	1	A707	1
4	1.5	A403	2
4	2	A404	2
4	3	A405	2
4	6	A406	2
4	9	A407	2

Table C-32 Measured vertical positions, name of the series and carriage number for location near vertical 4

Vertical	height (cm above bed)	series name	carriage
4a	1	A701	2
4b	1	A702	2
4c	1	A703	2
4d	1	A704	2
4e	1	A705	2
4f	1	A706	2
4g	1	A707	2

Table C-33 Measured vertical positions, name of the series and carriage number for vertical 5

Vertical height (cm series name carriage above bed)			
5	0.5	A306	1
5	1	A307	1
5	1	A501	1
5	1.5	A301	1
5	2	A302	1
5	3	A303	1
5	6	A304	1
5	9	A305	1

Table C-35 Measured vertical positions, name of the series and carriage number for vertical 6

Vertical height (cm series name carriage above bed)			
6	0.5	A201	1
6	0.5	A401	1
6	1	A202	1
6	1	A402	1
6	1	A601	1
6	1	A611	1
6	1	A602	1
6	1	A603	1
6	1	A604	1
6	1	A605	1
6	1	A606	1
6	1	A607	1
6	1.5	A203	1
6	1.5	A403	1
6	2	A204	1
6	2	A404	1
6	3	A205	1
6	3	A405	1
6	4.5	A207	1
6	6	A206	1
6	6	A406	1
6	9	A407	1

Table C-34 Measured vertical positions, name of the series and carriage number for location near vertical 5

Vertical height (cm series name carriage above bed)			
5a	1	A501	2

Table C-36 Measured vertical positions, name of the series and carriage number for location near vertical 6

Vertical height (cm series name carriage above bed)			
6a	1	A601	2
6a	1	A611	2
6b	1	A602	2
6c	1	A603	2
6d	1	A604	2
6e	1	A605	2
6f	1	A606	2
6g	1	A607	2

Table C-37 Measured vertical positions, name of the series and carriage number for vertical 7

Vertical	height (cm above bed)	series name	carriage
7	0.5	A101	2
7	1	A102	2
7	1	A801	2
7	1.5	A103	2
7	2	A104	2
7	3	A105	2
7	3	A802	2
7	6	A106	2
7	6	A803	2

Table C-38 Measured vertical positions, name of the series and carriage number for vertical 8

Vertical	height (cm above bed)	series name	carriage
8	0.5	A101	1
8	1	A102	1
8	1	A801	1
8	1.5	A103	1
8	2	A104	1
8	3	A105	1
8	3	A802	1
8	6	A106	1
8	6	A803	1

C-series

These tables show the measuring locations of the different experiments for series C. The order in which the experiments were performed are indicated by the increasing numbers.

Vertical	series name
-	c404 ¹³
1	c401 ¹⁴
2	c304
3	c201
3	c303
4	c302
4	c403
5	c301
6	c101 ¹⁵
6	c204
7	c203 ^{16,17}
7	c402
8	c202

¹³ Two hour wave duration; no measurements

¹⁴ Malfunctioning ADV

¹⁵ Half-hour measurement instead of hour measurement, ADV file not complete

¹⁶ 'Peilvoetje' in water during experiment

¹⁷ no ADV data

D-series

Series	Water	Grain size	accelerometer	microphone	Speed (m/s)
D101	-	110 µm		+	0.1
D102	-	110 µm		+	0.2
D103	-	110 µm	+		0.1
D104	-	110 µm	+		0.2
D201	-	Mix	+		0.1
D202	-	Mix	+		0.1
D203	+	Mix	+		0.1
D204	+	Mix	+		0.2
D205	+	Mix		+	0.1
D206	+	Mix		+	0.1
D207	+	Mix		+	0.2
D208	+	Mix		+	0.2

Grain size distribution mixture D-series

Begin x (m)	End x (m)	D ₅₀ (µm)	D ₁₀ (µm)	D ₉₀ (µm)
37.1	36.2	Gravel	Gravel	Gravel
36	33	197	145	267
31	28	92	57	144
26	23	273	198	404
21	18	146	93	243
17	14	350	191	597
13	10	411	314	559

Profile evolution

Tables showing profile evolution for the different profile measurements.

Profile time of profile evolution	
A106	4:01:08
A207	8:07:08
A309	13:20:47
A407	17:24:44
A607	22:38:23
A707	26:42:20
A904	29:36:53

Profile time of profile evolution	
B101	0:30:20
B102	1:31:01
B104	3:32:23

Profile time of profile evolution	
C101	0:34:31
C201	1:39:22
C302	7:03:37
C402	11:23:01
C404	14:33:24

D Set-up correction

Table D-39 Overview of uncorrected and corrected set-up values; mean and standard deviation over several tests (series A)

x	mean	stdev	mean corrected	stdev	number of measurements
2.80	-0.00231	0.000472	-0.00189	0.000269	48
6.56	-0.0022	0.000502	-0.00184	0.00029	48
7.97	-0.00232	0.000449	-0.00193	0.00026	48
8.44	-0.0022	0.000472	-0.00182	0.000275	48
15.50	-0.00283	0.000496	-0.00229	0.000331	9 (A1**_5, A8**_5)
18.00	-0.003	0.000368	-0.00256	0.000293	9 (A1**_6, A8**_6)
20.50	-0.00316	0.000515	-0.00346	0.000289	22 (A2**_5, A4**_5, A6**_5)
20.65	-0.00306	0.00036	-0.00291	0.000116	2 (A601_6, A611_6)
20.75	-0.00291		-0.00294		1 (A602_6)
20.80	-0.00335		-0.00324		1 (A603_6)
20.85	-0.00378		-0.00311		1 (A604_6)
21.00	-0.00304		-0.00313		1 (A605_6)
21.10	-0.00271		-0.00295		1 (A606_6)
21.20	-0.00359		-0.00337		1 (A607_6)
23.00	-0.00151	0.001348	-0.00385	0.000861	8 (A301_5..A307_5, A501_5)
23.15	-3.81E-03		-2.96E-03		1 (A501_6)
25.46	-1.79E-03	0.000599	-1.55E-03	0.000414	7 (A7**_5)
25.50	-2.35E-03	0.000674	-2.38E-03	0.000349	7 (A4**_6)
25.61	-2.61E-03		-1.81E-03		1 (A701_6)
25.71	-1.60E-03		-1.68E-03		1 (A702_6)
25.76	-1.97E-03		-1.70E-03		1 (A703_6)
25.81	-1.69E-03		-1.31E-03		1 (A704_6)
25.96	-1.14E-03		-9.81E-04		1 (A705_6)
26.06	-8.88E-04		-5.83E-04		1 (A706_6)
26.16	-2.95E-04		-3.40E-04		1 (A707_6)
28.00	-0.00136	0.000564	-0.0013	0.000291	9 (A2**_6, A308_5, A309_5)
30.50	0.00103	0.000564	0.001075	0.000338	5 (A301_6..A305_6)
33.00	0.002646	0.000228	0.002887	0.000199	4 (A306_6..A309_6)

Table D-40 zerolevel values WHM before test (series A)

	WHM01	WHM02	WHM03	WHM04	WHM05	WHM06
A101	9.06E-05	1.63E-04	1.15E-04	1.28E-04	8.07E-07	1.91E-04
A102	1.14E-04	1.58E-04	1.42E-04	2.21E-04	9.72E-05	2.82E-04
A103	3.69E-04	3.50E-04	-1.97E-06	1.38E-04	3.36E-05	1.07E-04
A104	8.51E-05	5.87E-05	-1.73E-04	-5.16E-05	-1.87E-04	7.29E-06
A105	4.83E-04	6.24E-04	5.35E-04	4.00E-04	2.99E-04	5.80E-04
A106	2.07E-05	6.89E-05	4.84E-05	1.07E-04	1.80E-04	-1.20E-04
A201	2.75E-05	1.46E-04	6.36E-05	1.30E-04	2.54E-05	6.78E-05
A202	-3.92E-05	3.22E-05	4.76E-05	1.19E-04	-1.89E-04	-4.83E-05
A203	-4.17E-05	2.99E-05	5.22E-05	2.45E-04	6.51E-05	-2.13E-04
A204	1.04E-04	3.26E-04	-9.46E-05	1.50E-04	1.71E-05	2.45E-04
A205	5.79E-05	2.25E-04	2.20E-04	4.86E-05	-3.95E-05	-9.21E-05
A206	9.17E-05	-1.26E-04	1.33E-04	2.80E-04	1.26E-04	-4.04E-05
A207	8.28E-05	6.52E-05	9.03E-05	-4.89E-05	1.84E-05	1.33E-04
A301	6.34E-05	-8.91E-05	3.60E-05	-8.93E-06	1.06E-04	-9.05E-09
A302	-8.33E-05	-6.18E-05	-1.28E-04	1.50E-04	-1.97E-04	-2.57E-04
A303	2.81E-04	1.70E-04	1.13E-04	4.12E-04	4.67E-04	1.41E-04
A304	1.42E-03	1.18E-03	1.07E-03	1.24E-03	7.13E-04	1.09E-03
A305	-1.78E-04	1.61E-04	-1.51E-04	2.69E-05	1.03E-04	-1.03E-04
A306	3.05E-04	2.36E-04	1.82E-04	8.41E-05	3.85E-04	1.77E-05
A307	3.77E-04	2.99E-05	2.82E-04	1.07E-04	1.87E-04	9.64E-07
A308	7.28E-05	1.31E-04	-5.42E-05	3.71E-05	-2.59E-05	1.09E-04
A309	2.80E-04	4.48E-04	1.70E-04	2.01E-04	2.51E-04	8.55E-05
A401	-6.18E-05	-1.56E-04	3.19E-04	1.33E-04	1.31E-04	1.69E-04
A402	2.97E-04	2.43E-04	7.67E-05	1.62E-04	4.06E-04	-2.71E-05
A403	3.08E-05	-2.12E-06	-1.64E-04	9.19E-05	2.53E-04	-9.61E-05
A404	1.33E-04	2.31E-04	-8.69E-06	1.79E-04	2.64E-05	1.51E-04
A405	1.49E-05	-1.31E-05	-1.94E-04	-5.51E-05	-2.01E-05	-2.82E-05
A406	1.22E-05	-1.20E-04	-2.57E-04	-5.51E-05	-3.01E-04	6.40E-05
A407	3.76E-04	3.88E-04	3.16E-04	9.43E-05	6.03E-05	1.74E-04
A501	-1.66E-04	9.62E-05	-1.88E-04	-1.08E-04	-1.92E-04	-1.03E-04
A601	6.57E-05	9.37E-05	6.32E-05	5.70E-05	1.91E-04	-1.54E-04
A602	-3.57E-05	-5.34E-05	1.45E-04	1.73E-04	-1.85E-04	-4.12E-04
A611	2.69E-04	-1.07E-04	-3.15E-05	-2.57E-05	-1.85E-04	-6.24E-04
A603	5.68E-05	1.20E-04	2.85E-04	5.90E-05	1.70E-04	-2.48E-05
A604	-1.16E-04	-2.89E-04	3.34E-04	-1.04E-04	-1.93E-04	2.18E-04
A605	1.67E-04	-2.66E-04	-2.00E-04	1.87E-04	1.87E-04	1.14E-04
A606	-1.55E-04	7.95E-05	-1.90E-04	-1.37E-05	-1.64E-04	-2.12E-04
A607	-1.83E-04	3.62E-05	-4.64E-04	2.27E-04	4.43E-05	4.60E-05
A701	4.74E-05	-7.47E-06	-7.19E-05	1.86E-04	2.72E-04	-6.23E-04
A702	1.01E-04	2.52E-04	9.71E-05	1.32E-04	3.39E-04	-9.81E-07
A703	9.55E-05	-1.08E-04	-1.12E-04	7.09E-05	-2.05E-04	9.96E-05
A704	-6.38E-05	5.78E-04	1.29E-04	3.66E-04	4.30E-04	2.68E-04
A705	1.78E-04	7.72E-05	1.27E-04	4.63E-05	-1.06E-05	-9.09E-05
A706	1.83E-04	-2.97E-05	6.90E-05	-1.31E-05	1.89E-04	-2.97E-05
A707	8.59E-06	-1.49E-04	-1.43E-04	1.57E-04	-2.08E-04	-1.07E-04
A801	6.75E-05	1.40E-04	6.32E-05	-6.91E-05	-1.89E-04	-1.61E-04
A802	3.42E-04	1.24E-04	-1.44E-05	3.03E-04	9.01E-05	7.05E-05
A803	-2.21E-04	1.24E-04	2.59E-04	-2.91E-04	6.01E-05	1.94E-05

Table D-41 zero level values WHM after test (series A)

	WHM01	WHM02	WHM03	WHM04	WHM05	WHM06
A101	-1.64E-03	-1.61E-03	-1.66E-03	-1.73E-03	-2.02E-03	-1.39E-03
A102	-4.66E-04	-3.64E-04	-2.79E-04	-2.83E-04	-1.35E-03	-2.72E-04
A103	-6.23E-04	-5.09E-04	-9.56E-04	-7.39E-04	-6.82E-04	-7.01E-04
A104	-1.02E-03	-1.10E-03	-1.26E-03	-1.04E-03	-1.42E-03	-1.04E-03
A105	-2.86E-04	-1.87E-04	-3.11E-04	-3.91E-04	-5.03E-04	-1.18E-04
A106	-4.16E-04	-4.01E-04	-4.98E-04	-3.44E-04	-1.37E-04	-3.54E-04
A201	-1.55E-03	-1.60E-03	-1.48E-03	-1.77E-03	1.08E-04	-1.26E-03
A202	-9.48E-05	8.88E-06	-3.93E-05	-3.54E-05	1.28E-03	1.80E-04
A203	4.76E-07	4.61E-05	1.67E-04	3.54E-04	1.37E-03	2.04E-04
A204	-1.64E-04	4.95E-05	-4.71E-04	-1.84E-04	8.69E-04	5.27E-05
A205	-1.15E-03	-9.16E-04	-8.66E-04	-1.08E-03	-1.36E-04	-7.83E-04
A206	4.01E-04	2.42E-04	4.12E-04	5.67E-04	1.11E-03	6.64E-04
A207	-1.75E-03	-1.75E-03	-1.77E-03	-1.94E-03	1.71E-04	1.12E-05
A301	-1.86E-03	-2.01E-03	-1.83E-03	-2.00E-03	6.76E-03	-7.70E-04
A302	4.53E-05	8.08E-05	1.91E-04	3.09E-04	5.99E-03	2.99E-04
A303	-2.27E-04	-1.21E-04	-1.10E-04	1.33E-04	5.15E-03	1.73E-04
A304	-1.24E-04	-1.71E-07	-6.33E-05	3.54E-04	4.76E-03	7.14E-04
A305	-8.35E-04	-3.16E-04	-6.50E-04	-4.82E-04	5.84E-03	4.86E-06
A306	-1.01E-03	-8.83E-04	-9.47E-04	-1.02E-03	6.49E-03	-1.01E-03
A307	-4.75E-04	-4.52E-04	-3.16E-04	-4.65E-04	6.86E-03	-3.32E-04
A308	-3.52E-04	-3.93E-05	-4.16E-04	-2.30E-04	-1.33E-03	9.63E-07
A309	-4.47E-04	-3.10E-04	-5.94E-04	-4.42E-04	-2.29E-04	-3.69E-04
A401	-1.55E-03	-1.61E-03	-1.36E-03	-1.44E-03	-5.43E-05	-1.01E-03
A402	-7.74E-04	-8.67E-04	-1.07E-03	-7.94E-04	2.35E-04	-2.15E-04
A403	1.04E-03	9.91E-04	8.95E-04	1.16E-03	2.37E-03	1.36E-03
A404	-2.57E-04	-4.09E-04	-4.89E-04	-3.43E-04	8.12E-04	5.23E-04
A405	-8.70E-04	-8.92E-04	-1.00E-03	-8.74E-04	-3.19E-04	-1.88E-04
A406	-1.36E-03	-1.48E-03	-1.52E-03	-1.26E-03	-5.90E-04	-7.98E-04
A407	9.86E-04	1.03E-03	9.30E-04	7.60E-04	1.61E-03	1.14E-03
A501	-2.13E-03	-1.29E-03	-2.03E-03	-1.92E-03	-2.91E-03	-1.81E-03
A601	-1.14E-03	-1.75E-04	-1.15E-03	-1.22E-03	9.77E-04	-1.12E-03
A602	-4.41E-04	9.64E-04	-1.46E-04	-2.15E-04	-2.89E-04	-3.49E-04
A611	-2.30E-04	-4.91E-04	-2.46E-04	-2.43E-04	1.68E-03	-2.50E-04
A603	-5.64E-04	-5.24E-04	-1.88E-04	-2.79E-04	1.20E-03	-2.55E-04
A604	-2.08E-03	-2.26E-03	-1.69E-03	-2.06E-03	-1.22E-03	-1.13E-03
A605	-7.51E-04	-1.25E-03	-1.11E-03	-6.30E-04	2.66E-04	2.89E-04
A606	-3.76E-04	-1.43E-04	-3.09E-04	-7.15E-05	8.48E-04	2.76E-04
A607	-1.42E-03	-1.21E-03	-1.60E-03	-7.58E-04	1.34E-03	-4.06E-04
A701	-1.85E-03	-1.80E-03	-1.58E-03	-1.33E-03	-1.19E-03	-2.23E-03
A702	2.43E-05	1.15E-04	-8.36E-05	-1.15E-04	3.36E-04	1.59E-04
A703	-8.77E-04	-4.45E-04	-7.44E-04	-4.77E-04	-8.02E-04	-4.51E-04
A704	-8.58E-04	-3.81E-04	-7.49E-04	-5.65E-04	-2.48E-04	-4.87E-04
A705	-7.87E-04	-1.00E-03	-9.27E-04	-1.01E-03	-3.09E-04	-4.18E-04
A706	-8.27E-04	-9.77E-04	-9.88E-04	-1.00E-03	-3.76E-04	-6.40E-04
A707	-4.22E-04	-3.54E-04	-4.28E-04	-2.38E-05	-9.87E-07	-1.75E-05
A801	-1.39E-03	-1.30E-03	-1.40E-03	-1.53E-03	-1.54E-03	-1.20E-03
A802	-1.12E-03	-1.32E-03	-1.47E-03	-1.12E-03	-1.27E-03	-1.21E-03
A803	-7.44E-04	-4.59E-04	-3.49E-04	-7.43E-04	-4.21E-04	-4.89E-04

Table D-42 Overview of uncorrected and corrected set-up values; mean and standard deviation over several tests (series C)

x	mean	stdev	mean corrected	stdev	no. measurements
2.8	-0.0035	0.000579	-0.00288	0.000347	12
6.56	-0.00337	0.000574	-0.00275	0.000355	12
7.97	-0.00354	0.000619	-0.00292	0.000371	12
8.44	-0.00338	0.000576	-0.00276	0.00034	12
15.5	-0.00423		-3.16E-03		c202 WHM06
18.0	-0.00405		-3.43E-03		c203 WHM06
18.0	-0.00366		-3.38E-03		c402 WHM06
20.5	-0.00371		-3.95E-03		c101 WHM06
20.5	-0.00091		-2.11E-03		c204 WHM06
23.0	-0.00436		-5.12E-03		c301 WHM06
25.5	-0.00286		-3.51E-03		c302 WHM06
25.5	-0.00325		-3.34E-03		c403 WHM06
28	-0.00326		-2.61E-03		c201 WHM06
28	-0.00173		-1.87E-03		c303 WHM06
30.5	-0.00156		-1.08E-03		c304 WHM06
33.0	0.002041		2.67E-03		c401 WHM06

Table D-43 zerolevel values WHM before test (series C)

	WHM01	WHM02	WHM03	WHM04	WHM06
c101	6.67E-05	-2.44E-04	1.42E-04	-1.92E-06	1.75E-04
c201	1.18E-04	-1.09E-04	-1.02E-04	-2.85E-04	8.57E-05
c202	5.88E-04	2.48E-05	5.34E-04	3.69E-04	3.89E-05
c203	1.78E-04	2.29E-04	1.55E-04	2.07E-04	-4.87E-06
c204	1.77E-04	-1.31E-06	-1.41E-04	2.11E-05	-2.31E-04
c301	2.39E-04	-8.18E-05	1.66E-04	-7.34E-05	5.75E-05
c302	6.15E-06	-1.23E-04	4.23E-05	-1.55E-04	-3.90E-05
c303	3.22E-04	1.66E-04	-2.51E-05	3.89E-04	3.60E-05
c304	2.55E-04	-4.30E-05	-2.51E-05	-9.00E-05	-2.69E-05
c401	4.09E-04	3.06E-04	2.50E-04	2.69E-04	2.75E-05
c402	6.05E-05	-3.18E-05	1.26E-04	6.54E-05	-2.28E-05
c403	1.22E-04	1.05E-04	-1.43E-04	4.02E-04	-3.00E-05

Table D-44 zero level values WHM after test (series C)

	WHM01	WHM02	WHM03	WHM04	WHM06
c101	-1.83E-03	-2.03E-03	-1.85E-03	-1.96E-03	6.49E-04
c201	-1.46E-03	-1.52E-03	-1.69E-03	-1.79E-03	-1.21E-03
c202	-2.08E-03	-2.53E-03	-2.27E-03	-2.34E-03	-2.09E-03
c203	-1.19E-03	-9.76E-04	-1.62E-03	-1.19E-03	-1.23E-03
c204	-8.69E-04	-9.10E-04	-1.06E-03	-7.78E-04	2.17E-03
c301	-5.22E-04	-8.91E-04	-6.11E-04	-8.06E-04	1.59E-03
c302	6.34E-05	-7.66E-05	6.98E-05	-1.72E-04	1.27E-03
c303	1.27E-04	2.60E-04	-7.62E-05	4.08E-04	3.04E-04
c304	-7.21E-04	-9.66E-04	-7.87E-04	-9.83E-04	-9.89E-04
c401	-1.14E-03	-1.40E-03	-1.05E-03	-1.24E-05	-1.24E-03
c402	no value	-2.27E-03	-1.08E-03	-1.09E-03	-5.70E-04
c403	-1.29E-03	-9.26E-04	-1.15E-03	-1.00E-03	1.56E-04

E Opcon calibration curves

Calibration measurements

The calibration measurements were conducted by stirring a known amount of sediment in a known amount of water. The measured voltage is recorded at each concentration. However, the measured voltage at each concentration is too high, since very fine particles in the water column do not contribute to the weight, but do contribute to the measured voltage. In other words, the actual concentration (measured from the weight of the sediments that were put in the vessel) is lower than the concentration (from now on named as “virtual” concentration) that belongs to the measured voltage. This “virtual” concentration is the actual concentration (in g/l) increased with the background concentration (in g/l and which is constant independent of the measured voltage). The background concentration (g/l) is the voltage measured at still water multiplied with the first order estimated calibration coefficients of the polynomial fit of the raw data points.

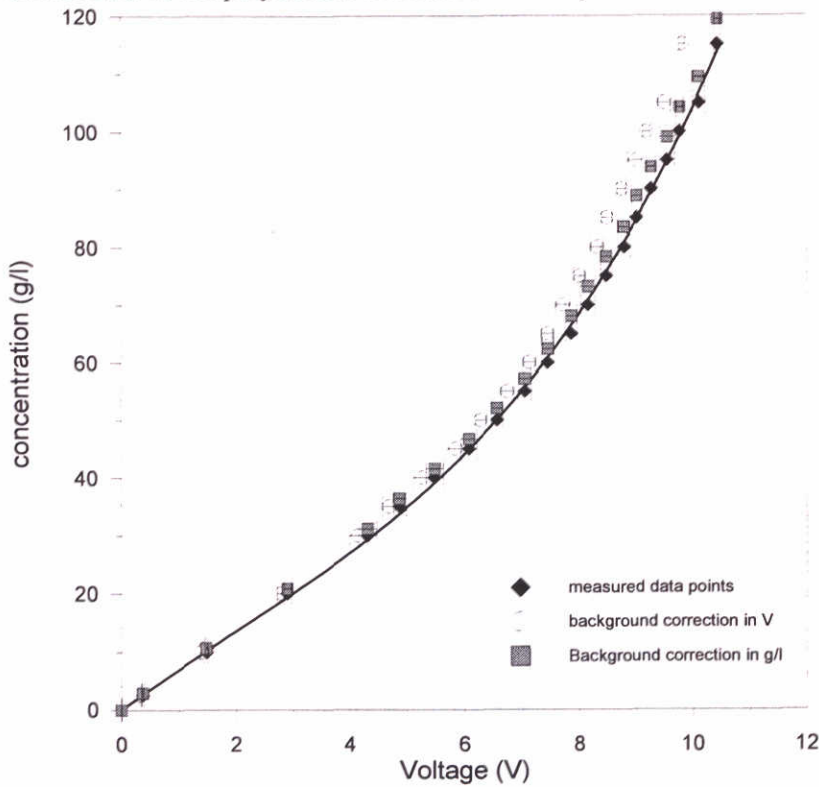


Figure E-51: The relation between concentration and Voltage. Dark squares represent the raw measurements, the open circles are the raw data when the background correction is done in V, the grey squares are the concentrations, after background correction in g/l. These data-points are used to fit the calibration curves.

In Figure E-51, the raw measured data points (black dots), the original calibration curve, with corrections in V and the calibration curve corrected with above described procedure are shown.

OpCon Calibration for various 0-level shiftings

In the beginning of the experiments, the zero shift of the OpCon was set to zero. During the experiments, it became apparent that the measured voltages exceeded 10V (which was designed as the maximum voltage for the linear part of the detector). Since the amplifier was already at its minimum, the zero shift of the OpCon was set to -2V to gain extra space for measuring. After that, an amplifier at the data acquisition system was used to translate the signal to -7.97V. After a period of measurements, it was decided to set the zero shift of the OpCon to 0V, and use the amplifier at the data acquisition system to translate the signal by -7.97 V to -7.97V.

Table E-45 gives an overview of the combinations of the zero-shifts.

Table E-45: Overview of 0-shift combinations during the various experiments

Range of measurements	0-shift OpCon	Total shift on data acquisition
A101-A207	0	0
A301-A303	-2	-2
A304-A607	-2	-7.97
A701-C404	0	-7.97

Since it was not clear what the effect of this zero shifting would be on the calibration curve, two calibration curves per instrument were constructed, one curve without a zero shift and one curve with a zero shift of -2V. Figure E-52 shows that the calibration curve is linear up to 30 g/l, but is not linear for larger concentrations. Therefore four third-order polynomials and four fourth-order polynomials were fitted through the data points. The chi-square of the different fits was used to decide which order of polynomial was appropriate. Table E-46 shows the calibration coefficients for OpCon 1 and OpCon 2 with different 0-level shiftings.

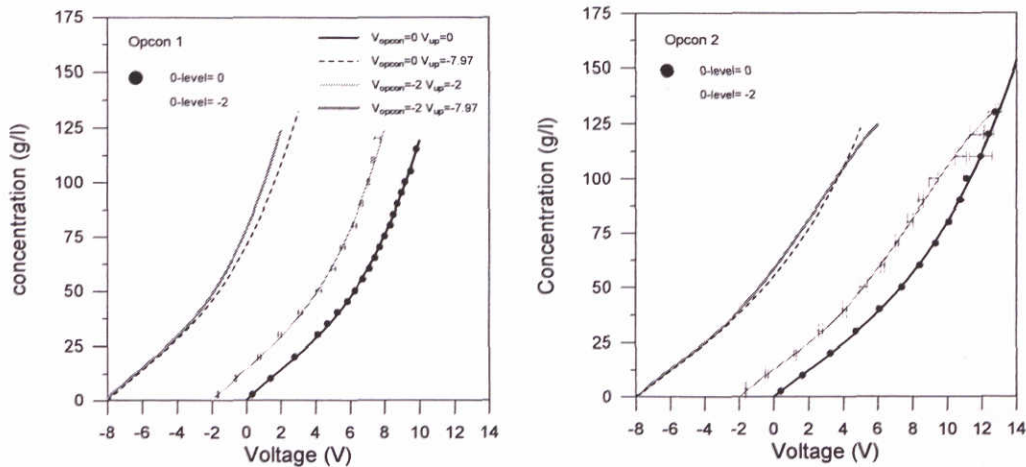


Figure E-52: Calibration curves for OpCon1 and OpCon2 with different zero level shiftings. The calibration curve with a zero level shifting of -7.97V (and a shift of -2V at the OpCon), is based on the data points from the measurements with a -2V zero shifting. These data points are translated with -5.97V. The calibration curve with a zero level shifting of -7.97V (and a shift of -0V at the OpCon), is based on the data points from the measurements with a -0V zero shifting. These data points are translated with -7.97V.

During the experiments, the OpCon voltage (with a zero level shift of -2V) was set to -7.97V by an amplifier connected to the data acquisition system. For the calibration of these measurements, the calibration curve with a zero level shifting of -2V should be translated by -5.97 V. Since this is not possible by simply adjusting the polynomial coefficients (but would be possible if the relation between concentration and voltage was linear), the calibration measurements are translated by -5.97 V and the polynomials are fitted to these data points. The polynomial coefficients are shown in Table E-46 and Figure E-52. An equal procedure is conducted for the calibration measurements that were done with a zero-shift of 0V at the OpCon.

Table E-46: Coefficients of the polynomials fitted through the calibration measurements with different zero shifting according to the function $(c)=A_0+A_1V+A_2V^2+A_3V^3+A_4V^4$ (where (c) is the sediment concentration (g/l) and V the measured voltage) the internal uncertainties of the fitted parameters are within brackets. The χ^2_{red} shows the quality of the fit.

OpCon	0-level OpCon	Total 0-level	A_0	A_1	A_2	A_3	A_4	χ^2_{red}
1	0	0	0 (0.008)	7.95(0.17)	-0.56 (0.07)	0.085(0.006)		0.4
1	-2	-2	15.0 (0.3)	7.5(0.3)	-0.02(0.06)	0.01(0.04)	0.010(0.004)	0.8
1	-2	-7.97	74(1)	16.6(0.4)	2.2(0.3)	0.24(0.06)	0.010(0.004)	0.8
1	0	-7.97	70.809 (0.008)	15.31 (0.17)	1.474 (0.07)	0.085 (0.006)		0.4
2	0	0	0 (0.006)	6.44(0.14)	-0.22(0.05)	0.035(0.004)		0.4
2	-2	-2	12.8(0.3)	5.88(0.12)	-0.084(0.015)	0.084(0.015)	-0.0045(0.0008)	1
2	-2	-7.97	57.2(0.5)	10.1(0.2)	0.45(0.05)	-0.024(0.004)	-0.0044(0.0007)	1
2	0	-7.97	55.328 (0.006)	9.676 (0.14)	0.623 (0.05)	0.035 (0.004)		0.4

(Un)certainty in calibration curve

Apart from the statistical uncertainties in the fits, an extra uncertainty is introduced. The calibration curves for different zero level shiftings are fits through data points. In the calibration, the measured voltage at a concentration of 0 g/l is zero. This 0-level is a data point and not a boundary condition for the fitting procedure. This implies that these fits will calculate a small sediment concentration, even when the measured voltage does not deviate from base level. Table E-47 shows these concentrations and the corresponding uncertainties in the suspended sediment concentrations. These uncertainties are calculated by assuming that the only error in the suspended sediment concentration comes from the uncertainty in the calibration fit. It is assumed that the uncertainty in the OpCon voltage output or uncertainties coupled to the OpCon mechanism are negligible. The concentrations that are calculated when the voltage does not deviate from base level, fall within the uncertainties.

Table E-47: Sediment concentrations calculated with the polynomial fits when the output voltage does not deviate from base level and their uncertainties.

OpCon	0-level OpCon (V)	Total 0-level (V)	Concentration at base level (g/l)	δc (g/l)
1	0	0	0	0.18
1	-2	-2	-0.01	0.43
1	-2	-7.97	0.33	1.12
1	0	-7.97	0.06	0.18
2	0	0	0	0.18
2	-2	-2	-0.03	0.32

2	-2	-7.97	-0.04	0.54
2	0	-7.97	0.06	0.18

Background concentration

Prior to and after each experiment were measurements with the OpCon were conducted, the voltage of the background concentration was measured. It is assumed that the background concentration (in g/l) is constant throughout the experiment and that the concentration measured at the end of the experiment reflects these constant conditions. The measured voltage of the background concentration corresponds to a certain concentration of very fine suspended sediments, which is constant independent of the total measured concentration. Since the calibration coefficients (relation between concentration and measured voltage) for the OpCon are not linear for higher concentrations, a background concentration (in g/l) should be subtracted instead of a background voltage.

The background concentration is calculated with the fit parameters that correspond to the specific measurement.

In the cd-zero measurements, the background levels are given in g/l and are calculated with the old calibration coefficients. These coefficients are used to recalculate the measured voltage, after which the new background is calculated by above described procedure.

Effect of wrong calibration on signal A701-C404

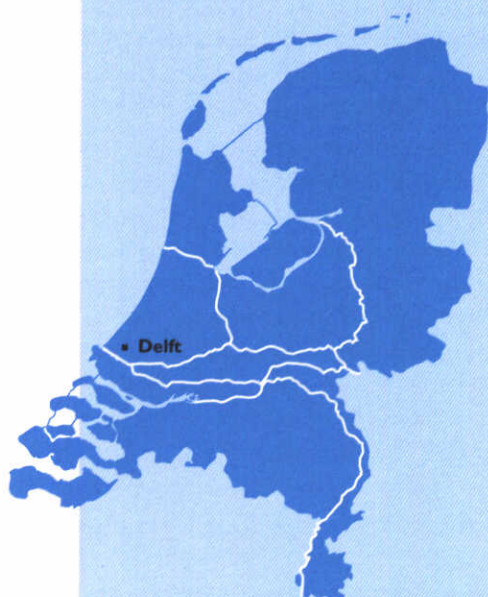
In the analysis of OpCon signals A701-C404, the translated calibration curve of -2V is used instead of the translated calibration curve of 0V. Figure E-52 shows that both calibration curves are almost similar in the region between -8 and 0V, but that at higher voltages, large differences may occur. Table E-48 shows the difference in the sediment concentration due to the wrong calibration coefficients at different voltages. For OpCon1, the suspended sediment concentrations that are calculated with the wrong calibration curve are overestimated. This effect is smaller for OpCon2.

Table E-48: Overview of the differences in the concentration due to the fitting with the wrong calibration curve. The uncertainty in the difference of OpCon1=1.1 g/l, the uncertainty in the difference of OpCon2 =0.8g/l.

Voltage	OpCon1			OpCon2		
	Concentration Calibration based on -2V	Concentration calibration based on -0V	Difference (g/l)	Concentration calibration based on -2V	Concentration calibration based on -0V	difference (g/l)
-7.97	0.33	0.06	0.26	-0.04	0.06	-0.10
-7.9	0.83	0.62	0.22	0.46	0.51	-0.05
-7.8	1.56	1.40	0.16	1.17	1.15	0.02
-7	7.45	7.30	0.14	6.47	6.12	0.35
-6	14.86	14.16	0.70	12.50	12.14	0.36
-5	22.29	20.91	1.38	18.39	18.15	0.24
-4	29.88	28.05	1.83	24.57	24.35	0.21
-3	38.05	36.11	1.94	31.36	30.96	0.40
-2	47.42	45.58	1.84	39.00	38.19	0.81
-1	58.85	56.97	1.88	47.61	46.24	1.37

0	73.45	70.81	2.64	57.20	55.33	1.87
1	92.55	87.59	4.96	67.68	65.66	2.02
2	117.73	107.84	9.89	78.86	77.45	1.41

Further, in A301-A303 for the A3 parameter is wrongly used 0.103 instead of 0.0103. At the moment of writing of this report this has not been corrected yet.



WL | delft hydraulics

Rotterdamseweg 185
postbus 177
2600 MH Delft
telefoon 015 285 85 85
telefax 015 285 85 82
e-mail info@wldelft.nl
internet www.wldelft.nl

Rotterdamseweg 185
p.o. box 177
2600 MH Delft
The Netherlands
telephone +31 15 285 85 85
telefax +31 15 285 85 82
e-mail info@wldelft.nl
internet www.wldelft.nl

